NEMATIC LIQUID CRYSTALS IN ELECTRIC AND MAGNETIC FIELDS

By

BARBARA JOAN FRISKEN

B.Sc., Queen's University, 1982
M.S., Northwestern University, 1984

A THESIS SUBMITTED IN PARTIAL FULFILLMENT OF

THE REQUIREMENTS FOR THE DEGREE OF

DOCTOR OF PHILOSOPHY

in

THE FACULTY OF GRADUATE STUDIES
(Physics)

We accept this thesis as conforming
to the required standard

THE UNIVERSITY OF BRITISH COLUMBIA
March 1989
© Barbara Joan Frisken, 1989

In presenting this thesis in partial fulfilment of the requirements for an advanced degree at the University of British Columbia, I agree that the Library shall make it freely available for reference and study. I further agree that permission for extensive copying of this thesis for scholarly purposes may be granted by the head of my department or by his or her representatives. It is understood that copying or publication of this thesis for financial gain shall not be allowed without my written permission.

Department of Physics

The University of British Columbia
Vancouver, Canada

Date March 5 1989

DE-6 (2/88)

Abstract

External electric and magnetic fields affect the orientation of liquid crystal molecules. Several aspects of these effects have been studied in the liquid crystal 4-n-pentyl-4′-cyanobiphenyl (5CB) with special attention focused on geometries where one field is applied along the direction of initial orientation and a second field is applied perpendicular to this direction to break the uniaxial symmetry of the sample.

Preliminary studies involved measuring the magnetic susceptibility of a nematic liquid crystal; for the first time, these measurements were made with a SQUID magnetometer. Details of the nematic ordering in 5CB over the temperature range of 15-40°C and in a magnetic field of 0.060T have been deduced from these measurements.

The influence of fields on molecular ordering has been studied theoretically by extending Maier Saupe mean field theory to include two fields. The influence of fields on fluctuations of the nematic director has been studied using continuum theory. These studies show that the effect of fields on fluctuations of the nematic director should dominate the experimental observations. Optical measurements are reported which demonstrate for the first time that a biaxial nematic phase can be induced by applying two fields to a sample with positive susceptibility anisotropies. This biaxial phase was studied in 5CB at 33.4°C for magnetic fields between .08-.42T and electric fields between 0-6x10^4V/m. The results agree with those predicted from fluctuation theory.

As the magnitude of the symmetry breaking field is increased, a transition to an elastically deformed state takes place; this Freedericksz transition is usually second order. Theory and measurements are reported here which show for the first time that this transition can be first order in a number of geometries for the liquid crystal 5CB. In conjunction with these measurements, a novel modulated phase has been observed.

This appears to be a stable, equilibrium phase in which the director remains in the plane defined by the initial alignment and the distorting field. Experimental investigations of this phase are presented and a simple model is proposed which predicts this behavior.

Table of Contents

Abstract ii

List of Tables vi

List of Figures vii

List of Symbols ix

Acknowledgements xi

1. Introduction 1

2. Magnetic Susceptibility of Liquid Crystals

2-1 Theory 8

2-2 Measurements of the diamagnetic susceptibility of 5CB using a SQUID magnetometer 11

2-3 Results and discussion 14

3. Field Induced Order

3-1 Molecular field theory

i) Field effects on orientational order 18

ii) Effects on bulk properties 30

3-2 Continuum theory

i) Field effects on fluctuation amplitudes 34

ii) Effects of fluctuations on bulk properties 41

3-3 Measurements of field induced biaxiality

i) Summary of previous experiments 44

ii) Experimental details 48

iii) Results 55

4. Freedericksz Transitions

4-1 Theory

i) Overview 61

ii) Introduction 63

iii) Landau theory 68

iv) Exact solution 72

4-2 Experimental details 76

4-3 Experimental results 79

5. Modulated Phases

5-1 Summary of modulated phases in nematics 89

5-2 Experimental results and discussion 95

5-3 Theory 103

6. Conclusions 108

Bibliography 110

Appendix A 114

Appendix B 119

List of Tables

I. Summary of experiments investigating the effects of fields on director fluctuations. 45

II. Free energy terms for geometries 1-6. 67

III. Coefficients of the Landau expansion for geometries 1-6. 71

IV. Comparison of theoretical and experimental data for the electric field induced bend and twist Freedericksz transitions. 82

List of Figures

1. Schematics of various liquid crystal phases. 2
2. Deformation modes possible in a nematic liquid crystal. 7
3. Magnetic susceptibility $\Delta\chi$ of the liquid crystal 5CB. 15
4. Order parameters Q and P and free energy F for e=0 and various values of h. 24
5. Phase diagram along the line e=0. 25
6. Order parameters Q and P and free energy F for e=h and various values of h. 27
7. Projection of the phase diagram onto the e-h plane. 28
8. Three dimensional plot of phase diagram. 29
9. Diagram of apparatus used to study electric field induced biaxiality. 49
10. Schematic diagram of temperature control apparatus. 52
11. Intensity transmitted by the sample between crossed polarizers. 56
12. Change in threshold with increasing magnetic field. 58
13. Increase of the transmitted light below Freedericksz transition due to fluctuation enhancement by the electric field. 59
14. Increase of the transmitted light below Freedericksz transition due to fluctuation enhancement by the electric field for several values of stabilizing magnetic field. 60
15. Six possible geometries for Freedericksz transitions. 64
16. Capacitance, order parameter and dimensionless free energy for the electric field induced bend transition as a funtion of 1/e. 74
17. Phase diagram for the electric field induced bend transition as calculated from theory for u=.56 and k=.14. 75
18. Diagram of apparatus used to study Freedericksz transitions. 77
19. Experimental results for the magnetic field induced bend transition. 80

20. Experimental results for the electric field induced bend transition. 81

21. Experimental results for the electric field induced twist transition at various ramping speeds. 83

22. Threshold voltage as a function of magnetic field for the electric field induced bend transition. 87

23. Cell geometry for observation of Williams domains. 91

24. Photographs of modulated phase. 96

25. Frequency dependence of threshold voltage for electric field induced bend Freedericksz transition. 98

26. Frequency dependence of threshold voltage for Williams domains. 100

27. Effect of magnetic field on inverse wavelength. 101

28. Dependence of θ_m, the free energy due to the deformation and the wavenumber q of the deformation of the voltage parameter e. 107

List of Symbols

$\underline{\underline{\alpha}}$	molecular polarizability
$\underline{B}$	magnetic induction
β	$(k_B T)^{-1}$
C	capacitance of cell
χ	diamagnetic susceptibility
$\underline{D}$	electric displacement vector
δ	optical phase difference
e	electric field parameter
ε	pseudopotential
$\underline{\underline{\epsilon}}$	dielectric susceptibility
$\underline{E}$	electric field
F	free energy density
$\mathbb{F}$	free energy
$\underline{F}$	average local field
$\underline{F}_i$	local field seen by i^{th} molecule
γ	anisotropy of elastic constants $1 - \frac{K_3}{K_1}$
h	magnetic field parameter
$\underline{H}$	magnetic field
I	intensity
K	average elastic constant
K_1	splay elastic constant
K_2	twist elastic constant
K_3	bend elastic constant
$\underline{\underline{\kappa}}$	molecular magnetic susceptibility
κ	anisotropy of elastic constants $1 - \frac{K_1}{K_3}$
$\hat{l}$	unit vector along the symmetry axis of the molecule
λ	wavelength
$\underline{M}$	magnetization
$\underline{\mu}$	molecular magnetic moment
N	refractive index
$\hat{n}$	director
$\underline{q}$	wavenumber of director fluctuation
$\underline{P}$	polarization
ρ	density
ρ_n	number density
$\underline{\underline{S}}$	order parameter tensor

T	temperature	
θ_m	maximum deformation angle of cell	
u	anisotropy of dielectric constants	$\frac{\epsilon_{\parallel}-\epsilon_{\perp}}{\epsilon_{\parallel}}$
V	volume	
$\mathbb{V}$	voltage	
$\mathbb{V}_{min}$	lower stability limit	
$\mathbb{V}_{th}$	threshold voltage	
$\mathbb{V}^*$	upper stability limit	
w	anisotropy of dielectric constants	$\frac{\epsilon_{\parallel}-\epsilon_{\perp}}{\epsilon_{\perp}}$
$W(\theta)$	anchoring potential per unit area	

Acknowledgements

I would like to thank my advisor, Peter Palffy-Muhoray, for his seemingly unlimited patience and guidance throughout my PhD program. I have learned a great deal from him during these years, especially on the topics of how to think about physics and of how to persist through all difficulties. I hope that many students and collegues will have the first hand opportunity that I have had to experience his contagious enthusiasm for natural phenomena.

I would also like to thank my parents for encouraging me to pursue a career that I feel I will continue to enjoy for many years to come. They offer a constant source of support for my many pursuits.

I would like to record my appreciation of the flexibility exhibited by the University of British Columbia and the Liquid Crystal Institute at Kent State University in allowing me to complete my research at the LCI. It is hard to imagine how this thesis would have turned out if I had been unable to move to Kent.

It is hard to do justice in such a small space to all of the friends and collegues who have helped make my years as a graduate student so fun and interesting. I would just like to say that I have appreciated their help and company through this time and look forward to future interactions.

Chapter 1: Introduction

Liquid crystals are primarily liquids but also share properties of crystalline materials [see, for example, de Gennes, 1974]. Usually, liquids are characterized by isotropic macroscopic properties and by the ability to flow while crystals are characterized by long range positional order which leads to anisotropic macroscopic properties. Like liquids, liquid crystals exhibit fluidity. They are made up of organic molecules characterized by anisotropic molecular properties and by short range molecular interactions which couple over many molecular diameters to produce long range orientational order. These characteristics result in anisotropic macroscopic properties as seen in the diamagnetic and dielectric susceptibilities and in optical birefringence.

There are several types of liquid crystalline order which lead to a variety of phases. Schematics of a few of the most common phases are shown in Figure 1.

The nematic phase is the least ordered liquid crystalline phase, being characterized by only long range orientational order. It is usually a uniaxial phase in that macroscopic properties are different along the direction of order and perpendicular to that direction. The standard physicists' view of the nematic phase is a uniaxial phase formed from hard, rod-like molecules ordering like pencils in a drawer. More realistically, the molecules should be considered to be lath- or book- like and flexible. Theoretical considerations of book-shaped molecules lead to predictions of biaxial phases [Straley, 1974]. Biaxial nematic phases have been found experimentally in lyotropic [Yu and Saupe, 1980], thermotropic polymer [Hessel and Finkelmann, 1986] and recently thermotropic monomeric systems [Malthete et al., 1986].

Most of the other liquid crystal phases are smectics: as well as possessing long range orientational order these phases are characterized by varying degrees of positional order - the molecules organize themselves in layers and can even have order within the

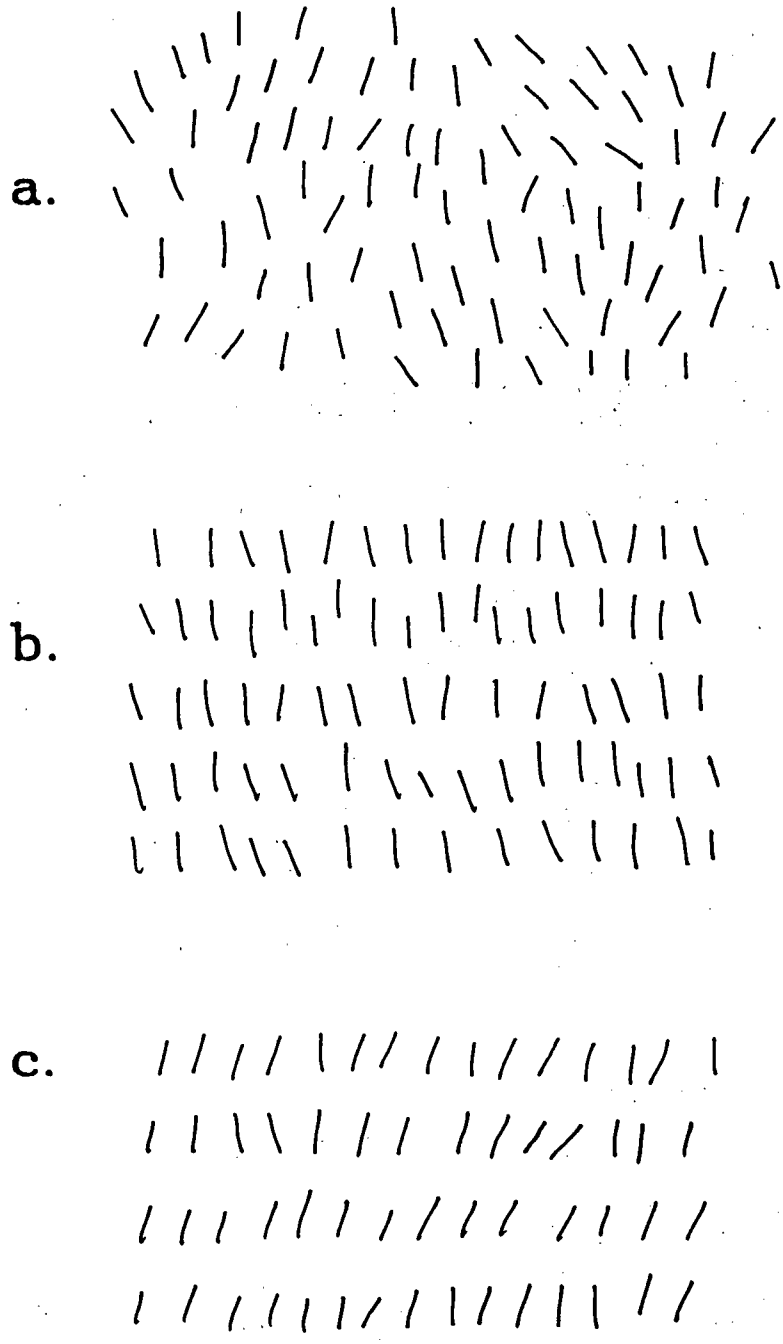

Fig. 1. Schematics of various liquid crystal phases. a) nematic, b) smectic A and c) smectic C. Each rod depicts the average direction of molecular orientation in the surrounding region.

layers, for example the hexatic phases where the in-plane ordering is hexagonal. Some of these phases are biaxial; here macroscopic properties described by second rank tensors are characterized by three components. This is the case for the tilted smectics where the director lies at an angle of 10-25 degrees to the axis perpendicular to the planes of the molecules.

Transitions between liquid crystal phases are the result of several mechanisms. In thermotropic liquid crystals, transitions occur from phases of lower to higher symmetry as the temperature is increased. In lyotropic liquid crystals, these transitions occur primarily as the concentration of rod-like aggregates in a liquid substrate is decreased.

The main concern of this thesis will be with nematic liquid crystals, in particular the effect of external fields on these systems. For theoretical purposes, the molecules will be considered be to uniaxial. In the nematic phase, molecules tend to align with partial ordering of their symmetry axes. This ordering can be described by an order parameter tensor $\underline{\underline{S}}$ where

$$S_{\alpha\beta} = \frac{1}{2} < 3\, l_\alpha l_\beta - \delta_{\alpha\beta} > \qquad [1.1]$$

where $\hat{l}$ is a unit vector along the symmetry axis of the molecule and the brackets $< >$ denote a volume average. In the principal axis frame, $\underline{\underline{S}}$ is diagonal and the order of a uniaxial phase can be described by the largest eigenvalue of the tensor. The frame is usually chosen so that this is the z component, so that the order is described by S_{zz} where

$$S_{zz} = S = \frac{1}{2} < 3\, \cos^2\theta - 1 >. \qquad [1.2]$$

Here θ is the angle between the cylindrical axis of the molecule and the eigenvector associated with the largest eigenvalue and the average is taken over available configurations. This definition has the property that if there is no orientational order and the system is isotropic, $S = 0$, while when the order is complete and all the molecules line up along the same axis, $S = 1$. The eigenvector associated with the

largest eigenvalue of $\underline{\underline{S}}$ in the principal axis frame is defined to be the director. In principle, the director can vary in space and time, though in a well aligned sample, the variations of the director will be small. To take these fluctuations into account, the order of the system in the lab frame is represented by the matrix

$$S_{\alpha\beta}(\underline{r}) = \frac{1}{2}\, S(\underline{r})\, [\, 3\, \hat{n}_\alpha(\underline{r})\, \hat{n}_\beta(\underline{r}) - \delta_{\alpha\beta}\,] \qquad [1.3]$$

where $\hat{\underline{n}}(\underline{r})$ is a unit vector along the director at a point $\underline{r}$ in the fluid. The directions $\hat{\underline{n}}(\underline{r})$ and $-\hat{\underline{n}}(\underline{r})$ are equivalent. The molecular order parameter is given by

$$S(\underline{r}) = \frac{1}{2} < 3\cos^2\theta - 1 >_{V(\underline{r})} \qquad [1.4]$$

and the average is taken over a volume $V(\underline{r})$ small compared to the wavelength of the director deformations.

The most important properties of liquid crystal phases, at least from a technological point of view, are related to their response to external electric and magnetic fields. External fields affect the liquid crystal by changing both the local ordering of the molecules and the thermal fluctuations of the director. These changes affect the properties of the bulk sample. Several aspects of these phenomena, particularly those related to the nematic phase, will be considered in this thesis.

Theory and measurement of the magnetic susceptibility will be discussed in the second chapter. The determination of the susceptibility of liquid crystals to applied fields is a fundamental problem in the study of these materials for several reasons. Firstly, the order parameter of the sample can in principle be determined by analyzing measurements of any second rank tensor property of the bulk material. Secondly, most applications of liquid crystals depend on their response to applied fields, and as this response is partly determined by the susceptibility anisotropy, knowledge of the susceptibility is of practical interest. In addition, information about the susceptibility anisotropies is sometimes necessary for the determination of other physical parameters, such as the elastic constants. One of the early projects of this thesis work involved the measurement of the magnetic susceptibility of a nematic liquid crystal with a SQUID

(Superconducting QUantum Interference Device) magnetometer. SQUID magnetometers had not been used previously in the measurement of magnetic properties of liquid crystals and the intrinsic sensitivity of the SQUID suggested that a more accurate measure of the order parameter might be obtained by using this method. This work was further motivated by the fact that magnetic susceptibility measurements are the easiest to relate to the order parameter. While the results for dielectric properties are difficult to analyze due to local field effects, the order parameter can be accurately determined from magnetic susceptibility measurements because the small magnetic susceptibility of liquid crystals makes the inclusion of local field corrections unnecessary in the analysis of the data.

The second aspect of the influence of fields on nematic liquid crystals studied was the effect of fields on the nematic order, particularly where fields were used to break the uniaxial symmetry of the sample. As a precursor to the experimental work, theoretical investigations were carried out to extend existing theories to the case of two fields. There are two contributions to the order of the bulk sample: (i) local orientational order of the molecules and (ii) fluctuations of the local order. Both of these are affected by external fields. The two contributions are usually considered separately; mean field theory can be used to discuss molecular ordering and continuum theory is used to discuss fluctuation effects. These theories are developed in Chapter 3. These two contributions affect different aspects of the macroscopic properties. Changing the orientational order of the molecules affects the average of the molecular polarizabilities and hence the macroscopic properties. The fluctuations of the director in a particular region of the sample change the principal axis frame of the anisotropic macroscopic properties in that region and so any change in the fluctuation spectrum will change the average properties for the sample. The magnitude and nature of the effects on the macroscopic properties are compared. In the last section of the chapter, other experiments investigating field induced order are discussed and finally, the experiments

performed for this thesis are described and the results are compared to theory.

External fields may compete with the elasticity of the bulk sample to influence the equilibrium distortions of the director. Distortions of the director may be viewed as being made up of the three principal modes shown in Figure 2. There are three elastic constants associated with the principal modes; the splay constant, K_1, the twist constant, K_2, and, the bend constant, K_3. Nematics can be distorted by competing boundary conditions and/or external fields. Boundary conditions are imposed by treating the container walls so that the molecules align at some specified direction to the walls. For example, conditions where the molecules are aligned to be perpendicular (homeotropic alignment), to be parallel (planar homogeneous alignment) or to be tilted with respect to the boundary can be obtained. If the fields are large enough to overcome the restraining elastic torques, bulk reorientation of the sample will occur. The fourth chapter deals with theory and experiment related to these phenomena, focusing on the effect of competing electric and magnetic fields.

The fifth chapter discusses a new modulated phase discovered in the course of the measurements described in Chapter 3. Phases where the director is modulated rather than uniform in space are not uncommon in the study of liquid crystals, and the various classes and mechanisms will be discussed. Theoretical and experimental characterization of the unique modulated phase discovered here will be described and related to previous results.

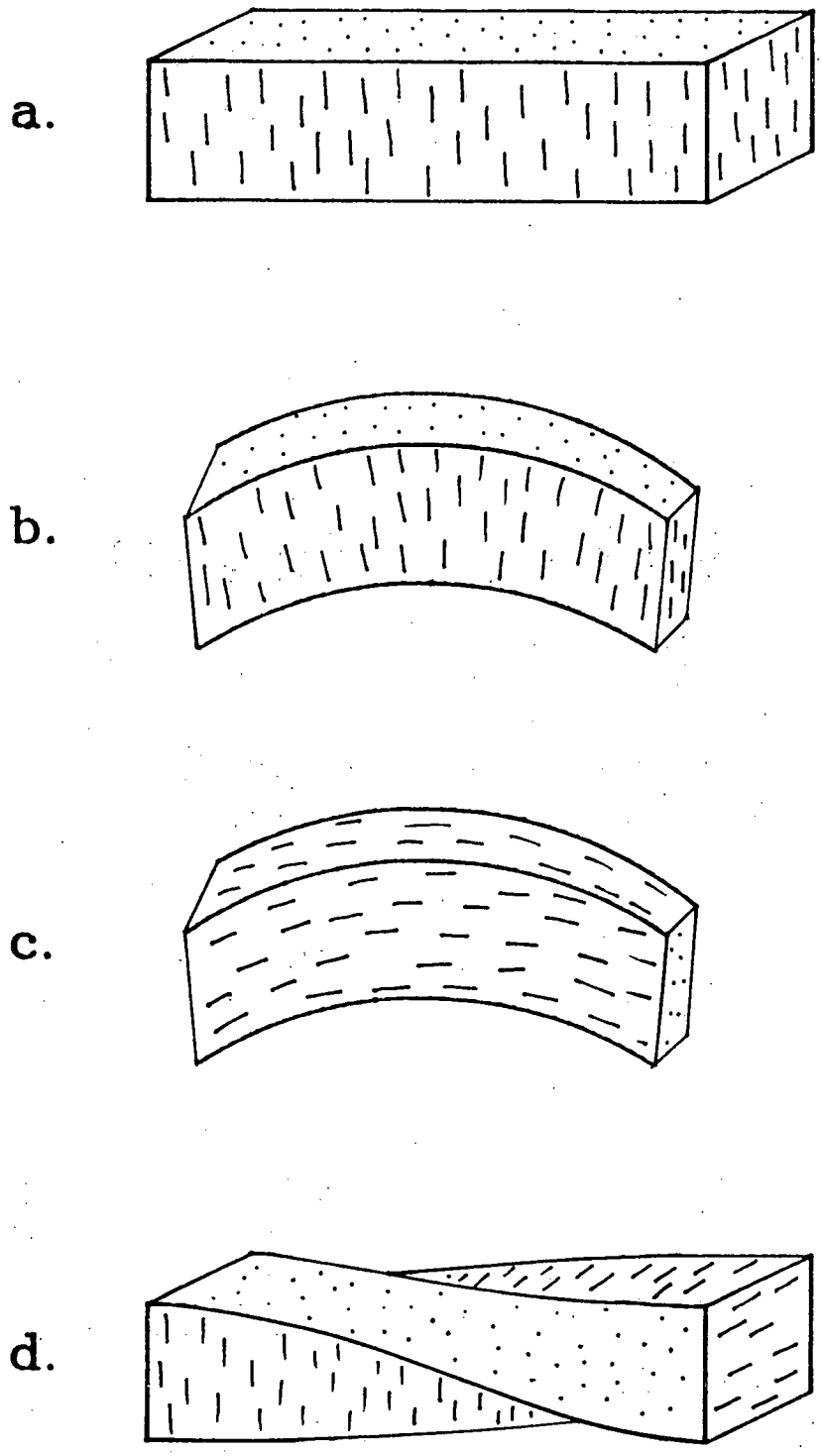

Fig. 2. Deformation modes possible in a nematic liquid crystal. a) undeformed state, b) splay mode, c) bend mode and d) twist mode.

Chapter 2: Magnetic Susceptibility of Liquid Crystals

2-1: Theory

Consider the effect of a magnetic field $\underline{H}$ on a nematic liquid crystal. The magnetic induction $\underline{B}$ is given by

$$\underline{B} = \mu_o (\underline{M} + \underline{H}) \qquad [2.1]$$

where $\underline{M}$ is the magnetization, $\underline{H}$ is the applied field and μ_o is the permitivity of free space. The magnetization is

$$M_\alpha = \chi_{\alpha\beta} H_\beta \qquad [2.2]$$

where $\chi_{\alpha\beta}$ are elements of the diamagnetic susceptibility tensor χ. In a uniaxial nematic liquid crystal with director along $\hat{z}$, this tensor is given by

$$\chi = \begin{bmatrix} \chi_\perp & 0 & 0 \\ 0 & \chi_\perp & 0 \\ 0 & 0 & \chi_{||} \end{bmatrix} \qquad [2.3]$$

where $\chi_\perp$ and $\chi_{||}$ are the components of χ perpendicular and parallel to the director. The average susceptibility is given by

$$\overline{\chi} = \frac{1}{3}\left[\chi_{||} + 2\chi_\perp\right] \qquad [2.4]$$

and the anisotropy of the suseptibility is defined as

$$\Delta\chi = \chi_{||} - \chi_\perp = \frac{3}{2}\left[\chi_{||} - \overline{\chi}\right]. \qquad [2.5]$$

It is interesting to note that while both $\chi_{||}$ and $\chi_\perp$ are negative, the anisotropy is positive for most liquid crystals. This is because the largest contribution to the molecular diamagnetism comes from the induced current carried by the delocalized electrons of the aromatic rings present in most liquid crystals. This makes a large negative contribution to the component of χ perpendicular to the director. Also note that here χ is a volume susceptibility; the mass susceptibility is related to the volume susceptibility through the density of the material ρ; $\chi^m = \chi/\rho$.

It is convenient to define the anisotropic part of the magnetic susceptibility

tensor,

$$Q_{\alpha\beta} = \chi_{\alpha\beta} - \frac{1}{3}\,\delta_{\alpha\beta}\,\chi_{\gamma\gamma}. \qquad [2.6]$$

This is a traceless, second rank tensor which will be zero in the isotropic phase. Interpretation of the anisotropic magnetic susceptibility in terms of the local microscopic order S as defined in Chapter 1 involves considering the relationship between microscopic and macroscopic susceptibilities. In the simplest case, the molecules are assumed to be uniaxial with components of the molecular magnetic susceptibility parallel ($\kappa_{||}$) and perpendicular ($\kappa_{\perp}$) to the long axis of the molecule. The $\hat{z}$ component of the molecular magnetic moment $\underline{\mu}$ induced by a field $\underline{H}$ acting along $\hat{z}$ of such a molecule oriented at an angle θ with respect to $\hat{z}$ is given by

$$\mu_Z = \kappa_{||}\,H\cos^2\theta + \kappa_{\perp}\,H\sin^2\theta. \qquad [2.7]$$

The average component of the magnetization per unit volume along $\hat{z}$ is then

$$M_Z = \rho_n <\mu_Z> = \rho_n\left[\,\overline{\kappa} + \frac{2}{3}\,\Delta\kappa <\frac{3}{2}\cos^2\theta - \frac{1}{2}>\right] H \qquad [2.8]$$

where ρ_n is the number density and $< >$ denotes an average over the sample volume. The susceptibility parallel to the director can be written

$$\chi_{||} = \rho_n\left[\,\overline{\kappa} + \frac{2}{3}\,\Delta\kappa\,S\,\right] \qquad [2.9]$$

where the molecular susceptibility anisotropy and the average molecular susceptibility are defined as

$$\Delta\kappa = \kappa_{||} - \kappa_{\perp} \quad \text{and} \quad \overline{\kappa} = \frac{\kappa_{||} + 2\kappa_{\perp}}{3}. \qquad [2.10]$$

Similarily, the magnetic moment of a molecule oriented at an angle θ with respect to $\hat{z}$ and ϕ with respect to $\hat{x}$, for $\underline{H}$ acting along $\hat{x}$, is

$$\mu_X = \kappa_{||}\,H\sin^2\phi\,\sin^2\theta + \kappa_{\perp}\,H\sin^2\phi\,\cos^2\theta. \qquad [2.11]$$

and so the average component of the magnetization per unit volume along $\hat{x}$ is

$$M_X = \rho_n\left[\,\overline{\kappa} - \frac{1}{3}\,\Delta\kappa <\frac{3}{2}\cos^2\theta - \frac{1}{2}>\right] H \qquad [2.12]$$

where the ϕ dependence averages out because the sample is cylindrically symmetric. The susceptibility perpendicular to the director can be written

$$\chi_{\perp} = \rho_n\left[\,\overline{\kappa} - \frac{1}{3}\,\Delta\kappa\,S\right]. \qquad [2.13]$$

Thus, for a uniaxial nematic made up of uniaxial molecules,

$$\overline{\chi} = \rho_n \, \overline{\kappa} \qquad [2.14]$$

$$\Delta\chi = \rho_n \, \Delta\kappa \, S. \qquad [2.15]$$

Then, the z component of the anisotropic part of the magnetic susceptibility tensor given by

$$Q_{zz} = \frac{2}{3} \, \Delta\chi = \frac{2}{3} \, \rho_n \, \Delta\kappa \, S \qquad [2.16]$$

is proportional to the order parameter of the nematic.

2-2: Measurements of the diamagnetic susceptibility of 4-n-pentyl-4′-cyanobiphenyl (5CB) using a SQUID Magnetometer

Measurements of the diamagnetic susceptibility are complicated by the fact that the susceptibility of liquid crystals is very small, typically $\Delta\chi \sim 10^{-6}$ MKS. A variety of sensitive techniques have been employed to measure this property. Most methods measure $\chi_{||}$ as they rely on the fact that a nematic sample placed in a strong magnetic field aligns along the field and will have a magnetization proportional to $\chi_{||}$. Measurements of $\overline{\chi}$ are made in the isotropic phase so that full information on $\Delta\chi$ can be obtained. The Faraday-Curie method [de Jeu and Claassen, 1978; Sherrell and Crellin, 1979] measures the magnetic force on a sample suspended in an inhomogeneous field. In this method, a small field gradient is present in the main, aligning field in the direction perpendicular to the director. The sample experiences a force in the direction of the field gradient proportional to the susceptibility; this force is measured with a sensitive balance. The Gouy balance method [Kneppe et al., 1982] measures the force on a cylindrical sample whose ends are placed in two uniform fields of different magnitude.

For this thesis, magnetic susceptibility has been measured with a SQUID (Superconducting QUantum Interference Device) system [Frisken et al., 1986]; here the magnetization induced in a sample by the stable, homogeneous field of a superconducting magnet is detected by a superconducting pick-up coil coupled to a SQUID magnetometer. It has been known for some time that SQUID devices offer the greatest potential for sensitive measurements of magnetic susceptibility, though there are practical challenges. SQUID devices operate at liquid helium temperatures while most liquid crystalline materials exhibit mesomorphic behavior near room temperature. The large temperature gradients necessitated by the close proximity of the sample and the superconducting pick-up coil make it difficult to achieve the full sensitivity inherent in a SQUID system. This general problem has been studied by Philo and Fairbank

[1977] among others.

The design of the SQUID susceptometer used was similar to that developed at Stanford [Philo and Fairbank, 1977; Day, 1972; Philo, 1977]. The system featured a direct access sample space which could be temperature controlled to within ±10 mK over the temperature range 100 K - 330 K. The temperature of the sample and the heat flow from the sample to the helium bath were controlled by a set of shields. A typical choice of shield operation temperature resulted in a helium loss rate of 12 l/day at a sample temperature of approximately 300 K. The temperature of these shields was regulated to ±10 mK to minimize contributions to the SQUID signal from temperature dependent paramagnetism of the shields. The sample magnetization was monitored by a pair of astatically wound superconducting pick-up coils which constituted the primary winding of the flux transformer. This was connected to a commercial SHE 330 SQUID system. A superconducting (NbTi) shield surrounding the pick-up coils and sample space stabilized the externally applied field and shielded out extraneous magnetic noise. The applied field was provided by a small superconducting magnet which was capable of producing fields up to 1 T, uniform to within ± 0.1% for a distance of 25 mm along the coil axis measured from the center of the coils. The maximum operating fields were limited to 0.1 T. Independent optical measurements showed that this field was sufficient to align the liquid crystal sample.

The liquid crystal sample used was 5CB or 4-n-pentyl-4′-cyanobiphenyl. This liquid crystal was used in all of the experiments discussed in this thesis. It is a simple liquid crystal in that it has only a nematic phase; homologues of this system with longer alkyl chains show smectic phases as well. It is frequently used by scientists investigating liquid crystal properties because it is chemically inert and longlived and has a nematic phase around room temperature. Also, its physical properties are well known, making it a suitable choice for the study of new phenomena as well as for the testing of new measurement techniques.

A portion of the sample material used in this experiment was obtained from BDH while the rest was synthesized by Dr. Gordon Bates at the University of British Columbia. The BDH sample was used without further purification. Approximately 200 mg samples were contained in 5 mm o.d. NMR tubes attached to quartz support rods. The sample assembly could be raised and lowered by a computer controlled servomotor and was contained in a helium atmosphere. At the beginning of each run, the sample tube was lowered and raised through the pick-up coil region at a fixed temperature and field, producing a signal as the sample tube passed through the coils. The signals produced by the astatic coils were opposite in polarity and the absolute susceptibility of the sample was obtained from this data. The accuracy of these results was limited by noise resulting from movement of the sample. Once the absolute susceptibility was obtained in this way, more accurate measurement of the relative susceptibility was made by holding the sample in one of the coils at a position of maximum signal and varying the temperature. With the sample in this position, it was heated above the nematic-isotropic transition temperature (35.3°C) in a field of 0.060 T. The sample was then cooled slowly in stages. At each stage the sample was equilibrated for at least 20 minutes; the output voltage of the SQUID system was monitored during this time. After reaching equilibrium, data were recorded every minute for a further ten minutes.

The instrument was calibrated using spectro grade benzene with a mass susceptibility of 8.82×10^{-9} m^3/kg [Handbook of Chemistry and Physics, 1970]. For a 273 mg sample of benzene in a field of 0.060 T, the flux appearing in the SQUID due to the sample corresponded to 54 flux quanta. Over a temperature range of 25°C, the susceptibility was found to be constant to within .02%. This represents the accuracy to which changes in the susceptibility could be measured in this apparatus. Absolute susceptibility (relative to benzene) could be determined to within 10%.

2-3: Results and Discussion

In the nematic phase of 5CB, the susceptibility tensor consists of two components, $\chi_{||}$ and $\chi_{\perp}$. The susceptibility anisotropy of 5CB is positive and the sample aligns with the director parallel to the magnetic field. The experimental configuration allowed for the measurement of susceptibility parallel to the field ($\chi_{||}$). Assuming that the molecular diamagnetic susceptibility is independent of temperature, the average mass susceptibility $\overline{\chi}^{m}$ is also independent of temperature and can be measured in the isotropic phase. Then $\Delta\chi$ can be determined from

$$\Delta\chi^{m} = \chi_{||}{}^{m} - \chi_{\perp}{}^{m} = \frac{3}{2}\left(\chi_{||}{}^{m} - \overline{\chi}_{iso}{}^{m} \right). \qquad [2.17]$$

The determination of $\Delta\chi^{m}$ requires corrections to be made for the temperature dependence of the susceptibility of the quartz sample tube. This was done by subtracting the signal due to the empty tube which was measured separately. It was also necessary to correct the data for a quasi-linear drift in the output ($< \frac{1}{4}$ flux quantum/hr) associated with the decrease in liquid helium level in the cryostat. The correction was calculated by a linear fit to the drift rate measured with the sample in thermal equilibrium.

The absolute value of the mass susceptibility in the isotropic phase was determined to be $8.37 \pm 0.08\text{x}10^{-9}$ m^3/kg. This differs by 1% from the value of $8.43\text{x}10^{-9}$ m^3/kg quoted by Sherrell and Crellin [1979]. This is well within the expected accuracy.

The results for the anisotropy of the susceptibility as a function of temperature are shown in Figure 3. Using the form of $\Delta\chi^{m}$ employed by Sherrell and Crellin [1979]

$$\Delta\chi^{m}(T) = A_o + A_1(T_{NI} - T)^{n} + A_2(T_{NI} - T) + A_3(T_{NI} - T)^{2} \qquad [2.18]$$

the results presented here can be compared to those of the above authors. A non-linear least squares fit of the data below the transition to this form gives $A_o = 8.338\text{x}10^{-10}$, $A_1 = 2.887\text{x}10^{-10}$, $A_2 = 6.510\text{x}10^{-11}$, $A_3 = 3.520\text{x}10^{-13}$ and $n = 0.63$ with $T_{NI} = 35.3°C$ where the results of Sherrell and Crellin [1979] are $T_{NI} = 35.7°C$, $A_o = 8.873\text{x}10^{-10}$

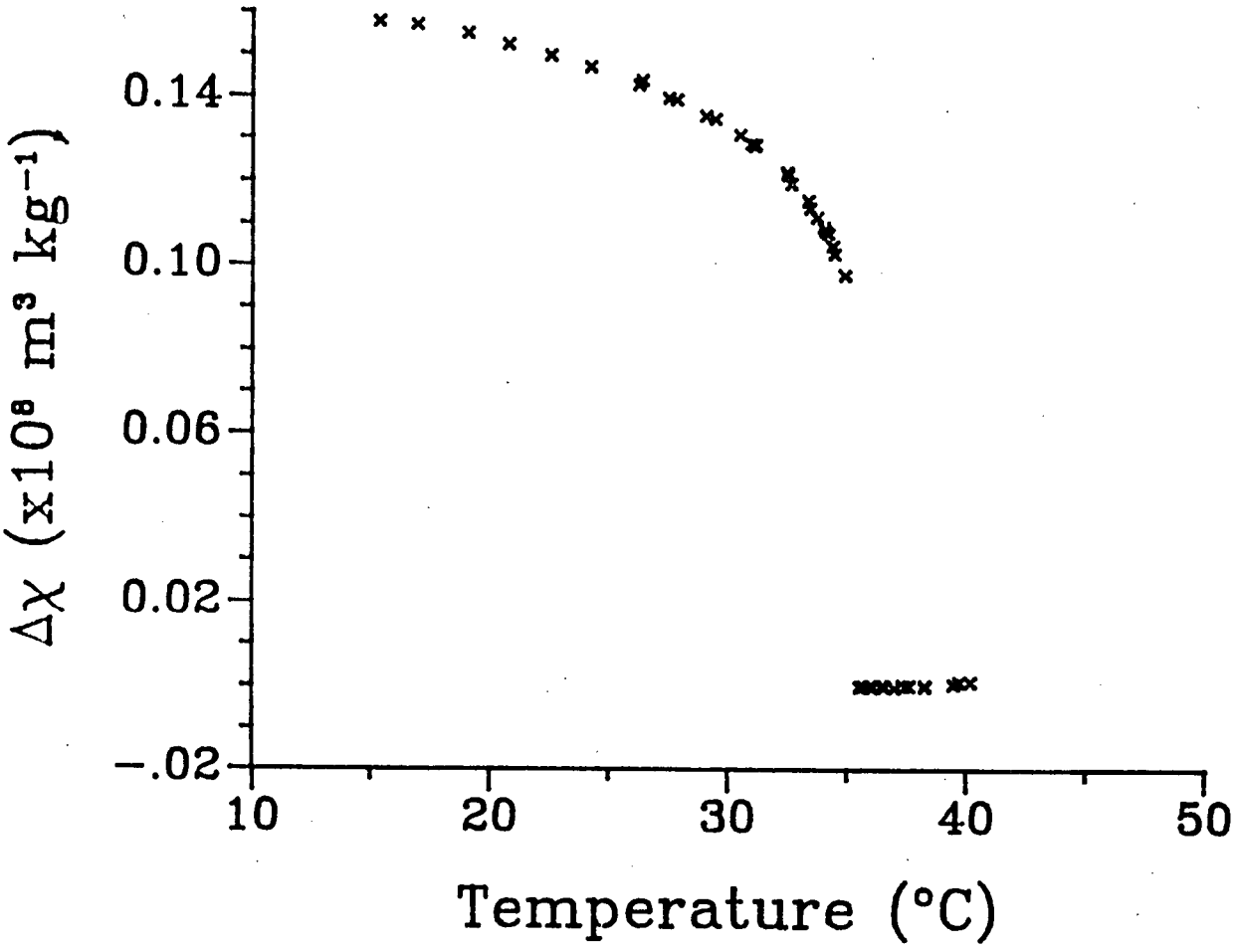

Fig. 3. Magnetic anisotropy $\Delta\chi$ of the liquid crystal 5CB (4-n-pentyl-4′-cyanobiphenyl).

m^3/kg, $A_1 = 3.414 \times 10^{-10}$ $m^3/kg/K^n$, $A_2 = 1.652 \times 10^{-10}$ $m^3/kg/K$, $A_3 = 7.277 \times 10^{-13}$ $m^3/kg/K^2$ and n = .7935. The data can also be compared to that of Buka and de Jeu [1982] if it is fit to an equation of the form

$$\Delta\chi^m(T) = \Delta\chi_o \left[1 - y \frac{T}{T_{NI}} \right]^z . \qquad [2.19]$$

Here, the best non-linear least squares fit provides values y=.9993, z=.1443 and $\Delta\chi_o = 2.36 \times 10^{-9}$ m^3/kg while Buka and de Jeu [1982] give values y=.9995, z=.141 and $\Delta\chi_o = 2.14 \times 10^{-9}$ m^3/kg with T_{NI} = 34.5°C. Chi-square χ^2 is 8.02×10^{-22} for the first fit and 1.68×10^{-21} for the second where

$$\chi^2 = \sum_i \frac{\left[y_i - y_f(x_i) \right]^2}{\sigma_i^2} . \qquad [2.20]$$

y_i are the data and y_f are the results of the fit to the data points. σ_i are the weighting factors of the data points. These are assumed to be equal to unity for all the data points. The temperature dependence of the measured anisotropy can be related to the order parameter through Eqn. [16].

The results shown in Figure 3 are comparable in accuracy to those obtained using more conventional techniques. This is in contrast to the four or five orders of magnitude of improvement which might be expected when using the SQUID technique [Philo, 1977b]. The accuracy of our results is limited by the low applied field, by noise and drift and by variations in the sample temperature. In the absence of field dependent noise, the sample magnetization and hence the SQUID sensitivity increases with applied field. Unfortunately, the apparatus used was originally designed for different experiments involving small applied fields. The theoretical limit on applied fields imposed by the Nb tubing shielding the pick-up coil leads was 0.15 T at the operating temperature of the shield. In practice, the Nb shield was effective only up to 0.06 T. In principle, the use of NbTi to shield the pick-up coil leads would allow the use of applied fields to at least as high as 5 T, but in practice, the full sensitivity implied by this field is difficult to attain. (For detailed discussion of the limitations

imposed by magnetic field noise, see Philo [1977b].) The range of improvement expected by increasing the applied field to 5 T is between one and two orders of magnitude, however, the extensive modifications required to change to NbTi shielding on the pick-up coils leads were not pursued. Noise and drift in the detected signal were due to many sources [Philo, 1977b], but the limiting factor appeared to be magnetic impurities in the aluminum form on which the SQUID pick-up coil was wound. This form contributed both to low temperature susceptibility noise and to drift due to temperature variations. Control of the temperature of the coil form was less effective (about 50 mK) than that employed by Philo [1977a, 1977b]. The temperature control of the sample was limited by the small sample space and the proximity of the helium bath. The sample space size was chosen to minimize liquid helium losses and to maximize the effectiveness of the shielding. With this experimental configuration, millidegree stability of the sample is obtainable but not the microdegree stability desired for detailed measurements close to the phase transition.

In summary, the sensitivity achieved in these measurements is comparable to that obtained by other techniques. Improvements to the apparatus should increase the sensitivity by about two orders of magnitude making it more sensitive than the Faraday-Curie and the Gouy balance techniques.

Chapter 3: Field Induced Order

3-1: Molecular Field Theory

3-1 (i): Field effects on orientational order

In the presence of two fields, the ordering will in general be biaxial, and two scalar order parameters which couple simultaneously to both fields will be required to describe the nematic ordering. Both the order of the nematic liquid crystal sample and the phase behavior of the system are affected by the presence of electric and magnetic fields [Frisken et al., 1987].

The effects of fields on molecular ordering can be described by two types of theories; both are mean field theories in that they ignore fluctuations. Previous theoretical work on biaxial phase behavior in the presence of external fields has mostly employed a phenomenological Landau-de Gennes expansion [Fan and Stephen, 1970; Priest, 1975; Keyes, 1978; Palffy-Muhoray and Dunmur, 1983; Gramsbergen et al., 1986]. Here the free energy of the system is expanded in terms of an order parameter with the addition of extra terms to describe the field energies. This type of expansion is complicated by two observations: that the expansion parameters may be field dependent [Palffy-Muhoray and Dunmur, 1983] and that the coefficients may take on different values in different regions of the phase diagram. Another problem with this approach is that the expansion is valid only for small values of the order parameter and thus may not provide an appropriate description of first order transitions. Alternatively, theories considering molecular interactions using a combination of attractive and repulsive potentials can be used to study the global features of the phase diagram. Various types of molecular statistical theories have been considered in discussions of liquid crystalline order, see for example Gelbart [1982].

We have used a molecular statistical model to describe the effect of fields on molecular ordering. The particular model used here is the Maier Saupe model [Maier

and Saupe, 1958; 1959; 1960]. This model, in spite of its simplicity, has been quite successful in describing the first order nematic-isotropic transition and has been extended to include the effect of a single field [Wojtowicz and Sheng, 1974] as well as other situations of interest to liquid crystals, for example binary mixtures [Palffy-Muhoray et al., 1985]. In this approach, the intermolecular interactions are replaced by an effective self-consistent pseudo-potential.

To expand the Maier Saupe theory to include the presence of external fields, we consider a nematic in the presence of an electric field $\underline{E}$ and a magnetic field $\underline{H}$. The molecules are assumed to be nonpolar and to have intermolecular interactions as well as electric and magnetic susceptibilities with cylindrical symmetry about the same axis. It can be shown that the general situation in which the fields are oriented in arbitrary directions is then equivalent to one in which one has a magnetic and an electric field oriented along two perpendicular axes. The free energy per molecule is written

$$F = - k_B T \ln z \qquad [3.1]$$

The partition function, z, can be expressed in terms of a single particle pseudopotential ε so that

$$z = \int d^2 l \exp(-\beta \varepsilon(\hat{l})) \qquad [3.2]$$

where $\beta = (k_B T)^{-1}$. $\hat{l}$ is a unit vector along the symmetry axis of the molecule and $d^2 l = d\Omega/4\pi = \sin\theta \, d\theta \, d\phi \, / \, 4\pi$. The pseudopotential is given by [Palffy-Muhoray et al., 1985]

$$\varepsilon(\hat{l}) = \rho\gamma - \frac{2}{3} \rho \, U \, S_{\alpha\beta} \left[\sigma_{\beta\alpha} - \frac{1}{2} S_{\beta\alpha}\right] - \frac{1}{2} D_{\alpha\beta} \, \sigma_{\beta\alpha} \qquad [3.3]$$

where γ is the isotropic liquid potential, ρ is the density and U represents the interaction strength. Summation over repeated Greek indices is assumed. The tensor order parameter is trace free and symmetric. It will be shown later to be given by the expression

$$S_{\alpha\beta} = \langle \sigma_{\alpha\beta} \rangle = \frac{1}{2} \langle 3 \, l_\alpha \, l_\beta - \delta_{\alpha\beta} \rangle. \qquad [3.4]$$

In the principal axis frame the order parameter has three components, S_{xx}, S_{yy} and

S_{ZZ}. It is convenient to define two new order parameters $Q = \langle q \rangle = \langle \sigma_{ZZ} \rangle$ and $P = \langle p \rangle = \langle \sigma_{XX} - \sigma_{YY} \rangle$, known as the uniaxial and the biaxial order parameters respectively. The order parameter tensor can now be written

$$\underline{\underline{S}} = \begin{bmatrix} -\frac{1}{2}(Q-P) & 0 & 0 \\ 0 & -\frac{1}{2}(Q+P) & 0 \\ 0 & 0 & Q \end{bmatrix}. \qquad [3.5]$$

The generalized tensor field $\underline{\underline{D}}$ is defined as

$$D_{\alpha\beta} = \frac{1}{3}\left[\Delta\kappa\, H_\alpha\, H_\beta + \Delta\alpha\, E_\alpha\, E_\beta\right] \qquad [3.6]$$

where E_α and H_α are cartesian components of the electric and magnetic fields, respectively. The molecular properties are assumed to be uniaxial; the anisotropies of the magnetic and electric molecular polarizabilities are given by

$$\Delta\kappa = \kappa_{\parallel} - \kappa_{\perp} \qquad \text{and} \qquad \Delta\alpha = \alpha_{\parallel} - \alpha_{\perp} \qquad [3.7]$$

where $\parallel$ and $\perp$ denote the components of the molecular susceptibility parallel and perpendicular to the long axis of the molecule.

The equilibrium free energy F_{eq} can be found by minimizing the trial free energy of Eqn. [3.1] with respect to $\underline{\underline{S}}$,

$$\frac{\partial F}{\partial S_{\alpha\beta}} = 0. \qquad [3.8]$$

This results in self-consistent equations for the components of $\underline{\underline{S}}$:

$$S_{\alpha\beta} = \frac{1}{Z}\int d^2l\, \sigma_{\alpha\beta} \exp\left(-\beta\varepsilon(\hat{l})\right) = \langle \sigma_{\alpha\beta} \rangle. \qquad [3.9]$$

An expression for the equilibrium free energy can then be obtained by substituting this solution for $\underline{\underline{S}}$ into Eqn. [3.1]. F_{eq} is then no longer a function of $\underline{\underline{S}}$ and in fact, it can be shown that $\underline{\underline{S}}$ is conjugate to $\underline{\underline{D}}$. This can be shown by differentiating F_{eq} with respect to $D_{\alpha\beta}$

$$\frac{\partial F_{eq}}{\partial D_{\alpha\beta}} = \frac{\partial F}{\partial D_{\alpha\beta}} + \frac{\partial F}{\partial S_{\gamma\delta}}\frac{\partial S_{\gamma\delta}}{\partial D_{\alpha\beta}} \qquad [3.10]$$

$$= \langle \sigma_{\alpha\beta} \rangle + 0$$

so that

$$\frac{\partial F_{eq}}{\partial D_{\alpha\beta}} = S_{\alpha\beta}\,.$$

There are two useful properties of $\underline{\underline{D}}$ that simplify the order parameter calculations. The first is that an arbitrary configuration of constant electric and magnetic fields is equivalent to a situation in which two fields are oriented along two perpendicular axis. To see this, consider the field tensor $\underline{\underline{D}}$ which is real and symmetric and therefore diagonizable. $\underline{\underline{D}}$ only enters the formalism through the term $D_{\alpha\beta}\sigma_{\beta\alpha}$ in the pseudopotential. In the principal axis frame for $\underline{\underline{D}}$, this term can be rewritten

$$D_{\alpha\beta}\sigma_{\beta\alpha} = D_{xx}\sigma_{xx} + D_{yy}\sigma_{yy} + D_{zz}\sigma_{zz}. \qquad [3.11]$$

Since $\underline{\underline{\sigma}}$ is traceless, an arbitrary term linear in Tr ($\underline{\underline{\sigma}}$) can be added to the field term,

$$D_{\alpha\beta}\sigma_{\beta\alpha} = D_{\alpha\beta}\sigma_{\beta\alpha} + a\,\delta_{\alpha\beta}\sigma_{\beta\alpha} \qquad [3.12]$$

where a is a constant. If a = $-D_{yy}$,

$$D_{\alpha\beta}\sigma_{\beta\alpha} = (D_{xx}-D_{yy})\sigma_{xx} + (D_{zz}-D_{yy})\sigma_{zz} \qquad [3.13]$$

and therefore the field term in the pseudopotential appears to involve only two fields oriented along two perpendicular axis. The two new field tensor components (D_{xx}-D_{yy}) and (D_{zz}-Dyy) will be functions of the original fields and the molecular anisotropies. Therefore, for a given non-orthogonal set of $\underline{E}$ and $\underline{H}$ fields, there always exists a set of orthogonal fields $\tilde{E}$ and $\tilde{H}$ which give the same tensor $D_{\alpha\beta}$ and thus the same free energy. Thus in studying the behavior of the liquid crystal on $\underline{\underline{D}}$ we need only look at orthogonal electric and magnetic fields. The second property involves the relationship between the principal axis frames for $\underline{\underline{D}}$ and $\underline{\underline{S}}$. The equilibrium free energy, F_{eq}, is a function only of the generalized field tensor $\underline{\underline{D}}$ and the temperature T. It contains scalar terms made up of the field tensor. There are only two such terms:

$$D_{\alpha\beta}D_{\beta\alpha} \quad \text{and} \quad D_{\alpha\beta}D_{\beta\gamma}D_{\gamma\alpha}. \qquad [3.14]$$

Since the order parameter is conjugate to the field tensor,

$$S_{\alpha\beta} = -\frac{\partial F_{eq}}{\partial D_{\alpha\beta}} \qquad [3.15]$$

so $\underline{\underline{S}}$ will contain terms like

$$D_{\beta\alpha} \quad \text{and} \quad D_{\beta\gamma}D_{\gamma\alpha}. \qquad [3.16]$$

In the principal axis frame for $\underline{\underline{D}}$, $\underline{\underline{D}}$ is diagonal and only the diagonal elements of $\underline{\underline{S}}$ will survive. Therefore, a principal axis frame for $\underline{\underline{D}}$ will also be a principal axis frame for $\underline{\underline{S}}$.

For special values of the fields degenerate situations may occur in which the order parameter is free to rotate about some axis at no energy cost.

Now consider the case where the magnetic field is applied along $\hat{z}$ and the electric field is applied along $\hat{x}$. In the principal axis frame, the pseudopotential becomes,

$$\varepsilon = -\rho\, U \left[Qq - \frac{1}{2} Q^2 + \frac{1}{3} \left(Pp - \frac{1}{2} P^2 \right) - hq + \frac{1}{2} e \left(q - p \right) \right] \qquad [3.17]$$

where the field parameters h and e are

$$h = \frac{\Delta\kappa\, H^2}{3\rho U} \qquad \text{and} \qquad e = \frac{\Delta\alpha\, E^2}{3\rho U}. \qquad [3.18]$$

Negative values of h and e correspond to negative susceptibility anisotropies.

Minimizing the free energy yields self-consistent equations for the average values of the order parameters

$$Q = \frac{1}{Z} \int d^2l\; q \exp\left(-\beta\varepsilon(\hat{l})\right) \qquad [3.19]$$

and

$$P = \frac{1}{Z} \int d^2l\; p \exp\left(-\beta\varepsilon(\hat{l})\right) .$$

Thus, the behavior of Q and P as a function of the three thermodynamic variables T, e and h can be determined. By expressing these equations in terms of integrals involving complex error functions and solving numerically using fixed point iteration for given values of the fields and the temperature, the order paramenters P and Q, the phase transition temperatures and the spinodal points can be calculated. Once the order parameters are known the corresponding free energy can be computed from [3.1]. The program used for these calculations is listed in Appendix A.

The calculations are simplified by the fact that the different regions of the e,h phase plane are symmetry related. It turns out that it is only necessary to compute the order parameters and the free energy for $0 \leq e \leq h$. Since the two fields in Eqn. [3.6] couple to the order parameters in the same way, the case $e > h$ can be handled by relabelling the electric and magnetic fields. In the case of a field with negative anisotropy parameters, we can use the fact that $\sigma_{\alpha\beta}$ is traceless to subtract a null term $b\delta_{\alpha\beta}\sigma_{\beta\alpha}$, where $\delta_{\alpha\beta}$ is the Kronecker symbol, from the pseudopotential given by Eqn.

[3.3]. If we choose b to be the largest of $-e$ or $-h$ we see that a field with negative anisotropy is equivalent to fields with positive anisotropy along the two perpendicular axis. Also, since the molecules are assumed to be nonpolar, positive and negative directions of the fields are equivalent. It is also important to note that there are equivalence relations between order parameters corresponding to a relabelling of the coordinate axes [Palffy-Muhoray et al., 1985].

The effect of a single field acting along the director of a material of positive susceptibility is well established [Wojtowicz and Sheng, 1974]. The first order isotropic-uniaxial nematic transition temperature increases with the field and ends at a critical point. The order parameters and the free energy for various values of h with e=0, reproducing results of Wojtowicz and Sheng [1974], were calculated from Eqn. [3.19] and [3.1] and are shown in Figure 4. Temperatures are given in units of the zero field nematic to isotropic transition temperature T_{NI}, while the free energy is given in units of $k_B T_{NI}$. The transition can be located by following the lowest free energy branch. Metastable states are expected between the transition and the spinodal points. As expected, the biaxial order parameter P is always zero.

The phase diagram for e=0 and both positive and negative h is shown in Figure 5. For positive h, the first order line ends in a critical point at h = .0097. For negative h, the first order line becomes a second order line at a tricritical point at h = −0.042. Accurate calculation of the tricritical point is made difficult by the fact that the free energy lines corresponding to different solutions have the same slope. The best method for calculation of the tricritical point calls for a series expansion in P of the free energy around the point; as knowledge of this value was not considered crucial for this work, this method was not pursued. As $h \to -\infty$ the ordering becomes two-dimensional as the director will be forced to lie in the plane perpendicular to the magnetic field, corresponding to $Q = -\frac{1}{2}$ when $\underline{H}$ is along z. At high temperatures the molecular symmetry axes will be distributed uniformly in this plane and the system will be

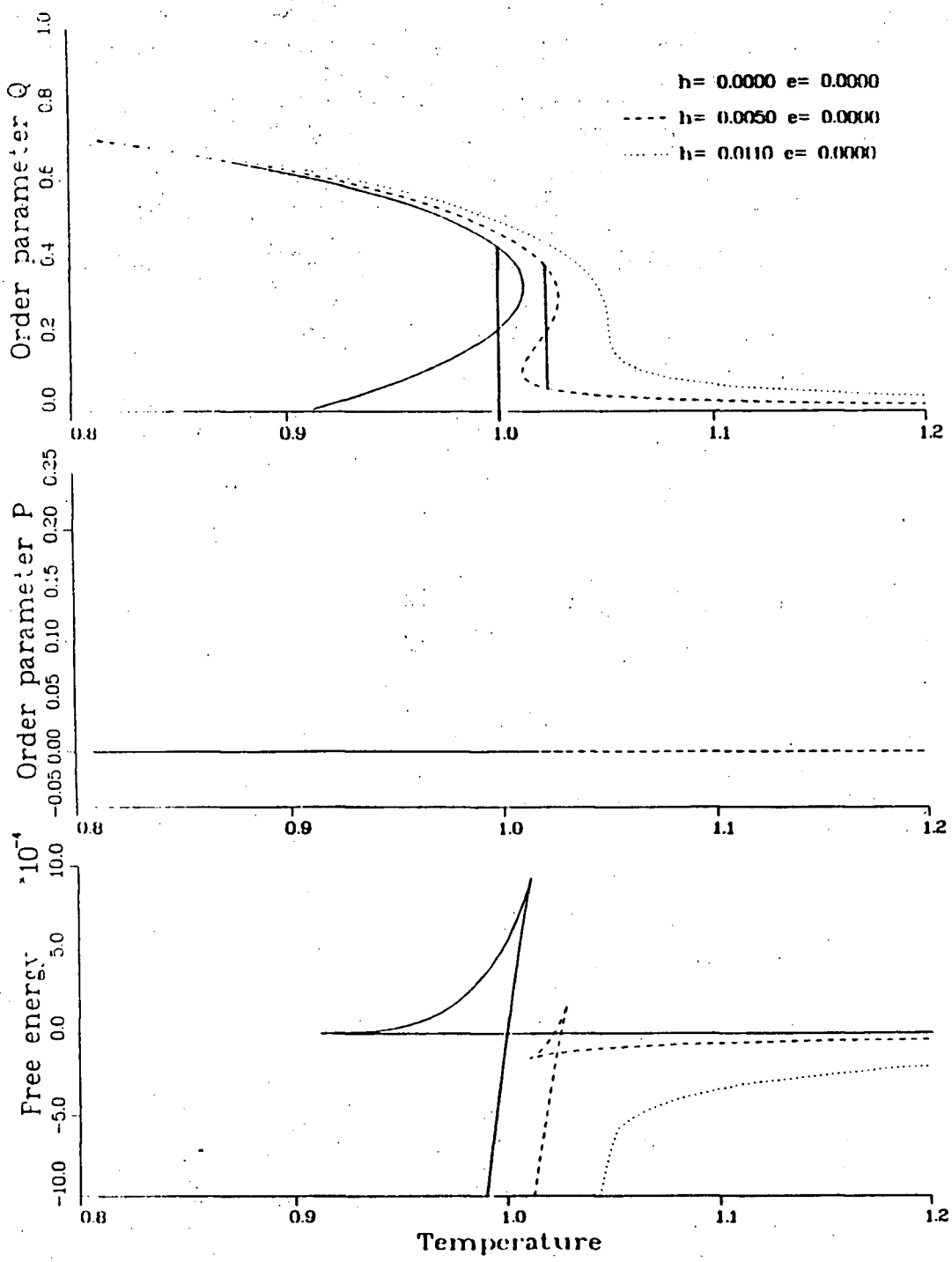

Fig. 4. Order parameters Q and P and free energy F for e=0 and various values of h. e $= \frac{\Delta\alpha\, E^2}{3\rho U}$ and $h = \frac{\Delta\kappa\, H^2}{3\rho U}$. The temperature is expressed in units of the nematic-isotropic transititon temperature T_{NI} and the free energy is expressed in units of $k_B T_{NI}$.

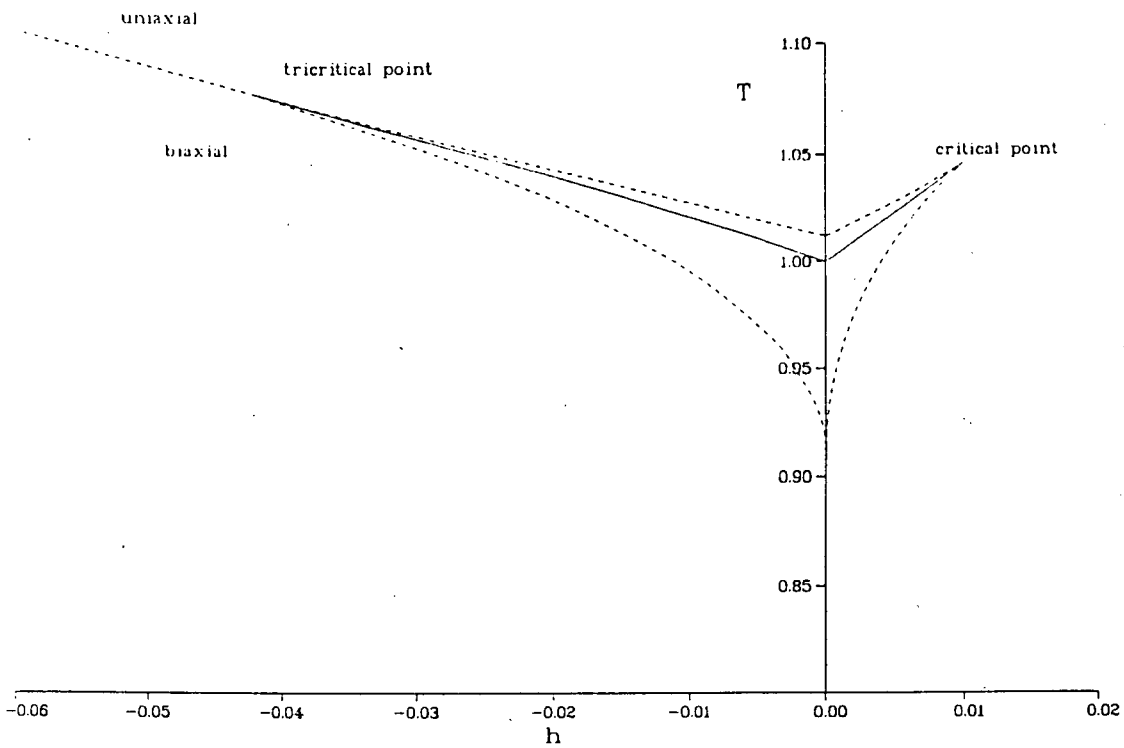

Fig. 5. Phase diagram along the line e=0. Solid lines represent first order transitions, dashed lines correspond to second order transtions, while dotted lines are spinodals. $e = \frac{\Delta\alpha\, E^2}{3\rho U}$, $h = \frac{\Delta\kappa\, H^2}{3\rho U}$ and T is in units of the nematic-isotropic transition temperature, T_{NI}.

uniaxial. At a certain temperature T_∞ there will be a symmetry breaking transition to a biaxial phase with $P \neq 0$. By expanding the free energy in P for $Q = -\frac{1}{2}$, T_∞ can be calculated to be 1.703. Numerical results show that the transition temperature approaches 1.703 monotonically from below; this result is different from that of the usual Landau approach [Palffy-Muhoray and Dunmur, 1983] where the transition temperature has a maximum for a finite field. The spinodals are shown as dotted lines.

To study the induced biaxiality, nonzero values of e are considered. Figure 6 shows the order parameter and the free energy for certain values of $h = e$. By symmetry this situation is equivalent to the case $h < 0$, $e = 0$ with h acting along y. The biaxial order parameter is a maximum at the nematic-isotropic transition and goes to zero as $Q \rightarrow 1$.

Figure 7 shows a projection of the phase diagram onto the e-h plane, with a three-dimensional plot of the phase diagram shown in Figure 8. The surface of first order transitions looks somewhat like an umbrella that has been turned inside out by the wind and with spokes in the $-e$,T and $-h$,T and e=h, T planes. In addition to the surface of first order transitions shown in Figure 8 there are three vertical sheets of transitions between two phases in which the biaxial order parameter P changes sign. There is neither latent heat nor spinodals associated with these transitions, which can take place continuously through a rotation in the x-y plane. The transition temperature T_{NI} has an absolute minimum T_{NI} for $e = h = 0$, and for small fields this temperature increases by an amount which is proportional to e or h (i.e. proportional to the field squared).

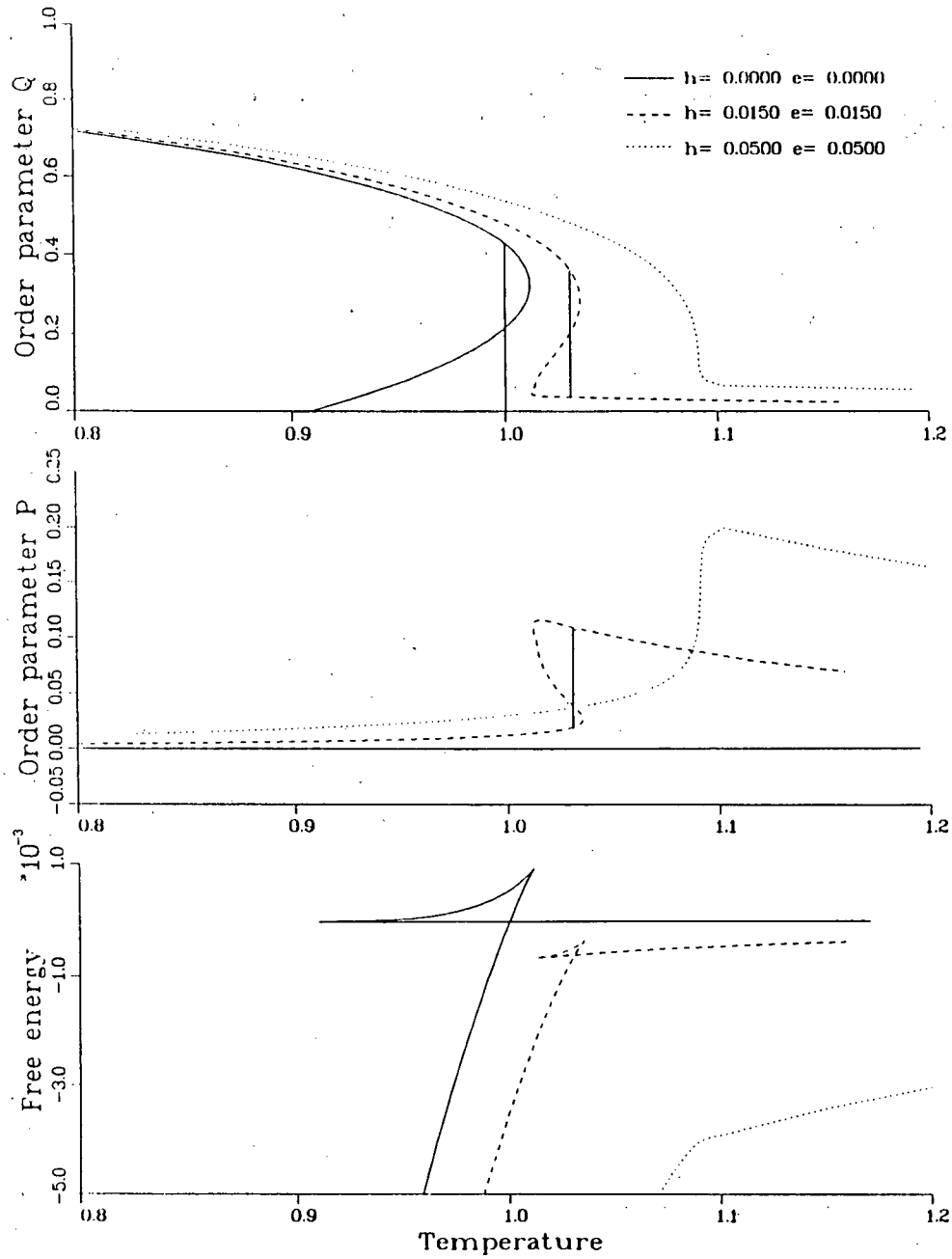

Fig. 6. Order parameters Q and P and free energy F for e=h and various values of h. e $= \frac{\Delta\alpha\, E^2}{3\rho U}$ and $h = \frac{\Delta\kappa\, H^2}{3\rho U}$. The temperature is expressed in units of the nematic-isotropic transititon temperature T_{NI} and the free energy is expressed in units of $k_B T_{NI}$.

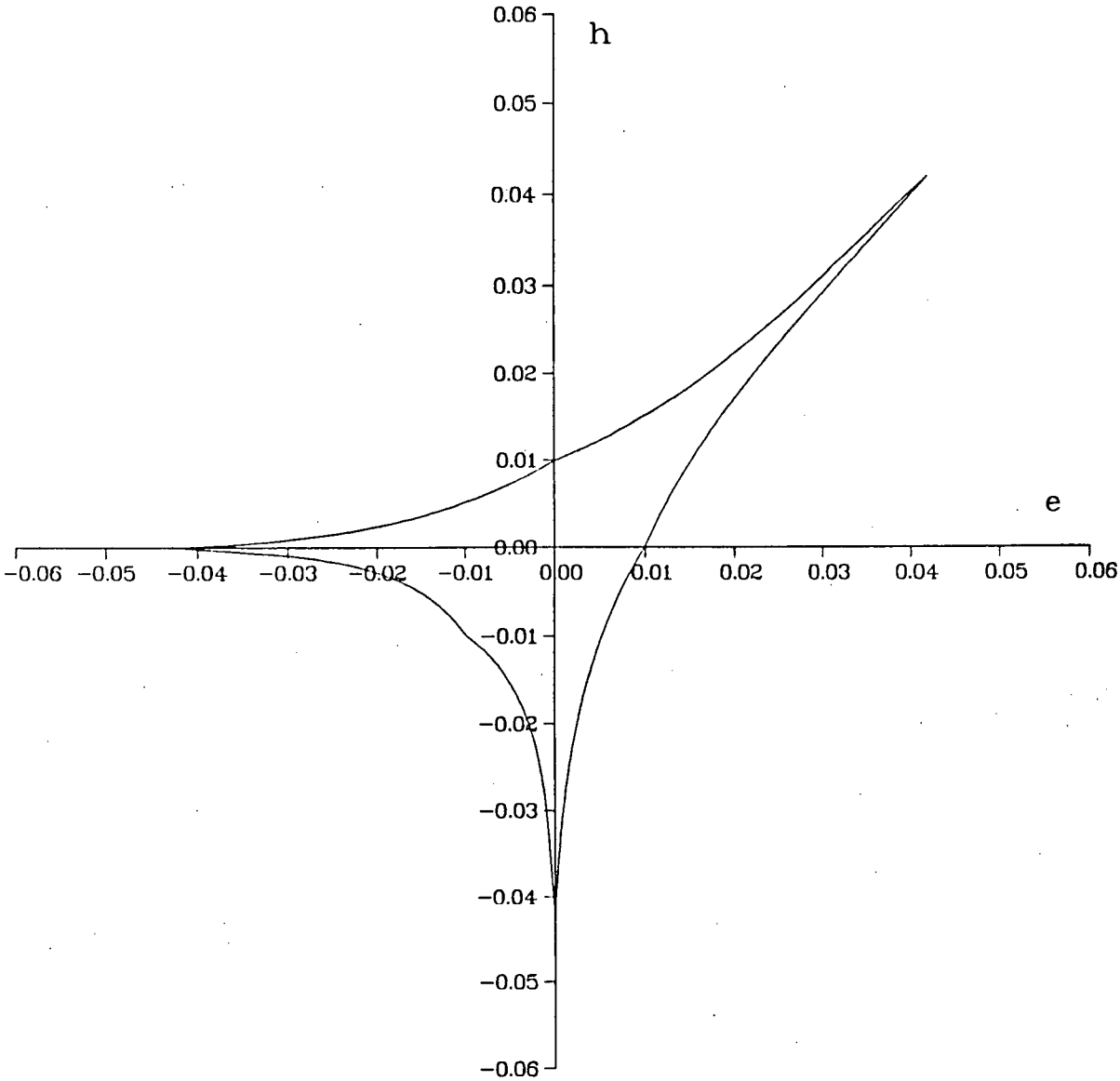

Fig. 7. Projection of the phase diagram on to the e-h plane. A surface of first order transitions is suspended between three symmetry related tricritical points and bounded by lines of ordinary critical points. $e = \frac{\Delta\alpha\, E^2}{3\rho U}$ and $h = \frac{\Delta\kappa\, H^2}{3\rho U}$.

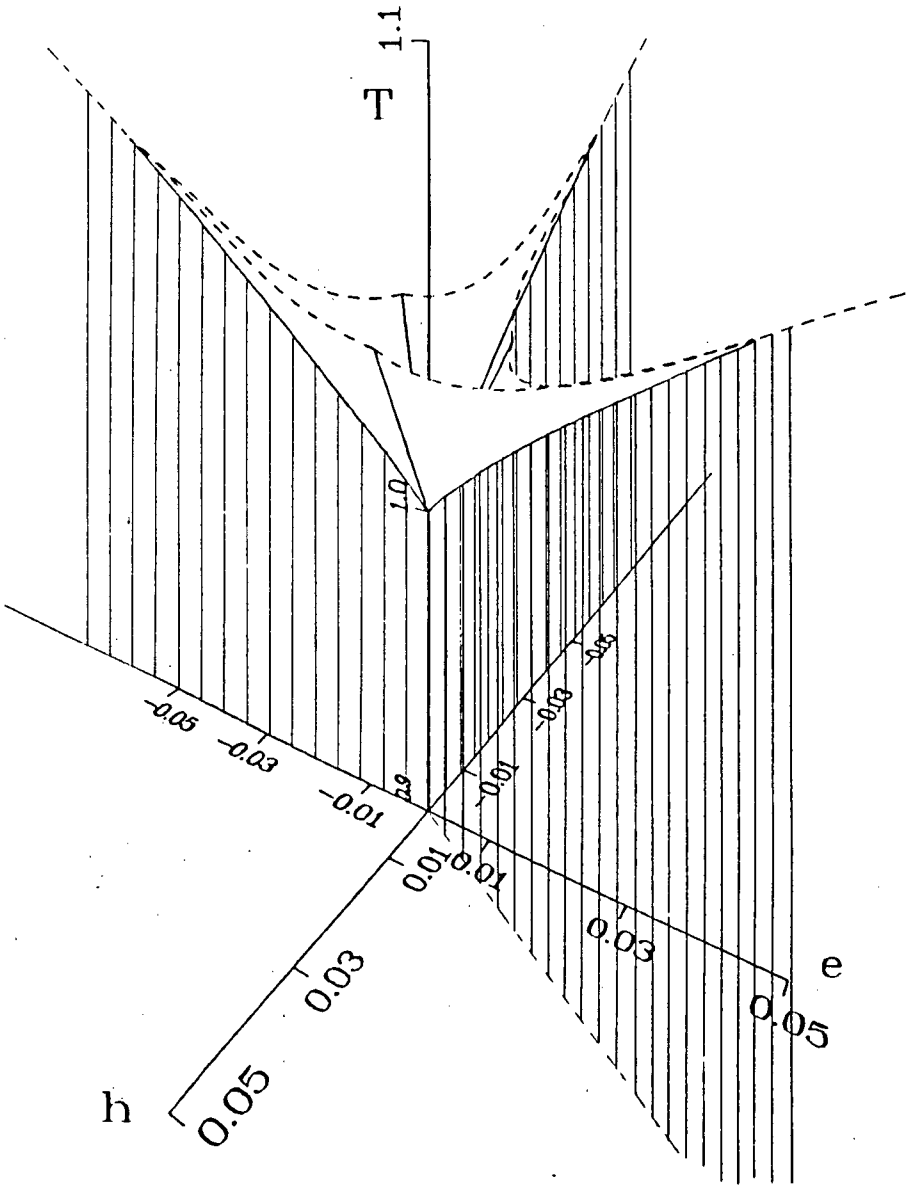

Fig. 8. Three dimensional plot of the phase diagram. $e = \frac{\Delta\alpha\ E^2}{3\rho U}$, $h = \frac{\Delta\kappa\ H^2}{3\rho U}$ and T is in units of the nematic-isotropic transition temperature, T_{NI}.

3-1 (ii): Effects on bulk properties

The fields needed to reach the critical or tricritical points are so large that the nature of these points cannot be investigated experimentally. For example, for 5CB where T_{NI} = 308 K, the ordinary critical point should occur at 1.045 T_{NI} = 322 K. With known [Frisken et al., 1986; Buka and Bata, 1986] values of the anisotropies $\Delta\chi$ and $\Delta\epsilon$, the critical field h=0.0097 would correspond to a magnetic field of 847 T or an electric field of 7.8x10^7 V/m. In the case of the tricritical point at h = e = 0.042, T = 1.078 T_{NI} = 332 K and the tricritical fields are 1765 T for the magnetic field and 1.62x10^8 V/m for the electric field.

It remains then to calculate how big an effect the induced biaxiality of the molecular ordering will have on measurable quantities. The induced biaxiality can be detected by measuring the change in birefringence of the sample with a laser incident along the axis of initial alignment of the sample placed between crossed polarizers. Birefringence is the macroscopic property which can be measured with the highest accuracy, measurements of changes of the birefringence of liquid crystal samples on the order of 10^{-7} have been reported [Malraison et al., 1980]. The birefringence of the sample is a bulk property and depends on both the molecular polarizability and the orientational order of the molecules.

When an electric field (such as that due to the incident laser beam) is present in the sample, the resulting electric displacement depends both on the applied electric field $\underline{E}$ and the polarization $\underline{P}$ of the system,

$$D_\beta = \epsilon_o E_\beta + P_\beta. \qquad [3.20]$$

The bulk dielectric tensor ϵ is defined

$$D_\beta = \epsilon_o \epsilon_{\beta\gamma} E_\gamma. \qquad [3.21]$$

Combining Eqn. [3.20] and Eqn. [3.21], an equation for the polarization can be obtained

$$P_\beta = \epsilon_o \left(\epsilon_{\beta\gamma} - \delta_{\beta\gamma}\right) E_\gamma. \qquad [3.22]$$

The polarization of the system has two sources: the permanent dipole moments

of the molecules and the molecular polarizability of the molecules. At optical frequencies, there is no contribution to the polarization from the permanent dipole moments. Then the polarization is due to the dipole moment induced by the local field $\underline{F}$ where the local field consists of the fields due to the dipole moments of the other molecules as well as the applied field. The dipole moment of the ith molecule $\underline{p}_i$ is

$$p_{i\beta} = \alpha_{\beta\gamma_L} F_{i\gamma} \qquad [3.23]$$

where $\underline{\underline{\alpha}}_L$ is the molecular polarizablility tensor in the lab frame and $\underline{F}_i$ is the local field seen by the ith particle. As with the case of the molecular magnetic susceptibility, the polarizability tensor in the molecular frame can be represented by a diagonal tensor

$$\underline{\underline{\alpha}}_M = \begin{bmatrix} \alpha_\perp & 0 & 0 \\ 0 & \alpha_\perp & 0 \\ 0 & 0 & \alpha_{||} \end{bmatrix} \qquad [3.24]$$

where $\alpha_\perp$ and $\alpha_{||}$ are the polarizabilities perpendicular and parallel to the symmetry axis of the uniaxial molecule. Transformation of the uniaxial molecular polarizability tensor to the lab frame involves the rotation matrix $\underline{\underline{T}}$ for two angles

$$\underline{\underline{T}} = \begin{bmatrix} \cos\phi\cos\theta & \sin\phi\cos\theta & -\sin\theta \\ -\sin\phi & \cos\phi & 0 \\ \cos\phi\sin\theta & \sin\phi\cos\theta & \cos\theta \end{bmatrix}. \qquad [3.25]$$

In the lab frame,

$$\underline{\underline{\alpha}}_L = \underline{\underline{T}}^{-1} \underline{\underline{\alpha}}_M \underline{\underline{T}} \qquad [3.26]$$

that is

$$\alpha_{\beta\gamma_L} = \bar{\alpha}_M \delta_{\beta\gamma} + \Delta\alpha_M [3\, l_{i\beta}\, l_{i\gamma} - \delta_{\beta\gamma}] \qquad [3.27]$$

where $\bar{\alpha}_M = \frac{1}{3}(\alpha_{||}+2\alpha_\perp)$ is the average polarizability, $\Delta\alpha_M = \frac{2}{3}(\alpha_{||}-\alpha_\perp)$ is the anisotropy of the molecular polarizability and $\hat{l}_i$ is the unit vector along the long axis of the ith molecule.

The polarization of the sample is then

$$\underline{P} = \rho_n < \underline{\underline{\alpha}}_L > \cdot \underline{F} = \rho_n [\, \bar{\alpha}\, \underline{\underline{I}} + \Delta\alpha \underline{\underline{S}} \,] \cdot \underline{F} \qquad [3.28]$$

where $\underline{\underline{I}}$ is the identity matrix, ρ_n is the number density, $\underline{\underline{S}}$ is the order parameter tensor defined in Eqn. [3.5] and $\underline{F}$ is the average local field. In deriving this relation, we have assumed a mean field view of the local field, that is, that the local field does not care about the orientation of the molecule so that the average over molecular orientation can be carried out independently of the average over $\underline{F}_i$.

Before continuing with considerations of the local field, it is worthwhile to summarize the extension of this derivation to the case of non-uniaxial molecules. In this case the polarizability tensor, as seen in the principal axis frame of the molecule, is written

$$\underline{\underline{\alpha}}_M = \begin{bmatrix} \alpha_1 & 0 & 0 \\ 0 & \alpha_2 & 0 \\ 0 & 0 & \alpha_3 \end{bmatrix}. \qquad [3.29]$$

Now the rotation matrix which will transform from the molecular frame to the lab frame will involve all three Euler angles. After averaging over all of the molecules in the sample, the anisotropic part of the polarizability tensor can be written [Bergersen et al., 1988]

$$\alpha_L = \frac{3}{2}(\alpha_3 - \overline{\alpha}) \begin{bmatrix} -\frac{1}{2}(Q-P) & 0 & 0 \\ 0 & -\frac{1}{2}(Q+P) & 0 \\ 0 & 0 & Q \end{bmatrix} + \frac{\alpha_1 - \alpha_2}{2} \begin{bmatrix} -\frac{1}{2}(D-C) & 0 & 0 \\ 0 & -\frac{1}{2}(D+C) & 0 \\ 0 & 0 & D \end{bmatrix} \qquad [3.30]$$

where in this case, there are four molecular order parameters (Q,P,D,C) which are given by

$$Q = \frac{1}{2}\langle 3L_{3z}^2 - 1\rangle \qquad [3.31]$$
$$P = \frac{3}{2}\langle L_{3x}^2 - L_{3y}^2\rangle$$
$$D = \frac{3}{2}\langle L_{1z}^2 - L_{2z}^2\rangle$$
$$C = \frac{3}{2}\langle L_{1x}^2 - L_{2x}^2 - L_{1y}^2 + L_{2y}^2\rangle.$$

$\hat{L}_i$ (i=1,2,3) are the vectors in the principal directions of the molecular polarizability. P and C are order parameters for the biaxial phase, while D is the contribution to the

uniaxial phase made by biaxial molecules. Even in a uniaxial phase, measurements of different macroscopic susceptibilities will reflect different linear combinations of the order parameters due to different molecular susceptibilities.

Calculation of the local field is a complicated problem. In principle, the calculation should sum the contributions of all of the induced dipoles as well as of the applied field, while, in practice, a variety of approximations have been used to simplify this problem. In order to obtain an order of magnitude estimate of the effect of molecular ordering on the birefringence, I will only consider the simplest model, proposed by Vuks [1966]. This assumes an isotropic form for the relation between the local and applied fields

$$\underline{F} = \frac{1}{3} (\bar{\epsilon} + 2) \underline{E}, \qquad [3.32]$$

where $\bar{\epsilon}$ is the average dielectric constant. Then the relation between the molecular polarizabilities and the dielectric constants can be written

$$\rho_n < \alpha_{ii_L} > = \frac{3\epsilon_o (\epsilon_{ii} - 1)}{(\bar{\epsilon} + 2)} . \qquad [3.33]$$

The refractive indicies N_i are simply related to the dielectric constants

$$N_i^2 = \epsilon_{ii}. \qquad [3.34]$$

For uniaxial molecules, the relation between the birefringence, the molecular polarizabilities and the biaxial order parameter is given by:

$$\Delta N = N_x - N_y \simeq \frac{\rho_n (\bar{\epsilon} + 2)}{3 \epsilon_o N_\perp} \Delta\alpha \, P \qquad [3.35]$$

For B = 0.44 T, E = 3×10^4 V/m, and using data from Dunmur and Tomes [1983], we find that $\Delta N = 3.7 \times 10^{-8}$, which should be just measurable with careful technique.

3-2: Continuum Theory

3-2 (i): Field effects on fluctuation amplitudes

In the continuum model, nematic liquid crystals are characterized by a director field $\hat{n}(\underline{r})$ which defines the local principal axis of some second rank tensor property. The director field exhibits thermal fluctuations which are opposed by elastic torques and which may be influenced by external magnetic and electric fields. The external fields couple to the director fluctuations via the anisotropic susceptibilities; for a material of positive susceptibility anisotropy, a field along the director will quench the fluctuations while one applied perpendicular to the director will enhance fluctuations parallel to the field. In the latter case, the uniaxial symmetry of the system is broken, and the sample becomes biaxial.

The amplitude of these fluctuations can be calculated by considering the effect of deformations of the director on the free energy developed for the continuum model by Frank [1958]. This calculation was first carried out by de Gennes [1968]. The derivation, extended to include two perpendicular fields, is outlined below.

Consider a sample with its average director along $\hat{z}$ with small variations of the director through the sample. These variations correspond to nonzero $\hat{x}$ and $\hat{y}$ components of the director; as the fluctuations are assumed to be small, $n_z >> n_x, n_y$. In the continuum model, the free energy density of the system due to elastic effects is

$$F_f = \frac{1}{2} K_1(\nabla\cdot\hat{n})^2 + \frac{1}{2} K_2(\hat{n}\cdot\nabla x\hat{n})^2 + \frac{1}{2} K_3(\hat{n}x\nabla x\hat{n})^2 \qquad [3.36]$$

where $\hat{n} = (\cos\phi\sin\theta, \sin\phi\sin\theta, \cos\theta)$, ϕ and θ are the azimuthal and polar angles, K_1, K_2 and K_3 are the splay, twist and bend elastic constants. Small fluctuations result in the elastic free energy increasing by an amount

$$\Delta F_f = \frac{1}{2}K_1(\partial_x n_x + \partial_y n_y)^2 + \frac{1}{2}K_2(\partial_y n_x - \partial_x n_y)^2 + \frac{1}{2}K_3\left[(\partial_z n_x)^2 + (\partial_z n_y)^2\right] \qquad [3.37]$$

where $\partial_i \Rightarrow \frac{\partial}{\partial i}$.

The experimental geometry under study makes use of a magnetic field $\underline{H}$ applied along the direction of initial alignment, $\hat{z}$, and of a voltage applied so as to result in an

electric field $\underline{E}$ (in the undistorted sample) perpendicular to this direction, say along $\hat{x}$. Because of the different magnitudes of the electric and magnetic susceptibility anisotropies, the two field energy terms have to be considered differently. In the case of the magnetic field, the susceptibility anisotropy is of the order of 10^{-6} MKS so that the magnetic field $\underline{H}$ and the magnetic induction $\underline{B}$ are essentially parallel. In the case of the electric field, the susceptibility anisotropy is of the order of 10 and the electric field $\underline{E}$ cannot be assumed to be parallel to $\underline{D}$.

The applied magnetic field results in a magnetization of the sample

$$M_\alpha = \chi_\perp H_\alpha + (\chi_{||} - \chi_\perp)\, n_\alpha n_\beta H_\beta$$

where $\chi_\perp$ and $\chi_{||}$ are the bulk susceptibilities transverse and parallel to the director. The free energy density due to the magnetic field is given by

$$F_m = -\frac{1}{2}\,\underline{B}\cdot\underline{H} \qquad [3.38]$$

with the magnetic induction given by

$$\underline{B} = \mu_o\,(\,\underline{H} + \underline{M}\,). \qquad [3.39]$$

The free energy density associated with the magnetic field is then

$$F_m = -\frac{1}{2}\,\mu_o\left[H^2+\underline{M}\cdot\underline{H}\right] = -\frac{1}{2}\,\mu_o\left[H^2 + \chi_\perp H^2 + (\,\chi_{||} - \chi_\perp)\,(\,\underline{H}\cdot\underline{n}\,)^2\right]. \qquad [3.40]$$

The orientation dependent part of the free energy density resulting from the action of a magnetic field applied along z in the presence of a small fluctuation is

$$\Delta F_m = \frac{1}{2}\,\frac{\Delta\chi B^2}{\mu_o}\,(n_x{}^2+n_y{}^2) = \frac{1}{2}\,h\,(n_x{}^2+n_y{}^2) \qquad [3.41]$$

where μ_o is the permeability of free space, $\underline{B} \simeq \mu_o\underline{H}$ is the magnetic induction and $\Delta\chi = \chi_{||} - \chi_\perp$.

The application of a voltage to electrodes parallel to the magnetic field results in an electric displacement $\underline{D}$

$$D_\alpha = \epsilon_o\epsilon_\perp E_\alpha + \epsilon_o(\epsilon_{||}-\epsilon_\perp)\, n_\alpha n_\beta E_\beta \qquad [3.42]$$

where ϵ_o is the permitivity of free space and $\epsilon_\perp$ and $\epsilon_{||}$ are the bulk dielectric susceptibilities transverse and parallel to the director. The sample volume is enclosed by one pair of metal surfaces, and two pairs of non-conducting surfaces. Assuming only

z dependence of $\underline{D}$ and $\underline{E}$, $\nabla\cdot\underline{D}=0$ implies that D_z is a constant and since the only charges are on the electrodes, $D_z=0$. By symmetry, $D_y=0$, as well. The set of equations [3.42] can then be written

$$D_x = \epsilon_o\epsilon_\perp E_x + \epsilon_o(\epsilon_{||}-\epsilon_\perp)(n_xE_x+n_yE_y+n_zE_z)\,n_x \qquad [3.43]$$
$$0 = \epsilon_o\epsilon_\perp E_y + \epsilon_o(\epsilon_{||}-\epsilon_\perp)(n_xE_x+n_yE_y+n_zE_z)\,n_y$$
$$0 = \epsilon_o\epsilon_\perp E_z + \epsilon_o(\epsilon_{||}-\epsilon_\perp)(n_xE_x+n_yE_y+n_zE_z)\,n_z.$$

For $n_y=0$, $E_y=0$. $\nabla x\underline{E}=0$, requires that E_x be a constant, in this case equal to $\mathbb{V}/d$, where $\mathbb{V}$ is the applied voltage and d is the spacing between the electrodes. Solving the equations above, we find that there is a z component to the electric field

$$E_z = -\frac{u\,n_xn_z\,E_x}{1-u\,n_x^2}. \qquad [3.44]$$

The x component of the displacement is given by

$$D_x = \frac{\epsilon_o\epsilon_\perp E_x}{1-u\,n_x^2} \qquad [3.45]$$

and the electric field contribution to the free energy density is

$$F_e = -\frac{1}{2}D_x\,E_x = -\frac{1}{2}\frac{\epsilon_o\epsilon_\perp E_x^2}{1-u\,n_x^2} \qquad [3.46]$$

where $u=\frac{\epsilon_{||}-\epsilon_\perp}{\epsilon_{||}}$. This form for the free energy due to a voltage applied parallel to the boundary planes was first derived by Arakelyan et al. [1984]. For small fluctuations, the corresponding change in the orientation dependent part of the free energy density is

$$\Delta F_e = -\frac{1}{2}\epsilon_o\epsilon_\perp u\,n_x^2\,E_x^2 = -\frac{1}{2}e\,n_x^2. \qquad [3.47]$$

Then the total change in the free energy averaged over the volume of the sample V is

$$\mathbb{F} = \int_V \Delta F = \int_V d^3r\,(\Delta F_f+\Delta F_m+\Delta F_e) \qquad [3.48]$$

Once the free energy is known, the probability of a particular director configuration occuring is given by

$$P(\hat{n}) = \frac{e^{-\beta\mathbb{F}(\hat{n})}}{\int d^2n'\,e^{-\beta\mathbb{F}(\hat{n}')}} \qquad [3.49]$$

where the integral is over all possible configurations.

Following Martinand and Durand [1972], the spatial variation of the director is expressed in terms of Fourier components

$$n_\alpha(\underline{r}) = \frac{1}{V} \sum_q n_\alpha(\underline{q}) \exp(-i\underline{q}\cdot\underline{r}) \qquad [3.50]$$

where

$$n_\alpha(\underline{q}) = \frac{1}{(2\pi)^3} \int_V d^3r\, n_\alpha(\underline{r}) \exp(i\underline{q}\cdot\underline{r}) \qquad [3.51]$$

Now the free energy can be expressed as a sum over q,

$$\mathbb{F}=\frac{1}{2V}\sum_q\{K_1(n_x q_x+n_y q_y)^2+K_2(n_x q_y-n_y q_x)^2+(K_3 q_z^2+h)(n_x^2+n_y^2)-e n_x^2\} \qquad [3.52]$$

With the goal of expressing the free energy in diagonal form, the summand can be written in the form $n_\alpha A_{\alpha\beta} n_\beta$ where

$$\underline{\underline{A}} = \begin{bmatrix} K_1 q_x^2+K_2 q_y^2+K_3 q_z^2+h-e & (K_1-K_2)q_x q_y \\ (K_1-K_2)q_x q_y & K_1 q_y^2+K_2 q_x^2+K_3 q_z^2+h \end{bmatrix} = \begin{bmatrix} a & b \\ b & c \end{bmatrix} \qquad [3.53]$$

The normal modes of the system are found by diagonalizing $\underline{\underline{A}}$ with a rotation transformation using the matrix $\underline{\underline{P}}$ where

$$\underline{\underline{P}} = \begin{bmatrix} \cos\gamma & -\sin\gamma \\ \sin\gamma & \cos\gamma \end{bmatrix} \qquad [3.54]$$

and

$$\cos\gamma = \sqrt{\frac{1}{2} - \frac{1}{2}\sqrt{\frac{(c-a)^2}{4b^2+(c-a)^2}}}\,. \qquad [3.55]$$

The eigenvalues are given by

$$\lambda_\pm = \frac{c+a}{2} \pm \frac{1}{2}\sqrt{4b^2+(c-a)^2} \qquad [3.56]$$

with eigenvectors

$$n_+ = \cos\gamma \cdot n_x + \sin\gamma \cdot n_y \qquad [3.57]$$

$$n_- = -\sin\gamma \cdot n_x + \cos\gamma \cdot n_y$$

Now the free energy can be written in quadratic form in terms of the amplitudes of the normal modes

$$\mathbb{F} = \frac{1}{2V} \sum_q \sum_\alpha n_\alpha^2\, \lambda_\alpha, \qquad \alpha = +,- \qquad [3.58]$$

Once the normal modes are known, the equipartition theorem can be used: for a classical system with free energy quadratic in the amplitudes $n_\alpha(\underline{q})$, the average energy per degree of freedom at thermal equilibrium is equal to $\frac{1}{2}\, k_B T$ so that the amplitudes of the normal modes can be expressed by

$$<n_\alpha{}^2(\underline{q})>_T = \frac{k_B TV}{\lambda_\alpha} \qquad [3.59]$$

The amplitudes of interest here will be the average value of the fluctuation amplitudes $<n_x{}^2+n_y{}^2>$ and the difference in the amplitudes $<n_x{}^2-n_y{}^2>$ where, in terms of the eigenvectors,

$$<n_x{}^2(\underline{q})+n_y{}^2(\underline{q})> = <n_1{}^2(\underline{q})+n_2{}^2(\underline{q})> = <n_1{}^2(\underline{q})>+<n_2{}^2(\underline{q})> \qquad [3.60]$$

$$<n_x{}^2(\underline{q})-n_y{}^2(\underline{q})> = <n_1{}^2(\underline{q})(\cos^2(\gamma)-\sin^2(\gamma))> - <n_2{}^2(\underline{q})(\cos^2(\gamma)-\sin^2(\gamma))>$$

for $<n_1 n_2> = 0$. If the amplitude difference is nonzero, the uniaxial symmetry of the sample is broken and the sample appears biaxial.

Solutions for these expressions for the amplitudes of the fluctuations can be found in three cases:

<u>case (i)</u>: E=0, one constant approximation (i.e. $K_1=K_2=K_3=K$)

In this case, $\lambda_+=\lambda_-=Kq^2+h$, where $q^2=q_x{}^2+q_y{}^2+q_z{}^2$ and

$$<n_x{}^2(\underline{q})+n_y{}^2(\underline{q})> = \frac{2k_B TV}{Kq^2+h} \qquad [3.61]$$

$$<n_x{}^2(\underline{q})-n_y{}^2(\underline{q})> = 0$$

These are the amplitudes in q-space. In r-space,

$$<n_x{}^2(\underline{r}) + n_y{}^2(\underline{r})> = \frac{1}{V}\sum_q <n_x{}^2(\underline{q}) + n_y{}^2(\underline{q})> \qquad [3.62]$$

If there is a continuum of wavevectors, the sum can be replaced by an integral over q. Then

$$<n_x{}^2(\underline{r}) + n_y{}^2(\underline{r})> = -\frac{2k_B T}{(2\pi)^3}\int_{q_m}^{q_M} \frac{4\pi q^2\, dq}{Kq^2+h} \qquad [3.63]$$

$$= \frac{k_B T}{\pi^2 K}\left[q_M - q_m - \frac{1}{\xi}\left[\arctan(\xi q_M) - \arctan(\xi q_m)\right]\right]$$

where $\xi = \sqrt{\frac{K}{h}}$. The integral extends over a volume in q-space bounded by q_m and q_M.

q_m is fixed by the sample dimension, and may be assumed to be zero for a macroscopic sample. q_M can be related either to the distance scale that defines local order, or to a fixed number of fluctuation modes. Both approaches result in a cutoff wavelength on the order of the intermolecular distance.

<u>case (ii)</u>: $E = 0$, $K_1 \neq K_2 \neq K_3$

In this case,

$$\lambda_+ = K_1 q_\perp^2 + K_3 q_z^2 + h \qquad [3.64]$$
$$\lambda_- = K_2 q_\perp^2 + K_3 q_z^2 + h$$

where $q_\perp^2 = q_x^2 + q_y^2$. The fluctuation amplitudes are given by

$$\langle n_x^2(r) + n_y^2(r) \rangle = \frac{k_B T}{(2\pi)^2} \sum_\alpha \frac{1}{2K_\alpha} \int_{q_m}^{q_M} \frac{d^3q}{q_\perp^2 + \frac{K_3}{K_\alpha} q_z^2 + h} \quad \text{for } \alpha = +,- \qquad [3.65]$$

$$\langle n_x^2(r) - n_y^2(r) \rangle = \frac{k_B T}{(2\pi)^2} \int_{q_m}^{q_M} d\phi \; q_\perp dq_\perp \; dq_z \; (\cos^2\phi - \sin^2\phi)$$
$$\times \left[\frac{1}{K_1 q_\perp^2 + K_3 q_z^2 + h} - \frac{1}{K_2 q_\perp^2 + K_3 q_z^2 + h} \right]$$

Introducing a stretched momentum vector into the first integral

$$q_\perp' = q_\perp \text{ and } q_z' = \sqrt{\frac{K_3}{K_\alpha}}\, q_z$$

the average fluctuation amplitude is

$$\langle n_x^2(\underline{r}) + n_y^2(\underline{r}) \rangle = \qquad [3.66]$$
$$\frac{k_B T}{2\pi^2} \sum_\alpha \frac{1}{\sqrt{K_\alpha K_3}} \left[q'_{M\alpha} - q'_{m\alpha} - \frac{1}{\xi_\alpha} \left[\tan^{-1}(\xi_\alpha q'_{M\alpha}) - \tan^{-1}(\xi_\alpha q'_{m\alpha}) \right] \right]$$

with $\xi_\alpha = \sqrt{\frac{K_\alpha}{h}}$. The difference term averages to zero on integration over ϕ, as expected for the case of no symmetry breaking field.

<u>case (iii)</u>: $E \neq 0$, one constant approximation.

This case provides the closest approximation to the experimental situation under

study. The eigenvectors of the two modes are given by

$$\lambda_+ = Kq^2+h \qquad [3.67]$$

$$\lambda_- = Kq^2+h-e$$

where the mean squared amplitude of the component of the normal modes of the director fluctuations perpendicular to $\underline{B}$ and

(a) along $\underline{E}$ is

$$<n_x{}^2(\underline{q})> = \frac{k_BT}{2\pi^2}\frac{1}{Kq^2+h-e} \qquad [3.68]$$

and

(b) perpendicular to $\underline{E}$ is

$$<n_y{}^2(\underline{q})> = \frac{k_BT}{2\pi^2}\frac{1}{Kq^2+h}\,.$$

Finally, the average amplitude of the fluctuations is

$$<n_x{}^2(\underline{r}) + n_y{}^2(\underline{r})> = \qquad [3.69]$$

$$\frac{k_BT}{2\pi^2K}\left\{2q_M-2q_m-\frac{1}{\xi_1}\left[\tan^{-1}(\xi_1q_M)-\tan^{-1}(\xi_1q_m)\right] - \frac{1}{\xi_2}\left[\tan^{-1}(\xi_2q_M)-\tan^{-1}(\xi_2q_m)\right]\right\}$$

while the difference of the fluctuation amplitudes is given by

$$<n_x{}^2(\underline{r})-n_y{}^2(\underline{r})> = \qquad [3.70]$$

$$\frac{k_BT}{2\pi^2K}\left\{-\frac{1}{\xi_1}\left[\tan^{-1}(\xi_1q_M)-\tan^{-1}(\xi_1q_m)\right] + \frac{1}{\xi_2}\left[\tan^{-1}(\xi_2q_M)-\tan^{-1}(\xi_2q_m)\right]\right\}$$

with $\xi_1 = \sqrt{\frac{K}{h}}$ and $\xi_2 = \sqrt{\frac{K}{h-e}}$. Thus, the electric field breaks the rotational symmetry of the sample by enhancing director fluctuations in the x-direction.

3-2 (ii): Effects of fluctuations on bulk properties

The effect of the fluctuations on the intensity of light transmitted through the sample can be calculated in two ways. The dielectric tensor is given by

$$\epsilon_{\alpha\beta}(\underline{r}) = \epsilon_{\perp}\delta_{\alpha\beta} + \Delta\epsilon\ n_{\alpha}(\underline{r})n_{\beta}(\underline{r}).$$

$\epsilon_{\perp}$ and $\epsilon_{\parallel}$ are calculated from the molecular polarizabilities as outlined in Section 3.1(ii) and the anisotropy of the dielectric constants is given by $\Delta\epsilon = \epsilon_{\parallel} - \epsilon_{\perp}$. The bulk dielectric tensor is calculated by averaging over the fluctuations of the local order in the sample

$$<\epsilon_{\alpha\beta}(\underline{r})> = \epsilon_{\perp}\delta_{\alpha\beta} + \Delta\epsilon <n_{\alpha}(\underline{r})n_{\beta}(\underline{r})> \qquad [3.71]$$

but $<n_{\alpha}(\underline{r})n_{\beta}(\underline{r})> = 0$ unless $\alpha = \beta$ as the fluctuations are uncorrelated so that

$$<\epsilon_{\alpha\alpha}(\underline{r})> = \epsilon_{\perp} + \Delta\epsilon <n_{\alpha}(\underline{r})n_{\alpha}(\underline{r})>, \qquad [3.72]$$

for α = x,y,z, with corresponding refractive indices

$$<N_{\alpha}{}^{2}(\underline{r})> = <\epsilon_{\alpha\alpha}(\underline{r})>. \qquad [3.73]$$

A difference in the mean square amplitudes of the modes leads to an induced birefringence for light propagating along the magnetic field.

Experimentally, the measured quantity is the average intensity I transmitted by the sample between polarizers crossed at ±45° to the electric field. This can be expressed

$$I = \frac{I_o}{2} <1 - \cos\delta> \simeq \frac{I_o}{4} <\delta^2>. \qquad [3.74]$$

I_o is the incident intensity and the phase difference δ induced by the sample is given by

$$\delta = \frac{2\pi l}{\lambda}\left[\ N_x - N_y\ \right] \simeq \frac{2\pi l\ \Delta\epsilon}{\lambda\sqrt{\epsilon_{\perp}}}\left[\bar{n}_x{}^2 - \bar{n}_y{}^2\right] \qquad [3.75]$$

where l is the thickness of the sample and λ is the wavelength of the incident light. $\bar{n}_i$ are the volume averaged fluctuation amplitudes. Then the intensity due to the induced birefringence is given by

$$I = \frac{I_o}{4}\left[\frac{2\pi l\ \Delta\epsilon}{\lambda\sqrt{\epsilon_{\perp}}}\right]^2 <[\bar{n}_x{}^2 - \bar{n}_y{}^2]^2> \qquad [3.76]$$

Alternately, the intensity can be calculated from light scattering theory as the scattering of light is governed by fluctuations of the dielectric tensor (de Gennes, 1974).

A light scattering experiment involves choosing the initial angle of polarization $\underline{i}$ and momentum $\underline{k}_i$ of ingoing light and the final angle of polarization $\underline{f}$ and momentum $\underline{k}_f$ of the outgoing light. The differential scattering cross section σ is given by

$$\sigma = \left[\frac{\omega^2 \epsilon_o}{c^2}\right]^2 <|\underline{i}\cdot\underline{\underline{\epsilon}}(\underline{q})\cdot\underline{f}|^2> \qquad [3.77]$$

where $\underline{q} = \underline{k}_i - \underline{k}_f$. For $\underline{i} \perp \underline{f}$ at $\pm 45°$ to the electric field and $\underline{q} = 0$,

$$\sigma = \left[\frac{4\pi^2 \epsilon_o}{\lambda^2 \bar{N}^2}\right]^2 \Delta\epsilon^2 <[\bar{n}_x{}^2 - \bar{n}_y{}^2]^2> \qquad [3.78]$$

with $\bar{N}$ the average refractive index and $\lambda = \frac{2\pi c}{\bar{N}\omega}$. The transmitted intensity will be proportional to σ:

$$I = f\, I_o\, \sigma = f\, I_o \left[\frac{4\pi^2 \epsilon_o}{\lambda^2 \bar{N}^2}\right]^2 \Delta\epsilon^2 <[\bar{n}_x{}^2 - \bar{n}_y{}^2]^2> \qquad [3.79]$$

where f is a geometrical factor related to the size of the detector.

In our theoretical calculations, we have considered the average of the difference of the squared fluctuation amplitudes $<n_x{}^2(\underline{r}) - n_y{}^2(\underline{r})>$ rather than the average of the square of the difference of the squared fluctuation amplitudes. This latter quantity can be written

$$<[n_x{}^2(\underline{r})-n_y{}^2(\underline{r})]^2> = < \left[[n_x{}^2(\underline{r})-n_y{}^2(\underline{r})]-<n_x{}^2(\underline{r})-n_y{}^2(\underline{r})>\right]^2> + <n_x{}^2(\underline{r})-n_y{}^2(\underline{r})>^2 \qquad [3.80]$$

where the first term represents the fluctuations about the mean. In principle, we could calculate the average $<[n_x{}^2(\underline{r}) - n_y{}^2(\underline{r})]^2>$ using Eqn. [3.49]. This calculation is involved and comparison of theory and data shows that pursuing this calculation is unnecessary in this case. Instead we make the assumption that the first term is a constant, at most contributing to the background intensity.[1] In this case, the average of the square of the difference of the fluctuation amplitudes can indeed be written in terms of the square of the average

---

[1]This problem could be avoided by measuring the light scattered at nonzero $\underline{q}$ where the intensity is proportional to $<n_x{}^2(\underline{r}) - n_y{}^2(\underline{r})>$. There will, however, always be a field-dependent background birefringence in this case as the probe beam is not traversing the cell along $\hat{n}$. It would be difficult to demonstrate biaxiality from data obtained in this way.

$$<[n_x^2(\underline{r})-n_y^2(\underline{r})]^2> = <n_x^2(\underline{r})-n_y^2(\underline{r})>^2. \qquad [3.81]$$

Using this approximation and the results of the previous section, we find in both cases that the intensity increases as $\epsilon_o\epsilon_\perp uE^2 \rightarrow \frac{\Delta\chi B^2}{\mu_o}$; however, it should be noted that this result was obtained assuming that the fluctuations were small.

To compare the magnitudes of the effect of the fields on molecular ordering and on fluctuations, the birefringence induced by field effects on the fluctuations can be calculated from

$$\Delta N = N_x - N_y = \sqrt{\epsilon_\perp + \Delta\epsilon <n_x^2>} - \sqrt{\epsilon_\perp + \Delta\epsilon <n_y^2>} \simeq \frac{\Delta\epsilon}{2\sqrt{\epsilon_\perp}}\left[<n_x^2> - <n_y^2>\right] \qquad [3.82]$$

For B=0.4 T and E=3x10^4 V/m,

$$\Delta N = 2.9\text{x}10^{-5}. \qquad [3.83]$$

Thus, the birefringence due to the fluctuations is expected to dominate the experimental observations. To observe birefringence due to molecular ordering, it would be necessary to investigate a situation where fluctuations were reduced. Such a situation occurs in the smectic phases where the splay and bend elastic constants diverge making fluctuations less favorable [Dunmur et al., 1985].

3-3: Measurements of the Field Induced Biaxiality

3-3 (i): Summary of previous experiments

Several experiments investigating field induced birefringence in thermotropic nematic liquid crystals have been attempted by a number of workers. The various geometries and other experimental parameters are summarized in Table I. The table shows a diagram of the geometry used, specifies the type (and method) of alignment, the material used, the susceptibility anisotropy being exploited and the cell thickness (l) and attempts to summarize both the conditions under which the measurements were undertaken and the results. There are three types of boundary alignment used in liquid crystals: planar or homogeous alignment refers to the director being parallel to the boundary at least in the region of the sample close to the boundary, in homeotropic alignment the director is perpendicular to the boundary. The alignment at the boundary can also be tilted.

Experiment 1 was the first to study the effect of fields on the orientation fluctuations. This experiment used the light scattering technique to show that both the intensity and the damping time of the fluctuations decreased as a stabilizing electric field was applied to the sample. Experiments 2-6 looked at the excess birefringence to study the effects of fields on the fluctuations, as in the experiments performed for this thesis. This is the most sensitive technique available; changes in the birefringence of the order of 10^{-5} - 10^{-8} can be measured, depending on the details of the technique used. Generally, the aligned sample is placed between crossed polarizers and the intensity of light passing through the apparatus is monitored with a photodiode. For experiments 2, 3, 5 and 6, this meant that the change in birefringence was observed in addition to the large birefringence of the field-free sample, making it necessary to experimentally subtract the zero-field birefringence using a Pockel's cell. Experiment 4 avoids this problem by using a negative magnetic anisotropy material. A magnetic field is applied along the direction perpendicular to the alignment. The effect of applying a field to a

Table I. Summary of experiments investigating the effect of fields on director fluctuations. l is the cell thickness. References: 1. Martinand and Durand [1972] 2. Poggi and Filippini [1977] 3. Malraison et al. [1980] 4. Seppen et al. [1986] 5. Dunmur et al. [1985] 6. Dunmur et al. [1987] 7. Frisken and Palffy-Muhoray [1989].

Ref.	Geometry	Alignment	Material	anisotropy	$l(\mu m)$	Measurements/Results
1		planar (rubbing)	MBBA	$\Delta\epsilon<0$	50	$0<E<6\times10^5$ V/m T=22°f=5KHz
						light scattering showed fluctuation quenching
2		Planar (SiO)	7CB	$\Delta\chi>0$	150	$0<H<2\times10^5$Oe, T=32.5°
						$\Delta\delta$ H
3		Planar (SiO)	8CB	$\Delta\chi>0$	200	T=37°, $0<H<2\times10^5$Oe
						$\Delta\delta$ H
			7CB, 8CB	$\Delta\chi>0$	200	$T_{NA}<T<T_{NI}$
						$\Delta\delta$ vs T
4		Homeotropic (hexadecanol-1)	nematic mixture	$\Delta\chi<0$	180	$0<H<12$T, T=22,62,42.1°
						ΔN H
						$25<T<72°$, H=10T
						ΔN vs T, induced biaxiality
5		Homeotropic (?)	5CB	$\Delta\epsilon>0$	15 55 111	T=28°,$0<E<5\times10^6$ V/m
						ΔN E^2, small fields ΔN E, large fields
			8CB	$\Delta\epsilon>0$	24	T=24.7°, $0<E<5\times10^6$ V/m
						ΔN E^2-all fields (Smectic)
6		Planar (?)	CN55	$\Delta\epsilon<0$	20	T=50°, $0<E<1.6\times10^6$ V/m
						ΔN E
			FDE55	$\Delta\epsilon<0$	25	T=22°, $0<E<1.6\times10^6$ V/m
						ΔN E
7		Homeotropic (silane)	5CB	$\Delta\epsilon>0$ $\Delta\chi>0$	500	T=33° $0<B<.5$ T $0<E<6.0\times10^6$ V/m
						induced biaxiality

negative anisotropy material is to quench the fluctuations in the direction parallel to the field. This makes the formerly uniaxial sample biaxial and the light propagating along the direction of the initial alignment is observed to increase from zero. However, negative magnetic anisotropy materials are rare (the one used in this experiment is actually a mixture of several liquid crystals) and this experimental method limits the range of materials that can be examined. Some recent theories have explored the effects of magnetic fields on mixtures of materials of positive and negative diamagnetic anisotropy [for example Kventsel and Sluckin, 1987].

In the case of the application of a single field, theory suggests that the birefringence will depend on the modulus of the applied field. The increase of the birefringence was observed to be linear with the increase of the applied magnetic field in Experiments 2-4. In Experiments 5 and 6, an ac electric field was used and the magnitudes of the frequency components (specifically the components at twice and four times the applied frequency) of the resulting intensity were shown to be consistent with a modular dependence of the fluctuation amplitudes on an applied field. Experiment 5 showed that the fluctuations are affected by the walls containing the sample; these act to quench the fluctuations as well. These authors also showed that at low field strengths and in the smectic phase the induced order varies as the square of the field strength, indicating that field-induced microscopic order is more important in this regime than fluctuation quenching.

Experiment 7 is the one attempted for this thesis; like Experiment 4, it measures field induced biaxial order. In this case, two fields are applied to a material of positive susceptibility anisotropy. The magnetic field is applied along the direction of initial alignment of the sample to stabilize the initial alignment. An electric field is applied perpendicular to this direction to break the uniaxial symmetry by enhancing, rather than quenching, the fluctuations in this direction. Assuming good initial alignment, the intensity of a probe laser transmitted by the sample between crossed

polarizers along the direction of initial alignment should be due to biaxiality induced by the competing electric field. The geometry does not restrict the experiments to a narrow range of materials and so studies of temperature and material dependence are possible. The details of this experiment will be considered in the next section. The results and a comparison of the results to the theory discussed earlier in the chapter can be found in the last section of the chapter.

3-3 (ii): Experimental Details

Figure 9 shows the experimental apparatus used to study field induced biaxiality in the nematic liquid crystal 5CB.

The first type of sample cell constructed for these measurements consisted of two glass plates (1.25 cm x 5 cm x .1 cm) separated by two stainless steel strips (.5 mm thick and 3 mm wide), and held together by Miller-Stephenson 907 epoxy. The two stainless steel strips were separated by about 2 mm to allow room for the laser beam to pass between them. The final sample volume was 2 mm wide, 5 cm long and .5 mm thick. Observation in the polarizing microscope of the switching characteristics of this cell indicated that the electric field was not very uniform inside the sample. Therefore, a second type of cell using larger electrodes was constructed. The cell consisted of two slender, rectangular pieces of glass (30.0 mm x 3.3 mm x 1.0 mm) separated by .5 mm and sandwiched between two stainless steel electrodes (30.0 mm x 12.5 mm x 0.5 mm) so that the electrodes were separated by 3.3 mm. This geometry required a special gluing procedure because of the small area for bonding. Armstrong 271 epoxy was found to make the best bond between the glass walls and the stainless steel electrodes. To prevent it from spreading over the glass, the glue was cured for one hour before being applied to the area to be bonded.

With a thickness of 500 μm, both types of samples are quite thick in comparison to the usual liquid crystal cell thickness of 10-25 μm. This choice was motivated by the fact that the optical phase shift is proportional to the thickness of the cell and thus the intensity will be proportional to the square of the thickness. This should make a large difference in the sensitivity of the apparatus to induced biaxiality. Following the calculations of Section 3-2 (ii), the phase shift induced by the field will be 7.2 mrad in a 25 μm cell and 0.14 rad in a 500 μm cell. The problems associated with working with a thick cell include the fact that fluctuations will be larger in thicker samples, decreasing the quality of the alignment and increasing the background intensity.

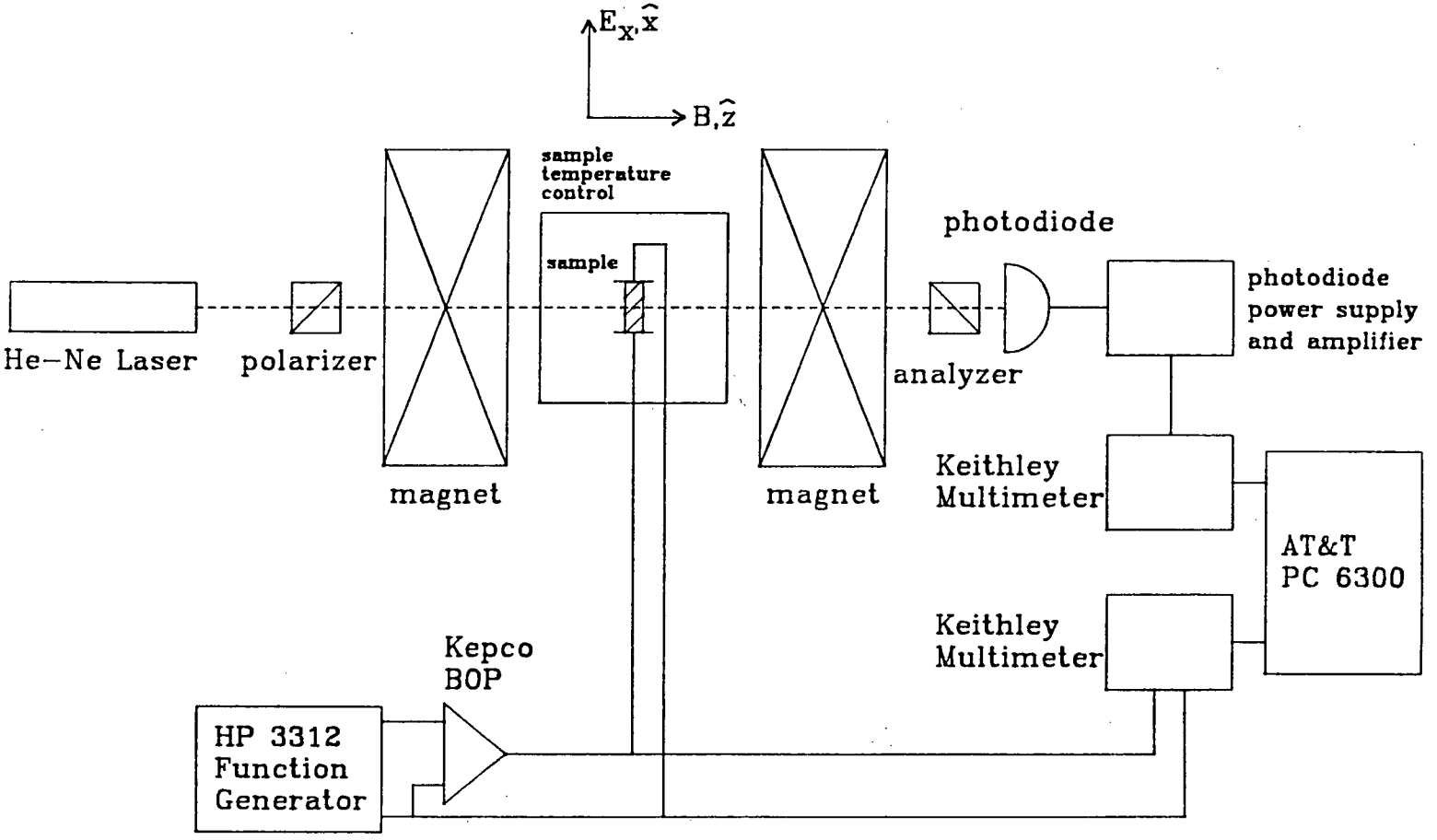

Fig. 9. Diagram of apparatus used to study electric field induced biaxiality.

To generate an electric field in the sample, a sinusoidal 1kHz voltage from a HP 3312A function generator was amplified in a Kepco bipolar amplifier and then applied to the stainless steel spacers via a step-up and isolation transformer. Experimentalists applying electric fields to liquid crystals usually use fields of frequencies of the order of 1 kHz or more as the director cannot follow these frequencies and sees instead the rms voltage. To ramp the voltage applied to the cell, a Bourne 3501S 10-turn 10kΩ potentiometer was used as a voltage divider. This potentiometer features highly linear resistance wire treated with a conductive coating to reduce jitter. By driving the potentiometer with a .25 rev/hr motor, a very uniform, linear ramping voltage could be obtained; at 115 V, a ramp of .2744 V/hr with a standard deviation σ of 4.75 mV per point was measured by a Keithley 197 Multimeter via an IEEE bus.

Alignment of the liquid crystal perpendicular to the glass plates (homeotropic alignment) was accomplished by two methods: by treatment of the glass surfaces as well as by application of a magnetic field. Lack of surface treatment lead to inhomogenieties in the director field at the surface. Surface treatment involved several steps. The glass was washed in an ultrasonic cleaner in a mixture of Liquinox detergent and diluted NH_3OH for 30 minutes. This was followed by a two hour rinse in distilled, de-ionized water. Next, the glass was soaked for 30 minutes in a .1% solution of Dow Corning X9-6136 silane and a 50-50 water-propanol mixture and then baked at 80°C for 30 minutes. This method consistently produced very satisfactory homeotropic alignment. Alignment was checked in a polarizing microscope. The liquid crystal used in the experiments was 5CB (4-n-pentyl-4′-cyanobiphenyl) synthesized by G.S. Bates at the Department of Chemistry, University of British Columbia. The nematic-isotropic transition temperature for the material studied here was measured to be 34.9°C measured with calibrated thermistors in a custom built temperature-controlled microscope stage.

The sample was contained in a thermostatted housing which was temperature

controlled in two stages. (See Figure 10.) Coarse temperature control was accomplished by circulating water from a temperature controlled bath through an outer jacket around the sample block. Fine control was obtained by passing current through heater wire wound around the inner sample block. The current applied to the wire heater was determined in a feedback loop. The temperature was sensed by a thermistor located in the block which was compared to a reference resistance in a Wheatstone bridge. The offset voltage from the bridge was detected and amplified in a null meter designed and built at UBC and the resulting voltage was used in the proportional/integral control of a Kepco OPS 40-0.5 operational power supply which provided current for the heater wire. The temperature was monitored by a second thermistor located in the sample block. A third thermistor in the sample block was used as a reference in the water bath temperature control circuit which caused the duty cycle of the water heater to vary according to how close the water temperature was to the set temperature, typically lower than the sample block temperature by 1-2°C. Using this temperature control procedure, the sample temperature was regulated to within ±1 mK.

Thermistors were used as the temperature sensing elements because they are easily calibrated and exhibit a large change of resistance with temperature (approximately ten times greater than platinum) in the temperature range of interest. The thermistors used were Fenwal GB41J1. They were calibrated using a HP 2804A quartz thermometer which was in turn calibrated against a triple point cell. Thermistors have a finite magnetoresistance. Rosenblatt [1981] found a change in temperature ΔT proportional to the square of the applied magnetic field

$$\Delta T = (1.025 \pm 0.015) \times 10^{-3} \text{mK kOe}^{-2} \cdot H^2. \qquad [3.84]$$

As the experiments performed for this thesis were done at constant magnetic field and the relative temperature was of more interest than the absolute tempterature, this was not considered to be a problem.

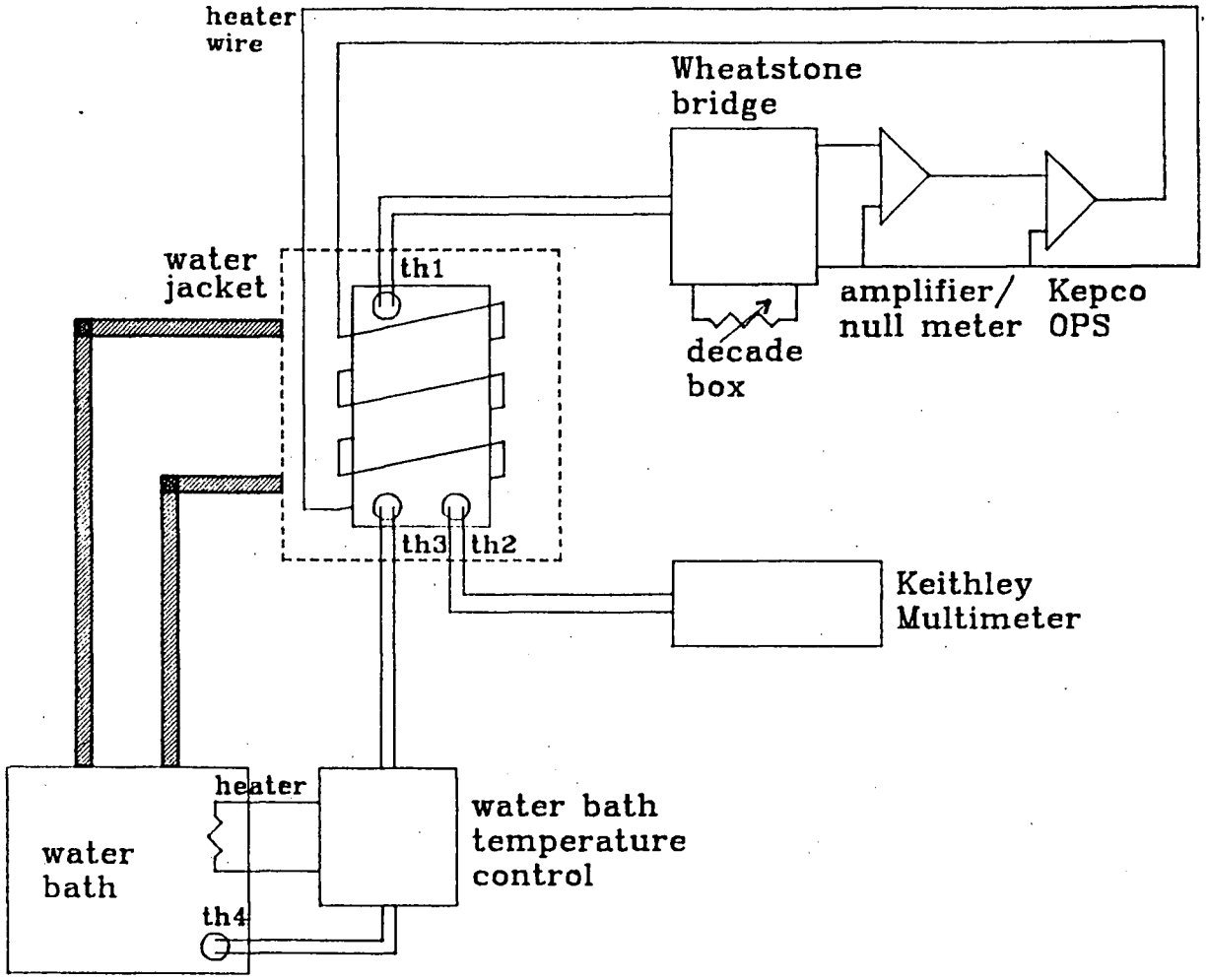

th1: control thermistor for heater feedback loop
th2: monitor thermistor to measure block temperature
th3: reference for water bath temperature control
th4: control thermistor for water bath temperature

Fig. 10. Schematic diagram of temperature control apparatus.

The thermostatted housing was placed between the poles of a water-cooled Harvey Wells electro-magnet powered by a Walker Scientific power supply. With a pole gap of eight inches (necessary to accomodate the thermostatted housing) the maximum field obtainable was 0.7 T. The field was stable to 1%. The sample was aligned so that the magnetic field was parallel to the initial sample alignment; 1″ diameter holes in the poles of the magnet made it possible to pass a laser beam through the sample parallel to the magnetic field. The field was calibrated in terms of the magnet current with a Rawson-Lush 824 rotating coil gaussmeter.

It was important to ensure that the direction of alignment of the liquid crystal in the sample cell was parallel to the direction of the magnetic field. Calculations showed that a misalignment of even a tenth of a degree would result in a birefringence which would increase with increasing magnetic field with a magnitude comparable to the effect due to the electric field. Minimizing this effect minimizes the background intensity. To facilitate aligning the magnetic field along the optic axis of the sample, the thermostatted housing was placed on a platform around which the magnet could be rotated independently.

The optics consisted of a PRA 5 mW HeNe laser (632.9 nm), polarizers and detection system. The polarizer/analyzer pair were Glan-Thompson prism polarizers supplied by Karl Lambrecht Corp. and had an extinction ratio of 10^{-6}. Such a high extinction ratio was necessary in order to make the zero field birefringence as small as possible to facilitate measurement of the induced biaxiality. The polarizers were mounted in holders which allowed for 3D positioning so that the direction of propagation of light through the prisms could be adjusted to be as close to the optic axis of the prisms as possible. The polarizer holders allowed rotation of the polarizer around the beam axis with a resolution of 0.005 rad. The direction of polarization of the analyzer was set to 45 degrees from the direction of the electric field and the polarizer was set at 90 degrees to the analyzer. The detection system consisted of a

Hamamatsu photodiode and a custom built amplifier. The specifications for this photodiode indicate an output voltage linear over fourteen decades of input intensity. Data collection was performed by an AT&T PC 6300 personal computer.

3-3 (iii): Results

Before starting the experiments on field induced biaxiality, attempts were made to investigate a second aspect of biaxiality and fluctuations. Fluctuations from the direction of initial alignment make the sample instantaneously biaxial; a stabilizing field should inhibit this biaxiality. By applying a stabilizing field at a frequency of the order of 5-10 Hz, it should be possible to follow the quenching of the fluctuations. To attempt this, a cell was constructed from two pieces of glass coated with indium tin oxide (ITO) and separated with .5 mm teflon spacers. The glass was treated so that the director would align homeotropically at the boundaries. By applying a voltage to the ITO surfaces, a low frequency electric field was induced along the initial director orientation. As a result, a large signal was observed which had frequency components which were harmonics of the frequency of the applied voltage. We found, though, that the signal observed at frequencies of the order of 10 Hz was due to an electrohydrodynamic instability as described by Nakagawa and Akahane [1983].

Using the cell described in the previous section, the behavior of the nematic sample in the presence of two fields was studied. A magnetic field was applied along the direction of initial orientation and a 1 kHz electric field was applied perpendicular to this direction to break the uniaxial symmetry of the sample. Typical results for the intensity transmitted by the sample between crossed polarizers while under the influence of two fields are shown in Fig. 11. The applied magnetic field is 0.33 T. As the voltage across the sample is increased (at a rate of $\simeq$ 50 V/hr), the intensity increases gradually at first and then abruptly at the reorientation transition, known as the Freedericksz transition. This transition will be discussed more thoroughly in the next chapter. The threshold voltage for this transition is found from the voltage at which the steep increase in intensity is seen and is shown on the graph as V_{th}. In this way, an estimate of 128.6 V for the threshold voltage can be obtained for this data. Above the transition, the birefringence continues to change as the reorientation

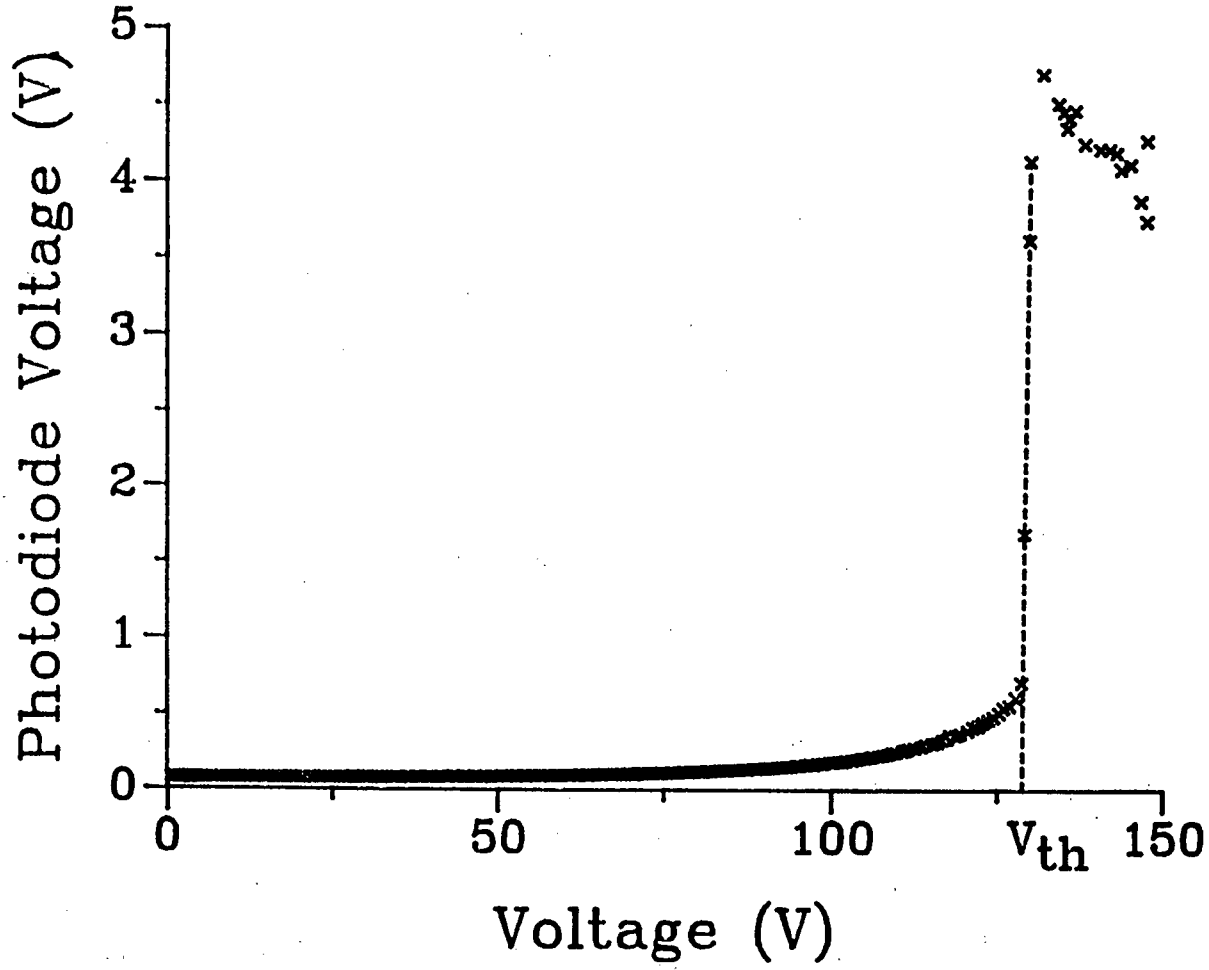

Fig. 11. Intensity transmitted by the sample between crossed polarizers. The applied magnetic field was 0.33 T and the voltage was ramped at a rate of 50 V/hr. The intensity increases abruptly at the threshold voltage, V_{th}.

progresses. The intensity of light transmitted fluctuates wildly because the thickness of the sample ($\sim$1000 λ) accentuates any non-uniformities of the sample. Fig. 12 shows that the behavior of the intensity is similar for different magnetic fields except that the reorientation threshold voltage increases with increasing magnetic field.

In most cases, the Freedericksz transition is second order [de Gennes, 1974]. In investigating the nature of the pretransitional behavior, a search for the critical divergence of the transmitted intensity associated with a second order transition was made. No critical divergence was observed, however, and the pretransitional increase in intensity can be adequately described by the theory for the orientation fluctuations discussed above. Fig. 13 shows the pretransitional intensity increase for the data of Fig. 11. The background has been subtracted. The solid curve shows the result of a least square fit of the data to the theoretical expression from continuum theory (Eqn. [3.76]) using the absolute amplitude of the intensity and the value of the threshold voltage as fitting parameters. The result of the fit is $\mathbb{V}_{th}$ = 131.1 V while the observed voltage is 128.6 V. This result is consistent with results of Chapter 4 which show that a first order transition occurs before the second order transition which previous work on Freedericksz transitions in static fields had led us to expect. The agreement of the fit to the data is very good, particularly in view of the approximations made in the theory. Fig. 14 shows the pretransitional intensity increase for the five sets of data of Fig. 12. The different magnitudes of magnetic field change the threshold voltage for the reorientation transition but not the shape of the pretransitional curves.

In the process of searching for the critical divergence of the transition, slower voltage ramps were made. During these runs, a pattern of diffraction spots was observed on the face of the photodiode holder. By direct observation, vertical stripes were seen in the cells. These results and their interpretation will be discussed in Chapter 5.

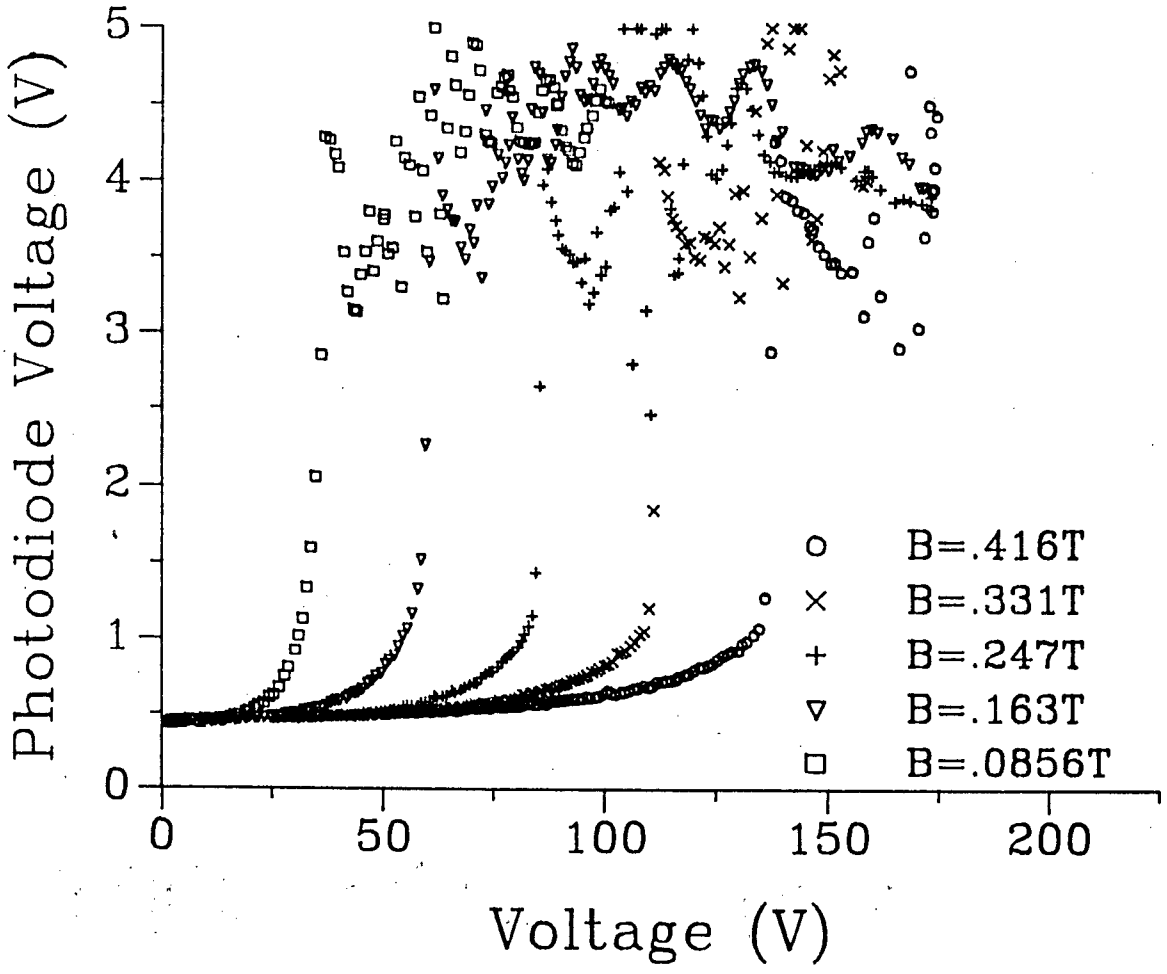

Fig. 12. Change in threshold with increasing magnetic field.

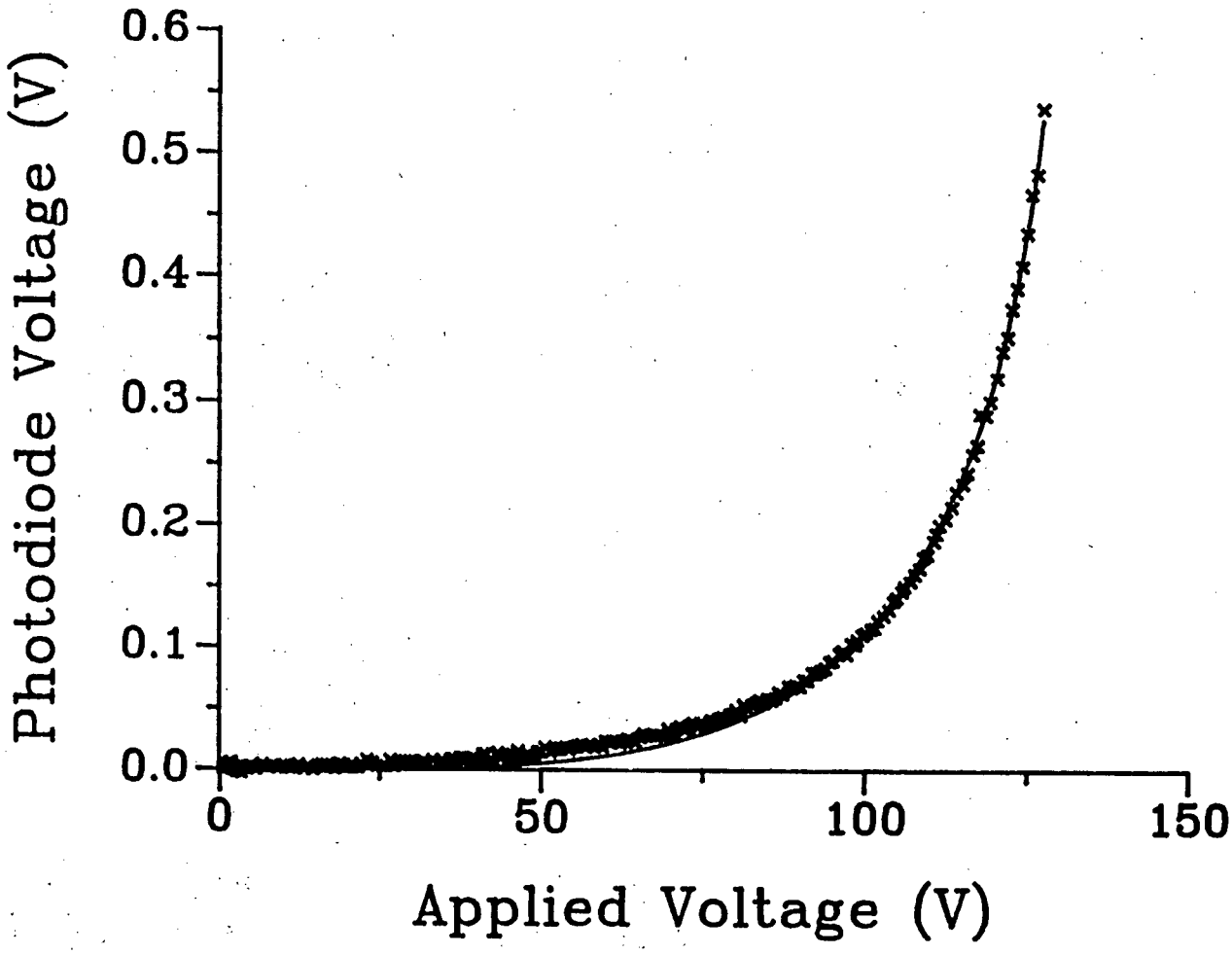

Fig. 13. Increase of the transmitted light intensity below the Freedericksz transition due to fluctuation enhancement by the electric field. The background has been subtracted. The solid curve is a least squares fit to the data using Eqn. [3.76].

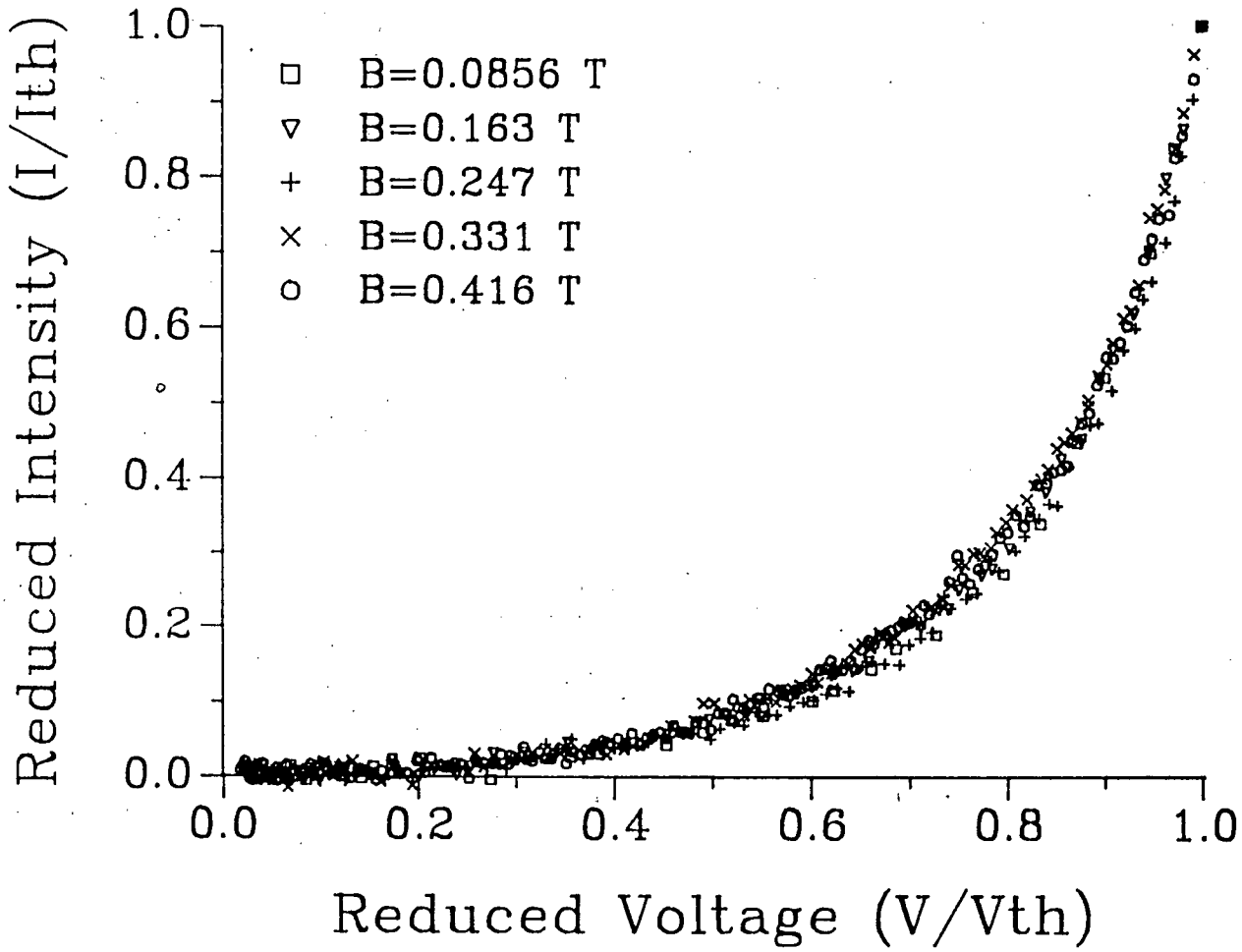

Fig. 14. Increase of the transmitted light intensity below the Freedericksz transition due to fluctuation enhancement by the electric field for several values of stabilizing magnetic field. The background has been subtracted and the data have been scaled by the threshold voltage and the maximum intensity at the threshold voltage.

4. Field Induced Order - Freedericksz Transitions

4.1 Theory

4.1 (i) Overview

A liquid crystal sample uniformly aligned between two parallel plane boundaries can undergo a transition to an elastically deformed state under the influence of external electric or magnetic fields. This transition, first observed by Freedericksz and Zolina [1933], has been the subject of considerable study.

Three different sample geometries may be distiguished. If the direction of molecular alignment at the boundaries is constrained to be perpendicular to the boundary planes, the initial deformation caused by the applied field is a bend. If the alignment is parallel, the initial deformation can be either a splay or a twist depending on whether the field is applied normal or parallel to the boundaries. For the case of a single static field applied either parallel or perpendicular to the boundaries, theoretical results [Gruler et al., 1972] predict all magnetic field induced transitions to be second order. Treatment of the electric field induced bend and splay transitions [Gruler et al., 1972; Deuling, 1972] suggests that these transitions should be second order as well. In these calculations for the electric field induced transitions, the bend geometry has been considered as a simple extension of the splay geometry and inhomogenieties of the electric field are ignored. After more careful consideration of the electrostatic problem, Arakelian et al. [1984] used a Landau approach to show that the electric field induced bend transition is expected to be first order; their results do not appear to be widely known. In general, the electric field induced bend and twist transitions have not received much attention, probably due to the unusual experimental geometry associated with applying an electric field parallel to the boundary planes.

For static fields, first order transitions have also been predicted to occur in systems of large conductivity anisotropy [Deuling and Helfrich, 1974] and have been

predicted and observed in systems where feedback is present [Wang et al., 1987]. First order transitions have been observed [Onnagawa and Miyashita, 1974] and studied theoretically [Motooka and Fukuhara, 1979; Fel and Lasene, 1986] for the case where the alignment at the boundary surfaces is tilted. First order transitions have been predicted in geometries where there are two fields, both perpendicular to the initial alignment direction [Barbero et al., 1988]. Several authors [Zel'dovich et al., 1981; Durbin et al., 1981; Ong, 1983] have suggested that the Freedericksz transition could be first order for systems with specific material properties if the transition is induced by an optical field. First order transitions have been predicted [Nersisyan and Tabiryan, 1984] and observed [Chen and Wu, 1988] if the transition is induced by an optical field in the presence of an additional electric field. They have also been predicted [Ong, 1985] and observed [Karn et al., 1986] for an optical field induced transition in the presence of an additional magnetic field.

In this chapter, theoretical and experimental aspects of the Freedericksz transition in the presence of two fields are investigated [Frisken and Palffy-Muhoray, 1989]. In the next section, expressions for the continuum free energy are derived for a variety of geometries. A simple Landau expansion of the free energy is used to investigate the equilibrium deformation qualitatively and to relate characteristics of the transitions to material properties. Because some of the transitions are found to be first order, exact solutions minimizing the continuum free energy are considered as well. To study the transition experimentally, dielectric measurements were made on samples of 5CB (4-cyano-4′-n-pentylbiphenyl) in the bend and twist geometry in the presence of an additional field stabilizing the initial alignment. The results of these experiments are compared with theory.

4.1 (ii) Introduction

As mentioned in the preceding section, there are three possible geometries for the Freedericksz transition; these can be labelled splay, twist and bend depending on the nature of the small angle deformation. If we consider Freedericksz transitions involving static fields and materials of positive susceptibility anisotropies, the transition can be induced by either a magnetic or an electric field perpendicular to the direction of initial alignment. In our case, we wish to consider the situation where a second field is applied along the direction of initial alignment to stabilize the alignment. The six possible experimental configurations satisfying these constraints are shown in Figure 15. For completeness, the nature of the deformation for all six transitions will be considered.

The bend transition (geometries 5 and 6) will be considered first in full; results for the other geometries are summarized in Table II and Table III. In the bend geometry, initial alignment is perpendicular to the glass plates. The director is assumed to be confined to the x-z plane so that it can be expressed in terms of the angle θ only:

$$\hat{n} = (\sin\theta \, , \, 0 \, , \, \cos\theta) \qquad [4.1]$$

where $\theta = \theta(z)$ is the angle between the director and the direction of alignment at the boundaries. Note that it is assumed in all six cases that the distortion depends only on z. The cell area in the x-y plane is A and the thickness (along $\hat{z}$) is l. At the center of the cell, ($z=l/2$) the deformation angle is a maximum ($\theta = \theta_m$) and here

$$\theta' = \frac{\partial\theta}{\partial z} = 0. \qquad [4.2]$$

The Frank free energy due to elastic deformations in this geometry is, in units of $AK_3\pi/2l$,

$$\mathbb{F}_f = \int_0^{\pi} \left[1 - \kappa \sin^2\theta\right] \theta'^2 \, dz \qquad [4.3]$$

where z has been scaled by l/π.

The field contributions to the free energy are different for the case of magnetic field induced bend and electric field induced bend. In both cases, the free energy due to

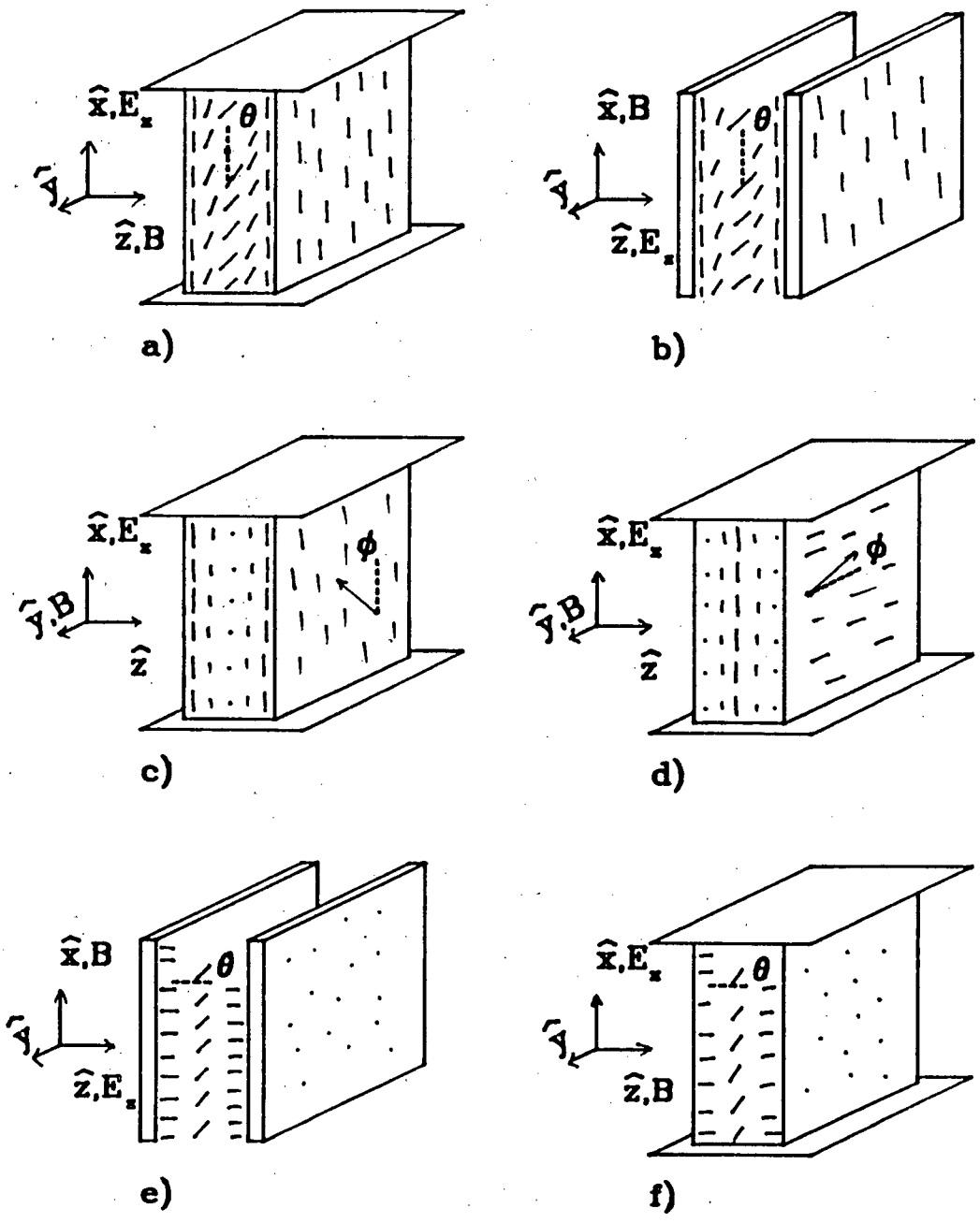

Fig. 15. Six possible geometries for Freedericksz transitions. a) geometry 1, magnetic field induced splay b) geometry 2, electric field induced splay c) geometry 3, magnetic field induced twist d) geometry 4, electric field induced twist e) geometry 5, magnetic field induced bend and f) geometry 6, electric field induced bend.

the magnetic field is calculated from Eqn. [3.32]. For a magnetic field along $\hat{x}$, the magnetic contribution to the free energy is

$$\mathbb{F}_m = -\frac{\mu_o \Delta\chi\, l^2}{K_3\pi^2} H^2 \int_0^\pi \sin^2\theta \, dz \qquad [4.4]$$

This geometry calls for application of an electric field along $\hat{z}$. In this case, the $\hat{x}$ and $\hat{y}$ components of $\underline{D}$ are zero and, from the requirement that $\nabla\cdot \underline{D} = 0$, the $\hat{z}$ component is independent of z, though it will depend on $\theta(z)$. Then, following Deuling [1972],

$$\mathbb{F}_e = -\frac{l^2}{K_3\pi^2}\int_0^\pi D_Z\, E_Z\, dz = -\frac{l^2}{K_3\pi^2} D_Z \int_0^\pi E_Z\, dz. \qquad [4.5]$$

$\nabla x\underline{E} = 0$ implies that E can be expressed as the gradient of some potential, U, in this case the geometry requires that E_Z is the only nonzero component of $\underline{E}$ as $U = U(z)$. The potential applied across the sample is

$$\mathbb{V} = \frac{l}{\pi}\int_0^\pi E_Z\, dz \qquad [4.6]$$

The relationship between D_Z and E_Z is given by

$$D_Z = \epsilon_o\, E_Z\, (\epsilon_\perp \sin^2\theta + \epsilon_{||}\cos^2\theta) \qquad [4.7]$$

By substituting [4.7] into [4.6], D_Z can be expressed as a functional of $\theta(z)$

$$D_Z = \frac{\epsilon_o\, \mathbb{V}\, \pi/l}{\int_0^\pi \frac{dz}{(\epsilon_\perp \sin^2\theta + \epsilon_{||}\cos^2\theta)}} \qquad [4.8]$$

and the electric field contribution to the free energy density in this geometry is

$$\mathbb{F}_e = -\frac{\epsilon_o\epsilon_{||}\mathbb{V}^2/K_3}{\int_0^\pi \frac{dz}{1 - u\sin^2\theta}} \qquad [4.9]$$

On the other hand, if the applied electric field is along $\hat{x}$ and the magnetic field is along $\hat{z}$, then the magnetic contribution to the free energy for the electric field induced bend deformation is

$$\mathbb{F}_m = -\frac{\mu_o \Delta\chi\, l^2}{K_3\pi^2} H^2 \int_0^\pi \cos^2\theta\, dz \qquad [4.10]$$

while the electric field contribution is

$$\mathbb{F}_e = -\frac{\epsilon_o\epsilon_\perp \mathbb{V}^2}{K_3}\left[\frac{l}{\pi d}\right]^2 \int_0^\pi \frac{dz}{1 - u\sin^2\theta} \qquad [4.11]$$

where $\mathbb{V}$ is the voltage applied to the cell, $u = 1 - \frac{\epsilon_\perp}{\epsilon_{||}}$ and $\epsilon_\perp$ and $\epsilon_{||}$ are the principal

values of the dielectric tensor, and d is the width of the cell.

Table II. Free energy terms for geometries 1-6. The geometries are shown in Fig. 15. $u=\frac{\Delta\epsilon}{\epsilon_{\parallel}}$, $w=\frac{\Delta\epsilon}{\epsilon_{\perp}}$, $\kappa=1-\frac{K_1}{K_3}$, $\gamma=1-\frac{K_3}{K_1}$. $h=\frac{\Delta\chi B^2 l^2}{\mu_o K_i \pi^2}$, and the free energies are expressed in units of $\frac{AK_i\pi}{2\,l}$ where i=1 for geometries 1 and 2, i=2 for geometries 3 and 4, and i=3 for geometries 5 and 6.

Geometry	$\hat{n}$	$\mathbb{F}_f$	$\mathbb{F}_m$	$\mathbb{F}_e$	e
1	$(\cos\theta,0,\sin\theta)$	$\int(1-\gamma\sin^2\theta)\theta'^2$	$-\int h\,\sin^2\theta$	$-\int\frac{e/w}{1+w\,\sin^2\theta}$	$\frac{\epsilon_o w V^2 l^2 \epsilon_{\parallel}}{K_1\pi^2 d^2}$
2	$(\cos\theta,0,\sin\theta)$	$\int(1-\gamma\sin^2\theta)\theta'^2$	$-\int h\,\cos^2\theta$	$-\frac{e/w}{\int\frac{1}{1+w\,\sin^2\theta}}$	$\frac{\epsilon_o\Delta\epsilon V^2}{K_1}$
3	$(\cos\phi,\sin\phi,0)$	$\int\phi'^2$	$-\int h\,\sin^2\phi$	$-\int\frac{e/w}{1+w\,\sin^2\theta}$	$\frac{\epsilon_o w V^2 l^2 \epsilon_{\parallel}}{K_2\pi^2 d^2}$
4	$(\sin\phi,\cos\phi,0)$	$\int\phi'^2$	$-\int h\,\cos^2\phi$	$-\int\frac{e/u}{1-u\,\sin^2\phi}$	$\frac{\epsilon_o u V^2 l^2 \epsilon_{\perp}}{K_2\pi^2 d^2}$
5	$(\sin\theta,0,\cos\theta)$	$\int(1-\kappa\sin^2\theta)\theta'^2$	$-\int h\,\sin^2\theta$	$-\frac{e/u}{\int\frac{1}{1-u\,\sin^2\theta}}$	$\frac{\epsilon_o\Delta\epsilon V^2}{K_3}$
6	$(\sin\theta,0,\cos\theta)$	$\int(1-\kappa\sin^2\theta)\theta'^2$	$-\int h\,\cos^2\theta$	$-\int\frac{e/u}{1-u\,\sin^2\theta}$	$\frac{\epsilon_o u V^2 l^2 \epsilon_{\perp}}{K_3\pi^2 d^2}$

4.1 (iii): Landau Theory

Landau theory provides a qualitative description of phase transitions from which much can be learned about the physical nature of the system being studied. It is based on the assumptions that near the critical point, the order parameter of the system is small and that the free energy can be expanded in powers of this order parameter. Once the free energy is known, all other thermodynamic quantities of the system can be calculated.

A Landau free energy can be constructed by assuming a deformation of the director field of the form

$$\theta = \theta_m \sin z \qquad [4.12]$$

and expanding the free energy $\mathbb{F} = \mathbb{F}_f + \mathbb{F}_e + \mathbb{F}_m$ in terms of the order parameter θ_m. In order to investigate whether the transition is first or second order, the expansion must include powers of θ_m up to sixth order. In this way, the dimensionless Landau expansion is obtained:

$$\mathfrak{F} = a\,\theta_m{}^2 + \frac{b}{2}\,\theta_m{}^4 + \frac{c}{3}\,\theta_m{}^6 \qquad [4.13]$$

where the coefficients are given explicitly in Table III for the six cases considered. (The twist deformations are assumed to have a form $\phi = \phi_m \sin z$.) Minimizing $\mathfrak{F}$ with respect to θ_m results in three solutions for θ_m, whether or not they have physical meaning depends on the parameters of the system. The null solution (θ_m=0) is always an extremum. Minimizing $\mathfrak{F}$ yields an expression for θ_m in terms of the coefficients of the free energy expression,

$$\theta_m{}^2 = \frac{-b \pm \sqrt{b^2 - 4ac}}{2c} \qquad [4.14]$$

The transition is second order for b,c > 0 and the transition occurs when a=0. A first order transition will occur for b < 0, c > 0 when $a = \frac{3\,b^2}{16\,c}$. At the first order transition, the value of the order parameter is given by

$$\theta_m = \sqrt{-\frac{3b}{4c}}\,. \qquad [4.15]$$

The third solution corresponds to a local maximum of the free energy and occurs when

$a = \frac{b^2}{4c}$.

Below the transition, $<\theta_m> = 0$. However, the mean square deviations from the average are not zero, and these fluctuations can be expressed [Landau and Lifshitz, 1980]

$$<\theta_m{}^2> = k_B T \left[\frac{\partial^2 \mathcal{F}}{\partial \theta_m{}^2}\right]^{-1}_{\theta_m=0} \qquad [4.16]$$

For the electric field induced bend transition,

$$<\theta_m{}^2> = \frac{k_B T}{1+h-e} \qquad [4.17]$$

Thus, fluctuations of the order parameter diverge as $e \rightarrow 1+h$.

Using the material parameters for 5CB [Bunning et al., 1981; Frisken et al., 1986; Dunmur et al., 1978], b is positive and the magnetic field induced bend transition and electric field induced splay transition are second order if they are induced by a magnetic field. b is negative and the transition is predicted to be first order:

1) when the bend transition is induced by an electric field with and without a stabilizing magnetic field
2) for both types of twist transition with and without a stabilizing field and
3) when the splay transition is induced by a magnetic field in the presence of a stabilizing electric field.

The tricritical point occurs at a, b = 0 and should be accessible in some of these transitions in materials with appropriate dielectric and elastic constants.

Several details indicate that the quantitative predictions of Landau theory may not be entirely accurate. The Landau expansion will be most accurate in the vicinity of the tricritical point and less accurate when the transition is first order. The value of the order parameter at the first order transition is large, suggesting that the transition is strongly first order and that Landau theory may not provide a good description. The results are unsatisfactory in other ways; θ_m has values greater than $\pi/2$, which is unphysical but is not surprising as there are no constraints on θ_m in this theory. As

well, when solving the equations describing the twist deformation, c goes negative for u $> .6$, which indicates that the expansion should include higher terms.

Table III. Coefficients of the Landau expansion for geometries 1-6. The geometries are shown in Fig. 15 and the symbols are defined in Table II.

Geometry	a	b	c	Criteria for first order
1	$1+e-h$	$\frac{1}{2}[-\gamma+h-e(3w+1)]$	$\frac{1}{8}[\gamma-\frac{2}{3}h+e(15w^2+10w+\frac{2}{3}]$	$e\geq\frac{1-\gamma}{3w}$
2	$1+h-e$	$\frac{1}{2}[-\gamma-h+e(w+1)]$	$\frac{1}{8}[\gamma+\frac{2}{3}h-e(3w^2+4w+\frac{2}{3}]$	$h\leq\frac{-\gamma-1-w}{w}$
3	$1+e-h$	$\frac{1}{2}[h-e(3w+1)]$	$\frac{1}{8}[-\frac{2}{3}h+e(15w^2+10w+\frac{2}{3}]$	$e\geq\frac{1}{3w}$
4	$1+h-e$	$\frac{1}{2}[-h-e(3u-1)]$	$\frac{1}{8}[\frac{2}{3}h-e(15u^2-10u+\frac{2}{3}]$	$h\geq\frac{1-3u}{3u}$
5	$1+e-h$	$\frac{1}{2}[-\kappa+h-e(1-u)]$	$\frac{1}{8}[\kappa-\frac{2}{3}h+e(3u^2-4w+\frac{2}{3}]$	$e\leq\frac{\kappa-1}{u}$
6	$1+h-e$	$\frac{1}{2}[-\kappa-h-e(3u-1)]$	$\frac{1}{8}[\kappa+\frac{2}{3}h-e(15u^2-10u+\frac{2}{3}]$	$h\geq\frac{1-3u-\kappa}{3u}$

4.1 (iv): Exact Solution

Experiments were performed to investigate the electric field induced twist and bend deformations. Because these transitions were expected to be strongly first order, an exact minimization of the continuum free energy was pursued in order to enable comparison between theory and experiment. The free energies for these two geometries (see Table II) are minimized by the Euler-Lagrange equation

$$\frac{\partial I}{\partial \theta} - \frac{d}{dz}\frac{\partial I}{\partial \theta'} = 0 \qquad [4.18]$$

where I is the integrand of the free energy integral. For the bend geometry,

$$I = (1 - \kappa \sin^2\theta)\ \theta'^2 - \frac{e/u}{1 - u \sin^2\theta} - h \cos^2\theta. \qquad [4.19]$$

This equation covers the twist geometry as well, if we set κ=0 and replace K_3 by K_2 in the definitions of e and h. Solutions of the Euler-Lagrange equation are extrema of the free energy. Solving Eqn. [4.18] and Eqn. [4.19] gives, at the center of the cell,

$$\frac{l}{2} = \int_0^{\theta_m} \sqrt{\frac{(1 - \kappa \sin^2\theta)(1 - u \sin^2\theta)(1 - u \sin^2\theta_m)}{\left[e - h\,(1 - u \sin^2\theta)(1 - u \sin^2\theta_m)\right](\sin^2\theta_m - \sin^2\theta)}}\ d\theta \qquad [4.20]$$

which can be solved for θ_m at a given voltage and magnetic field. Once θ_m is known, the free energy $\mathbb{F}$ and capacitance C can be calculated from

$$\mathbb{F}(\theta_m) = 2\int_0^{\theta_m} d\theta \left[(1 - \kappa \sin^2\theta)\ \theta' - \frac{\left[e + h \cos^2\theta\ (1 - u \sin^2\theta)\right]}{(1 - u \sin^2\theta)\ \theta'}\right] \qquad [4.21]$$

$$C(\theta_m) = 2C_o\int_0^{\theta_m} \frac{d\theta}{(1 - u \sin^2\theta)\ \theta'}$$

where C_o is the cell capacitance when $\theta_m = 0$ and

$$\theta' = \sqrt{\frac{\left[e - h\,(1-u \sin^2\theta)(1-u \sin^2\theta_m)\right](\sin^2\theta_m - \sin^2\theta)}{(1-\kappa \sin^2\theta)(1-u \sin^2\theta)(1-u \sin^2\theta_m)}} \qquad [4.22]$$

The integrals in Eqn. [4.20,4.21] are badly behaved in the limit $\theta_m \rightarrow \pi/2$; they are usefully expressed in terms of elliptic integrals as outlined by Morris and Palffy-Muhoray [1986]. Since the transition is first order, Eqn. [4.20] will be satisfied by two non-trivial values of θ_m for voltages in the range $\mathbb{V}_{min} < \mathbb{V} < \mathbb{V}^*$, where $\mathbb{V}_{min}$ and $\mathbb{V}^*$

are the stability limits of the transition. An iterative numerical method was used to solve Eqn. [4.20] for e, given θ_m and h, and then the free energy and the capacitance were calculated. The listing of the program used for these calcuations can be found in Appendix B. The capacitance, order parameter θ_m and free energy as functions of 1/e for several values of h are shown in Fig. 16. The e-h phase diagram for the bend transition is shown in Fig. 17. The results for the twist transition are similar, although for 5CB this transition is less strongly first order.

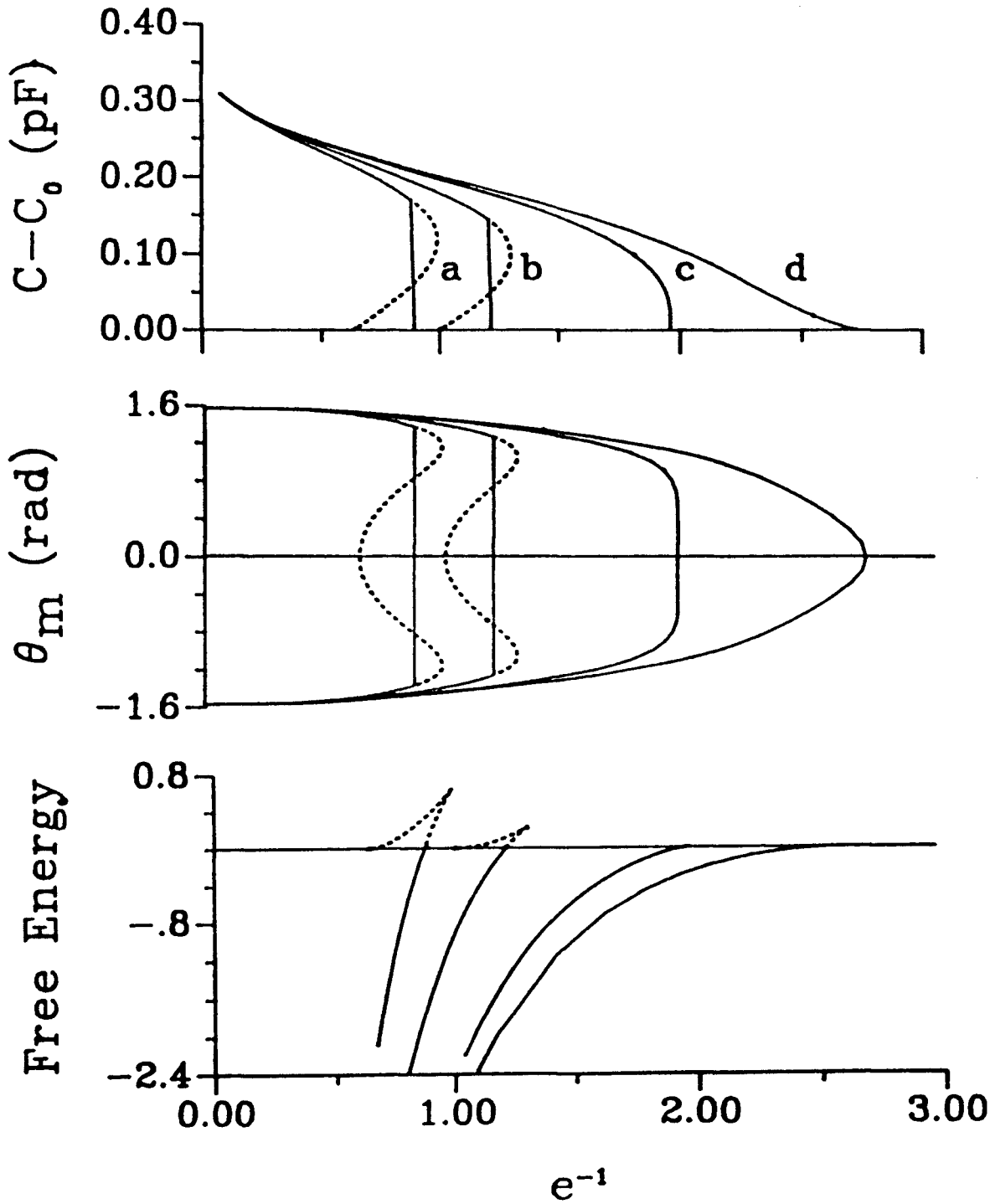

Fig. 16. Capacitance C, order parameter θ_m and dimensionless free energy F for the electric field induced bend transition as a function of the inverse of the electric field parameter e. The magnetic field parameter h is a) h=.573, b) h=0.0, c) h=−.489 and d) h=−.632 where $h = \frac{\Delta\chi B^2 l^2}{\mu_o K_3 \pi^2}$. $e = \frac{\epsilon_o \Delta\epsilon V^2 l^2 \epsilon_\perp}{K_3 \pi^2 d^2 \epsilon_\parallel}$ and C_o is the capacitance of the cell when $\theta_m = 0$.

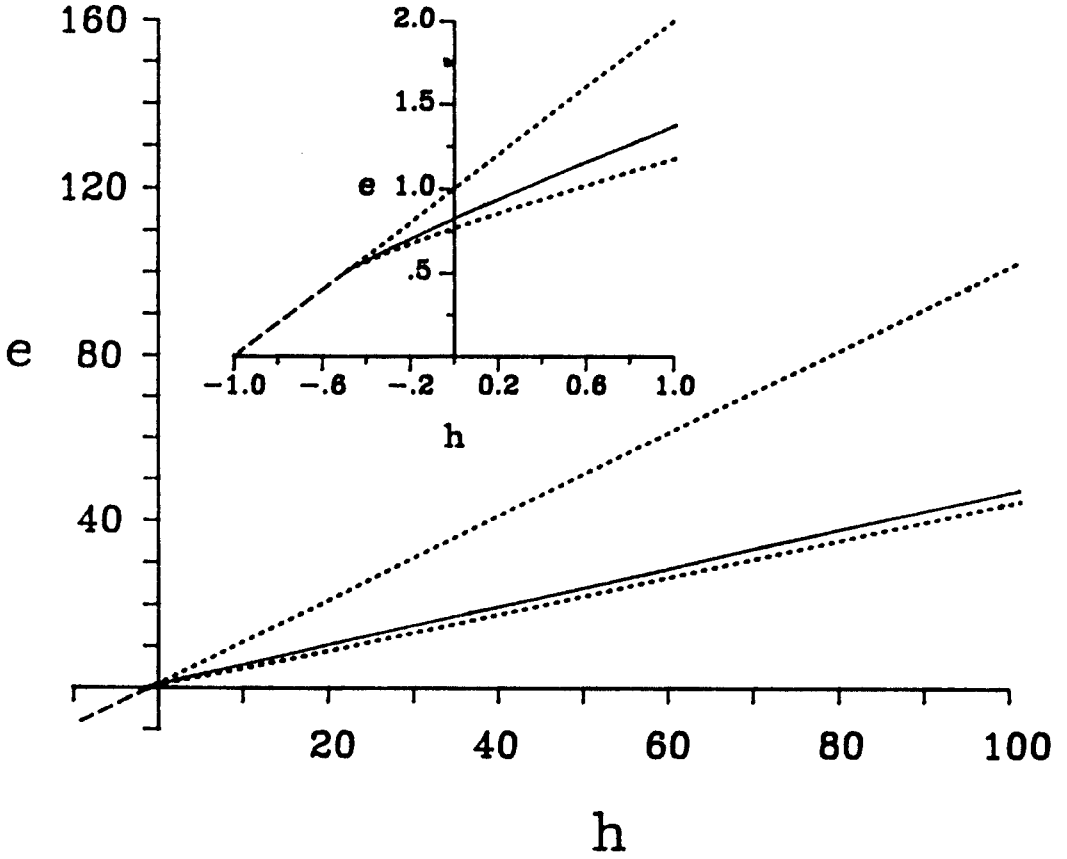

Fig. 17. Phase diagram for the electric field induced bend transition as calculated from theory for $u=\frac{\Delta\epsilon}{\epsilon_{||}}=.56$, $\kappa=1-\frac{K_1}{K_3}=.14$. Here, $e = \frac{\epsilon_o u V^2 l^2 \epsilon_\perp}{K_3 \pi^2 d^2}$ and $h = \frac{\Delta\chi B^2 l^2}{\mu_o K_3 \pi^2}$. Negative values of h correspond to negative diamagnetic anisotropy. The solid line indicates first order transitions, the dashed line second order transitions and the dotted lines the limits of the spinodal region. The inset shows detail near the tricritical point which occurs at h=−.489 and e=.511.

4.2: Experimental Details

Two types of cells, using different methods of surface treatment, were constructed for use in investigating the electrically and the magnetically driven transitions. To apply an electric field parallel to the boundary planes, cells were constructed with large stainless steel electrodes and slender glass plates as described in Chapter 3. In order to apply an electric field perpendicular to the boundary planes, the second type of cell consisted of two pieces of ITO (indium tin oxide) coated glass separated by two .5 mm teflon spacers 3.5 mm apart. The ITO coating acts as a transparent conductor. To induce director alignment parallel to the glass, the plates were treated with a solution of poly(vinyl formal) and chloroform and were buffed when dry [Gleeson, 1988]. The liquid crystal used in the experiments was 5CB. The cells used to investigate the electric field induced bend transition could be placed in the thermostatted housing with temperature control of ± 1 mK described in Chapter 3. The other cells were mounted directly on the support between the poles of the electromagnet.

The transition was investigated by measuring the capacitance of the cell. (Fig. 18). The capacitance monitors the average deformation of the cell rather than the deformation in the small area probed by the laser beam. The capacitance was measured with a GenRad 1615-A capacitance bridge. Cells constructed to measure the electric field induced transitions typically had capacitances of the order of 2 pF which could be measured accurately to $\sim 1 \times 10^{-3}$ pF. The measurements were made using an external signal from a HP3312 function generator amplified by a Kepco BOP 72-5 operational amplifier followed by a transformer. A lock-in amplifier (EG&G 5102) was used to detect the null. Measurements were made at 2 kHz, with voltages across the sample ranging from 0-60 V_{rms} applied via the bridge. In the case of the electric field induced bend transition, the sample approached equilibrium slowly at voltages near the critical voltage; data points were taken once an hour, 0.25 V apart. Samples undergoing the

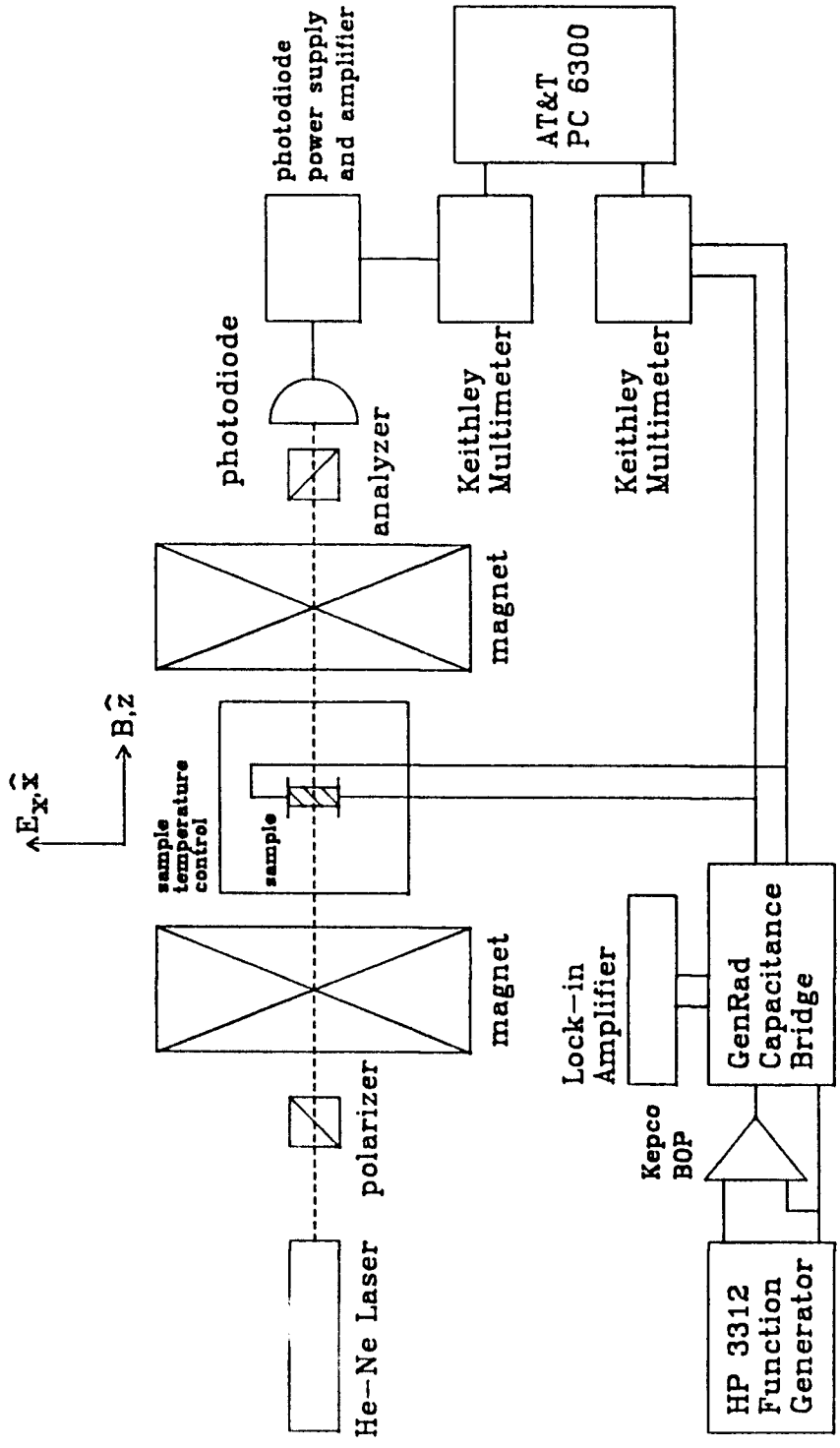

Fig. 18. Diagram of apparatus used to study Freedericksz transitions.

magnetic field induced bend transition approached equilibrium much faster; here measurements were made every 10 minutes. Measurements of the electric field induced twist transition were made at a variety ramping speeds.

4.3: Experimental Results

Typical sample results for the magnetic field induced bend transition are shown in Fig. 19. They show no evidence of hysteresis within experimental error, in agreement with the predictions of theory that the transition should be second order.

Fig. 20 shows experimental results for the electric field induced bend transition in the presence of a 0.12 T magnetic field applied so as to stabilize the initial alignment. These are typical results for this geometry, showing clear evidence of hysteresis. $\mathbb{V}_{min}$ and $\mathbb{V}^*$ are estimated from the voltages where the derivative of the capacitance with respect to voltage is a maximum, and the threshold voltage $\mathbb{V}_{th}$ is estimated to be the average of these. Table IV shows the experimental values of the threshold voltage $\mathbb{V}_{th}$ and the transition width $\Delta\mathbb{V}$ together with theoretical values calculated using the material parameters of 5CB. There is good agreement between measured and predicted values in all cases except that the experimentally observed width of the transition at nonzero magnetic field is significantly less than predicted by theory. Although this discrepancy is not wholly understood at this time, it is worth noting that the theoretical results are sensitively dependent on the form of the electric field contribution to the free energy. For example, if inhomogenieties of the electric field are ignored, the transition is predicted to be second order. In our system, $l/\mathrm{d} = .15$, and higher order terms in Eqn. [4.21] may play a significant role.

Initial capacitance measurements of the electric field induced twist transition resembled the results for the bend transition shown in Fig. 20. Further experiments involving a variety of voltage sweep speeds show that the hysteresis decreases as the ramping speed is decreased. Fig. 21 compares results from measurements at a variety of run speeds in zero magnetic field showing decreasing hysteresis. As the capacitance bridge must be nulled manually, the minimum ramp speed is determined in part by how long the experimentalist can stay awake. (The minimum ramp speed is also determined by the stability and resolution of the capacitance bridge and associated

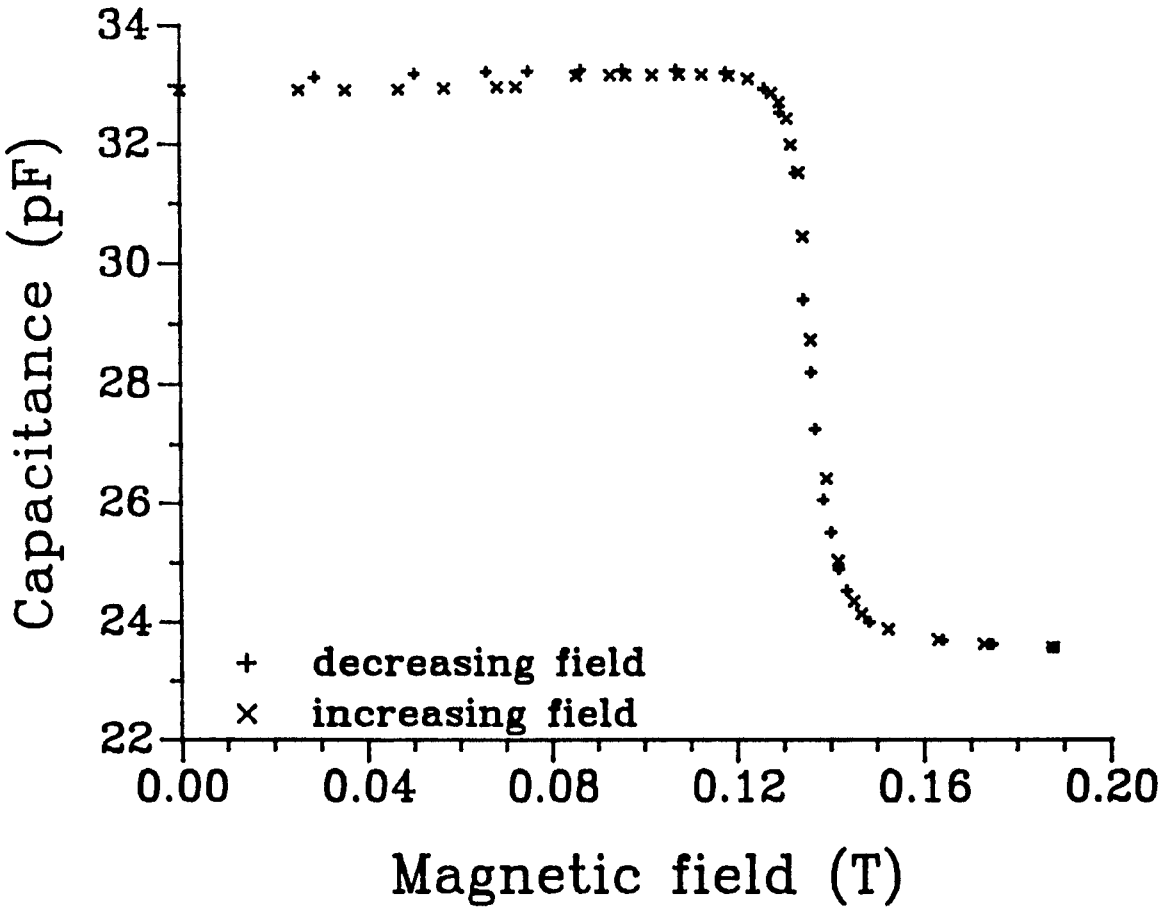

Fig. 19. Experimental results for the magnetic field induced bend transition. A voltage of 6.42V has been applied to stabilize the initial alignment.

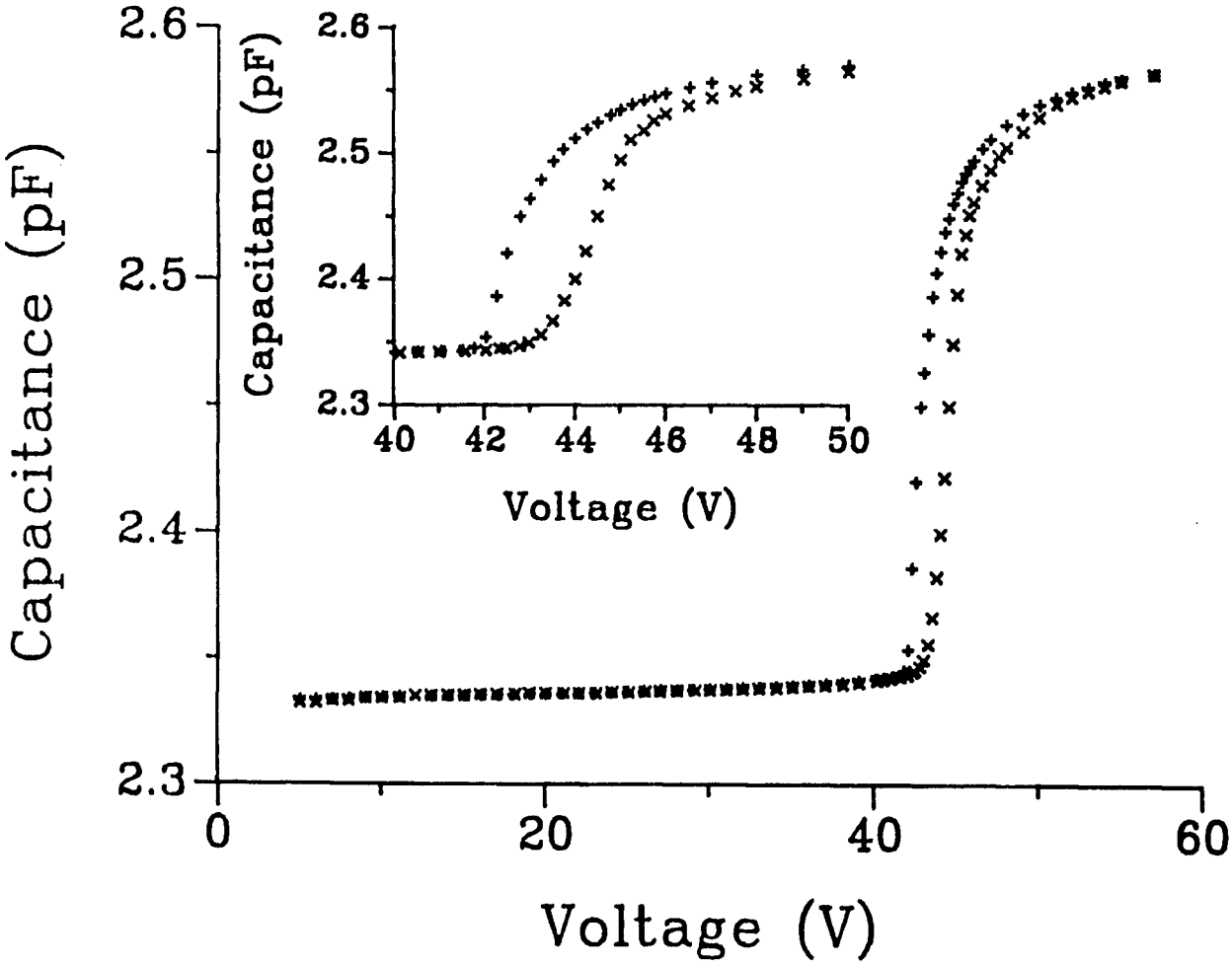

Fig. 20. Experimental results for electric field induced bend transition. A magnetic field of 0.12T has been applied to stabilize the initial alignment. The temperature is 33.4°C. The inset shows detail of the hysteresis. (x-increasing field, +-decreasing field).

Table IV. Comparison of theoretical and experimental data for the electric field induced bend and twist Freedericksz transitions. B is the applied magnetic field, V_{th} is the threshold voltage for the transition and ΔV is the width of the transition.

Transition Geometry	Temperature (°C)	B (T)	Theory		Experiment	
			V_{th}(V)	ΔV(V)	V_{th}(V)	ΔV(V)
Bend	33.4	0	6.14	0.50	5.1±.1	0.5±.1
		0.12	46.9	19	43.5±.1	1.8±.1
Twist	22.5	0	6.62	1.39	7.8±.1	0.5±.1
		0.12	57.1	38.5	50±.1	0.5±.1

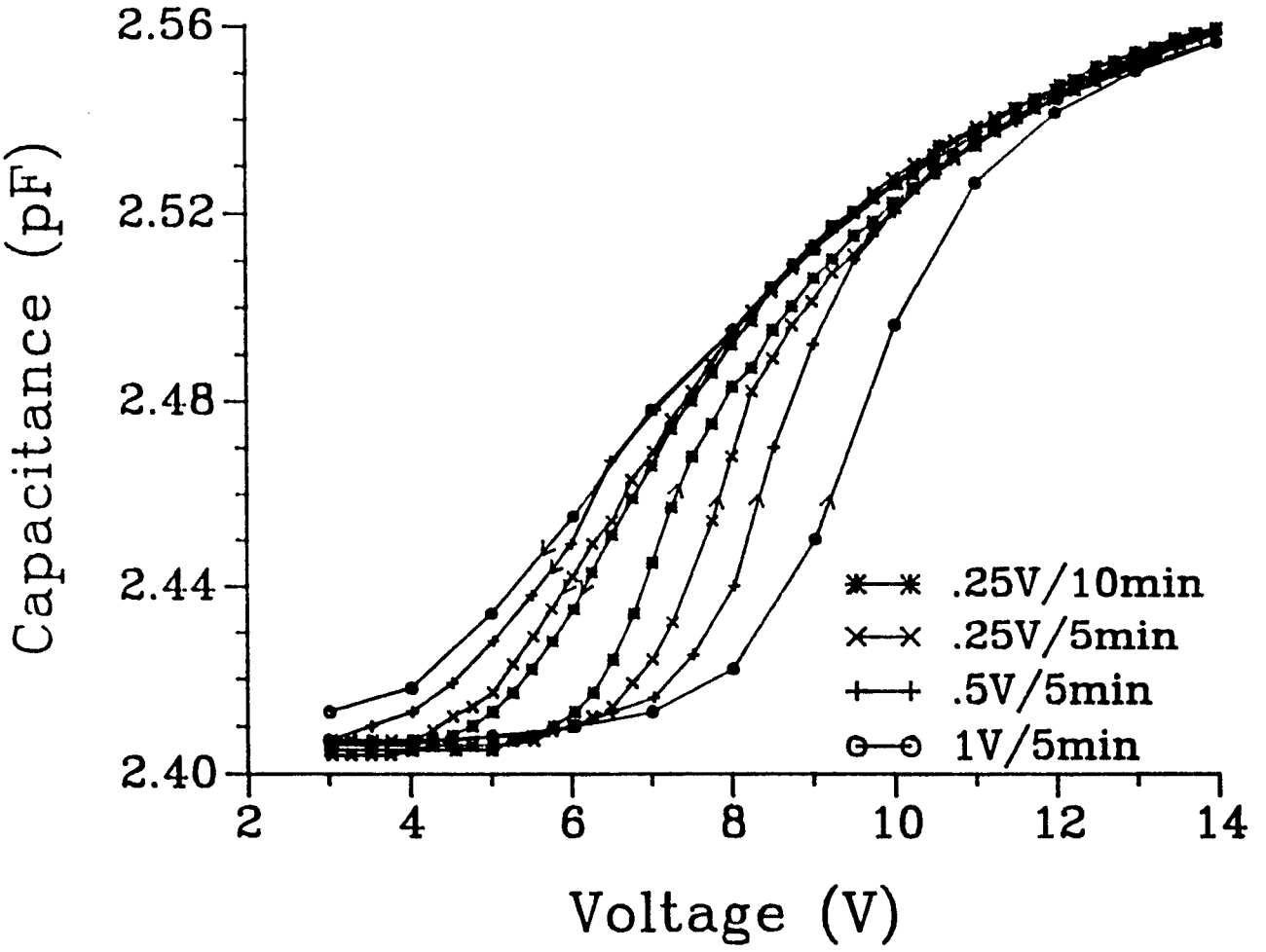

Fig. 21. Experimental results for the electric field induced twist transition at various ramping speeds.

electronics. This was typically on the order of 1×10^{-3} pF/day.) According to the results shown in Fig. 21, the hysteresis will tend to zero at infinitely small run speeds. Attempts have been made to investigate experimental reasons for this discrepancy from a theory which was so successful in the case of the bend transition.

The first experimental aspect considered was the homogeneous planar boundary alignment required for a twist cell. In this case, the director rotates in the plane of this boundary and the deformation is opposed by the in-plane rather than the out-of-plane anchoring of the director. The in-plane anchoring potential is typically smaller than the out-of-plane one by a factor of ~10. A related problem is that there seems to be a difference in the stability of the alignment for glass treated with silane (homeotropic alignment) and glass treated with PVF (planar alignment). The alignment of samples made with glass treated with PVF seems to deteriorate over a time period of weeks while the alignment of samples made with glass treated with silane persists unchanged over a period of months.

The usual calculation of the threshold characteristics for the Freedericksz transition involves the assumption that the anchoring is infinitely strong. This calculation can be extended to include finite anchoring by introducing an anchoring potential per unit area

$$W(\theta) = \frac{1}{2} W_o \theta^2. \qquad [4.23]$$

A finite anchoring potential leads to a nonzero angle θ_o at the boundary between the director and the direction of the alignment or easy axis. When the anchoring term is included, the twist free energy (in units of $\frac{AK_2\pi}{2l}$ with z scaled by l/π) is given by

$$\mathbb{F} = \int_0^{\pi} dz \left\{ \theta'^2 - \frac{e/u}{1 - u \sin^2\theta} - h \cos^2\theta + \frac{W_o \theta^2}{K_2} \left[\delta(z=0) + \delta(z=\pi) \right] \right\} \qquad [4.24]$$

where $\frac{e}{u} = \frac{\epsilon_o \epsilon_\perp \mathbb{V}^2}{K_2} \left[\frac{l}{\pi d} \right]^2$ and $h = \frac{\Delta\chi B^2}{\mu_0 K_2} \left[\frac{l}{\pi} \right]^2$. A trial solution is

$$\theta = \theta_o + (\theta_m - \theta_o) \sin z. \qquad [4.25]$$

The angle θ_o can be determined from the boundary conditions which result from

minimizing the free energy

$$K_2\theta' - W_o\theta = 0 \Rightarrow K_2\,(\theta_m - \theta_o)\,\frac{\pi}{l} - W_o\theta_o = 0. \qquad [4.26]$$

and thus

$$\theta_o = \frac{\theta_m}{1+\frac{lW_o}{K_2\pi}} = \frac{\theta_m}{1+\omega}.$$

Expanding the free energy in θ up to order ${\theta_m}^6$ and ${\theta_o}^2$, yields

$$\mathcal{F} = a{\theta_m}^2 + \frac{b}{2}{\theta_m}^4 + \frac{c}{2}{\theta_m}^6 \qquad [4.27]$$

where

$$a = \frac{\omega}{1+\omega} - \frac{(e-h)}{\pi^2}\,\frac{2+\omega^2}{(1+\omega)^2}$$

$$b = -\frac{1}{2}\left[\frac{(3u-1)e+h}{\pi^2}\right]\frac{11-2\omega+\omega^2}{(1+\omega)^2}$$

and

$$c = \frac{1}{8}\left[-(15u^2-10u+\frac{2}{3})\frac{e}{\pi^2} + \frac{2}{3}\frac{h}{\pi^2}\right]\frac{28-4\omega+\omega^2}{(1+\omega)^2}.$$

These expressions reduce to the previous results as $\omega \rightarrow \infty$. Out of plane anchoring strength for 5CB is $\sim 3\text{x}10^{-4}\text{J/m}^2$ [Gleeson and Palffy-Muhoray, 1989], so that with $K_2 \sim 3\text{x}10^{-12}$N and $l = 5\text{x}10^{-4}$m, $\omega \sim 10^4$. Thus, allowing for finite anchoring does not appreciably change the characteristics of the phase transition.

Another possibility is that adjacent domains of opposite orientation form during the transition, and eventually anneal into a uniform sample. These transient domains are often associated with Freedericksz transitions (more in Chapter 5). Regions of misalignment were occasionally observed in the twist cell, though mainly when the voltage was swept quickly through the threshold voltage. It is possible that the evolution and movement of these domains obscures the hysteresis of the twist transition. With this conjecture in mind, a more careful proceedure was developed to check for hysteresis in the capacitance. The voltage was held constant at a voltage below the transition while a magnetic field was applied at an angle about 5° off of the initial alignment. In this way, the symmetry of the deformation is broken and the formation of domains as the cell goes through the Freedericksz transition is suppressed. The voltage was then increased to a value well above the transition for zero magnetic field and the

capacitance was allowed to equilibriate. After equilibriation, the magnetic field was slowly decreased. After equilibriating again at this high voltage without the magnetic field, the voltage was ramped down to a voltage V_1 halfway through the transition and the capacitance was allowed to equilibriate again to C_{high}. Keeping the voltage constant, the magnetic field was increased to realign the sample, after it was decreased the capacitance was allowed to equilibriate to C_{low}. The difference between C_{high} and C_{low} was taken to be due to hysteresis. In this way, the capacitance difference between the high and low state could be measured without changing the voltage. This was advantageous because the hysteresis seemed to be sensitive to electrical and physical noise. Following this method, a small (~.006pf) hysteresis was measured in the twist cell at 7.25 V (B=0.0T) in an experiment lasting 4 hr.

In principle, it should be easier and more accurate to measure the hystersis optically as this probes a smaller area of the cell. Thus the results should not be affected by defects in the cell as long as a defect-free region can be selected. In practice, it is not possible to measure the twist transition optically as the polarization of the light follows the optic axis of the sample and reemerges parallel to the incident direction of polarization. (This adiabatic approximation holds as long as the length scale of the deformation is longer than the wavelength of light.) In the case of the bend transition, the transition is to a modulated rather than uniform phase and optical detection is obscured by the periodic variations in the local anisotropy. (The modulated phase observed in conjunction with the electric field induced bend transition will be described in Chapter 5.)

Optical methods were used to measure the transition voltage as a function of applied field. Fig. 22 shows results for the electric field induced bend transition voltages as a function of magnetic field for T=33.4°C. The transition was indicated by an abrupt increase in the intensity of light transmitted by the sample between crossed polarizers (as described in Chapter 3). These data for the threshold voltages can be compared to

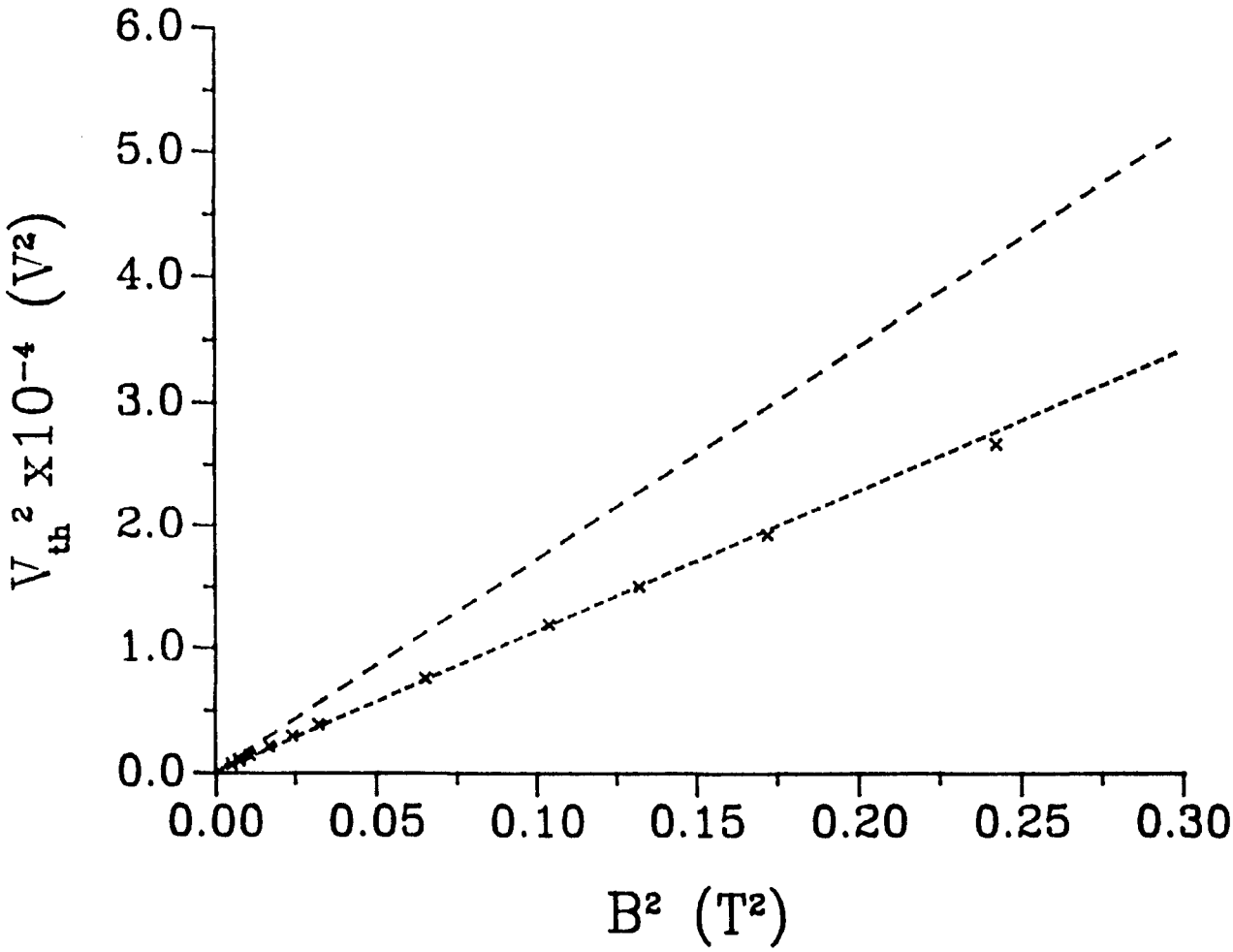

Fig. 22. Threshold voltage as a function of magnetic field for the electric field induced bend transition. For the dashed line, $\Delta\chi$=1.22x10^{-6} MKS [Frisken et al., 1986], u=.453 and $\epsilon_\perp$u=3.94 [Dunmur et al., 1978]. For the dotted line, $\Delta\chi$=.968x10^{-6}mKs [Buka and de Jeu, 1982], u=.544 and $\epsilon_\perp$u=3.97 [Ratna and Shashidhar, 1977].

the values calculated by exact minimization of the free energy as outlined in Section 4.1 (iv), but agreement with theory depends critically on the values of elastic, dielectric and diamagnetic constants used. This critical dependence on material parameters is shown in Fig. 22 where the dashed and dotted lines show two curves calculated for different values of physical constants taken from different sources. The agreement of the data with the second set of parameters is probably fortuitous rather than indicative of the accuracy of this particular set of parameters as it was found that these slopes could be made to vary by significant amounts by making slight changes in the temperature even within the same source of material parameters.

Chapter 5: Modulated Phases

5-1: Summary of Modulated Phases in Nematics

The initial goal of this thesis was to investigate the effect of two perpendicular fields on the molecular and long range orientational order of a nematic liquid crystal. As discussed in Chapter 3, it was observed that as a transverse electric field was applied to a homeotropic nematic sample, the light intensity transmitted by the sample between crossed polarizers increased and that this increase was adequately explained by continuum theory. At higher fields, the sample reoriented. In order to investigate the transition region more carefully, slower voltage sweeps were made. During these runs, a line of diffraction spots was noticed, and it was discovered that the uniform nematic phase had deformed into a phase in which the director was modulated in space.

This discovery was unexpected and led to interesting theoretical and experimental investigations of the properties of the modulation. These will be discussed in the following sections, but first, a brief review of the types and mechanisms of modulated phases in nematics is provided to help put this discovery in perspective.

There are two main classes of modulated phases in nematics, distinquished by the presence or absence of material flow within the sample.

The first class can be further categorized by the mechanisms responsible for creating the flow. Flow can be attributed to charges injected at the electrodes. Flow can result from the formation of space charges inside the sample which is caused by dielectric and conductive effects. Modulated structures are sometimes seen in conjunction with the reorientation of the molecules in a field, especially if the field is applied quickly, and these are associated with a coupling of flow and reorientation - this last example is a transient effect and disappears as realignment is completed. The first and second mechanisms require the action of an electric field; the third can occur for any reorienting field. The different mechanisms can be distinquished by their

dependence on the frequency of the applied field, by their dependence on the presence of a magnetic field and by their dependence on time. The first two mechanisms received a great deal of attention early in the study of liquid crystals, with a more recent resurgence of interest in these effects due to connections with the fields of turbulence and chaos. Transient effects and stable, non-flow related modulations are a more recent topic of investigation. The mechanisms will be discussed briefly below.

A dc or very low frequency ac (< 10 Hz) voltage applied to a sample can result in an instability at a threshold voltage which is of the order of a few volts. The applied voltage is found to cause injection of carriers at the electrodes of the sample cell [Nakagawa and Akahane, 1983a and 1983b] and the effect is frequency dependent because carrier injection is suppressed at higher frequencies. The forces caused by the external field applied to the non-uniform carrier concentration leads to convective flows. This instability can be observed in isotropic liquids, in the nematic phase of liquid crystals and for nematics of both positive and negative dielectric anisotropy. It was first described by Felici [1969] and is similar to the Benard instability which occurs in liquids and is attributed to the competing effects of temperature gradient and gravitational effects.

The second mechanism for instabilities occurs mainly in nematics where the conductivity anisotropy and the dielectric anisotropy have opposite sign so that there is a possibility of a competition between the effects due to these two material parameters [Williams, 1963]. These instabilities are usually studied at frequencies greater than $\sim$ 20 Hz so that the possibility of carrier injection is diminished. The competition of conductive and dielectric anisotropies leads to the formation of space charge in the sample, the resulting field causes a flow of ions through the liquid crystal. The director is reoriented by the flow, disrupting the initial alignment. A schematic diagram of the standard experimental configuration is shown in Figure 23. The cell typically consists of a nematic liquid crystal between two glass plates which are coated by transparent

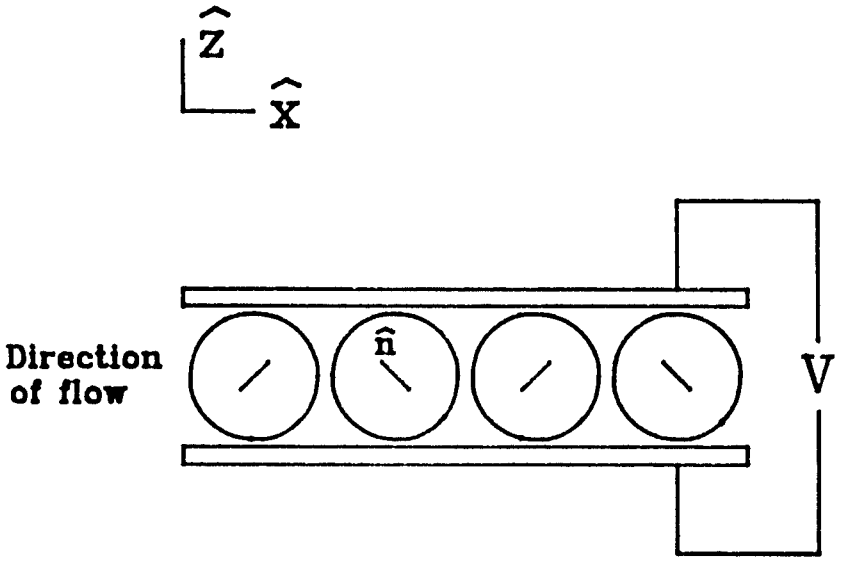

Fig. 23. Cell geometry for observation of Williams domains.

electrodes and are treated so that the director lies in the plane of the glass, along $\hat{x}$. The thickness of the cell is usually of the order of $50\mu m$. A voltage is applied between the electrodes; at 60 Hz in the liquid crystal MBBA, the threshold voltage for the instability is about 6.7 V. The instability results in a periodic distortion of the director with a wavevector along $\hat{x}$ and a wavelength on the order of the cell thickness. At voltages just above the threshold voltage, the sample is composed of cylindrical domains, called Williams (or Williams-Kapustin) domains. Because the material is birefringent, these convective cells are easily visible. The threshold voltage for the instability is observed to increase with frequency [The Orsay Liquid Crystal Group, 1970], essentially because a larger field is necessary to compensate for the shorter time period available for space charge build-up. At larger voltages, more complex structures are observed [Joets and Ribotta, 1986]. Because the instability involves a realignment of the director, the threshold for this effect is affected by a stabilizing magnetic field. The threshold voltage increases and the period decreases as the magnetic field is increased [Berman et al., 1976].

Spatially periodic, transient instabilities are often observed in a sample undergoing a Freedericksz transition [de Jeu et al., 1972; Carr, 1977; Guyon et al., 1979; Hurd et al., 1985]. Even though both the initial and the final equilibrium states are spatially uniform, the transition from one to the other can involve the formation of adjacent domains with opposite reorientation. The resulting textures eventually relax to a uniform state and the dynamics of the formation have been discussed in terms of the elastic and viscous anisotropy, the field strength and the boundary conditions of the sample. Interest in this phenomenon has revived with the study of lyotropic liquid crystals. These systems are characterized by longer relaxation times so that the textures are longer lived and more dramatic than in the case of thermotropic liquid crystals. It is still a relatively short lived phenomenon; even in the lyotropics, the domains form on time scales on the order of 20-40 s.

The second class of modulated phases are equilibrium states and do not involve flow; two types have previously been reported. Both are associated with large elastic constant anisotropy.

The first was reported by Cladis and Torza [1975] and involves the observation of a stable, striped phase as a bent nematic is cooled into the smectic A phase. Further experimental and theoretical analysis is discussed by Chu and McMillan [1977], Gooden et al. [1985] and Allender and Hornreich [1987]. A bent nematic is obtained either by applying a magnetic field perpendicular to the initial homeotropic alignment, thus forcing a reorientation of the sample, or by preparing a sample with homeotropic boundary conditions on one plate and planar boundary conditions on the other. As the smectic A transition is approached from above, the elastic constants associated with bend (K_3) and twist (K_2) deformations diverge. The bend deformation is unfavorable energetically and the director splays out of the plane defined by the field and the direction of the director at the boundary. In this case the transition to the modulated phase occurs above the threshold field for the Freedericksz transition; the stripes grow out of the deformed nematic as the elastic constants diverge. It has been found that the wavelength of the deformation is somewhat smaller than the sample thickness and that the wavelength decreases with increasing field.

The second observation of a stable periodic phase was made more recently by Lonberg and Meyer [1985]. In this case, a periodic twist-splay deformation replaces the expected uniform splay distortion at the Freedericksz transition in a polymer liquid crystal where the splay elastic constant is much larger than the twist elastic constant. The experimental conditions are those of the traditional splay Freedericksz transition; the polymer is contained between two glass plates treated to induce planar alignment at the boundaries and a magnetic field is applied perpendicular to the plates. Instead of the expected uniform distortion, over a time period of several hours in a field greater than the critical field a periodic phase develops. This periodic phase is also

characterized by a director which has a component perpendicular to the plane defined by the initial alignment and the field; this configuration reduces the deformation energy associated with the large splay elastic constant. Lonberg and Meyer [1985] were also able to show that the wavelength of the distortion is expected to decrease with decreasing splay constant, going to zero at $K_1/K_2 \sim 3.3$. However, it is difficult to find experimental systems where this parameter can be varied by substantial amounts. Further theoretical studies [Miraldi et al., 1986; Zenginoglou, 1987] have investigated the role of weak anchoring and a stabilizing field in this deformation.

5-2: Experimental Results and Discussion

In the case of the electric field induced bend transition when the competing magnetic field is nonzero, we have observed that the transition is not to a uniform but rather to a modulated phase. Figure 24 shows this modulated phase, viewed along the magnetic field direction ($\hat{z}$) with a single polarizer oriented with its direction of polarization parallel to the direction of the electric field ($\hat{x}$). The value of the magnetic field here is 0.33 T. The wavevector of the stripes is primarily in the direction of the electric field, and we have observed wavelengths ranging from 0.2 l to 1.1 l in a variety of cells under different conditions (for the example shown, $l = 0.5$ mm and the width of the sample is d = 5.3 mm). For voltages slightly above the threshold ($\sim$ 3 - 5 %) the stripes form slowly ($\sim$10 min) and persist indefinitely. If the voltage is increased, the stripes disappear. Details of the experimental studies of this deformation will be discussed in this section. The last section will describe the theory. Modulated structures were not observed in association with either the magnetic field induced bend transition or the electric field induced twist transition.

The modulated phase observed in conjunction with the electric field induced bend transition was studied optically. The sample was illuminated with a uniform white light source. A Wild KM339 travelling telescope was used for direct observation. To photograph the cell, a lens with a focal length of 50 cm was used to magnify and focus the image onto Kodak TMAX film in a 35 mm Nikon FG camera. Photos were taken at ASA 1600 with exposures of $\sim$ 0.25 s. The film was developed and the photos were printed in house.

As the modulated phase forms slowly, the most uniform examples of the distortion are obtained when the voltage near the transition is increased at a rate $<$ .5 V/hr. The uniformity is also dependent on the cleanliness of the sample and on the uniformity of the thin layer of epoxy between the glass and the electrodes. As the voltage is increased, the first indication of the approach of the transition is that the

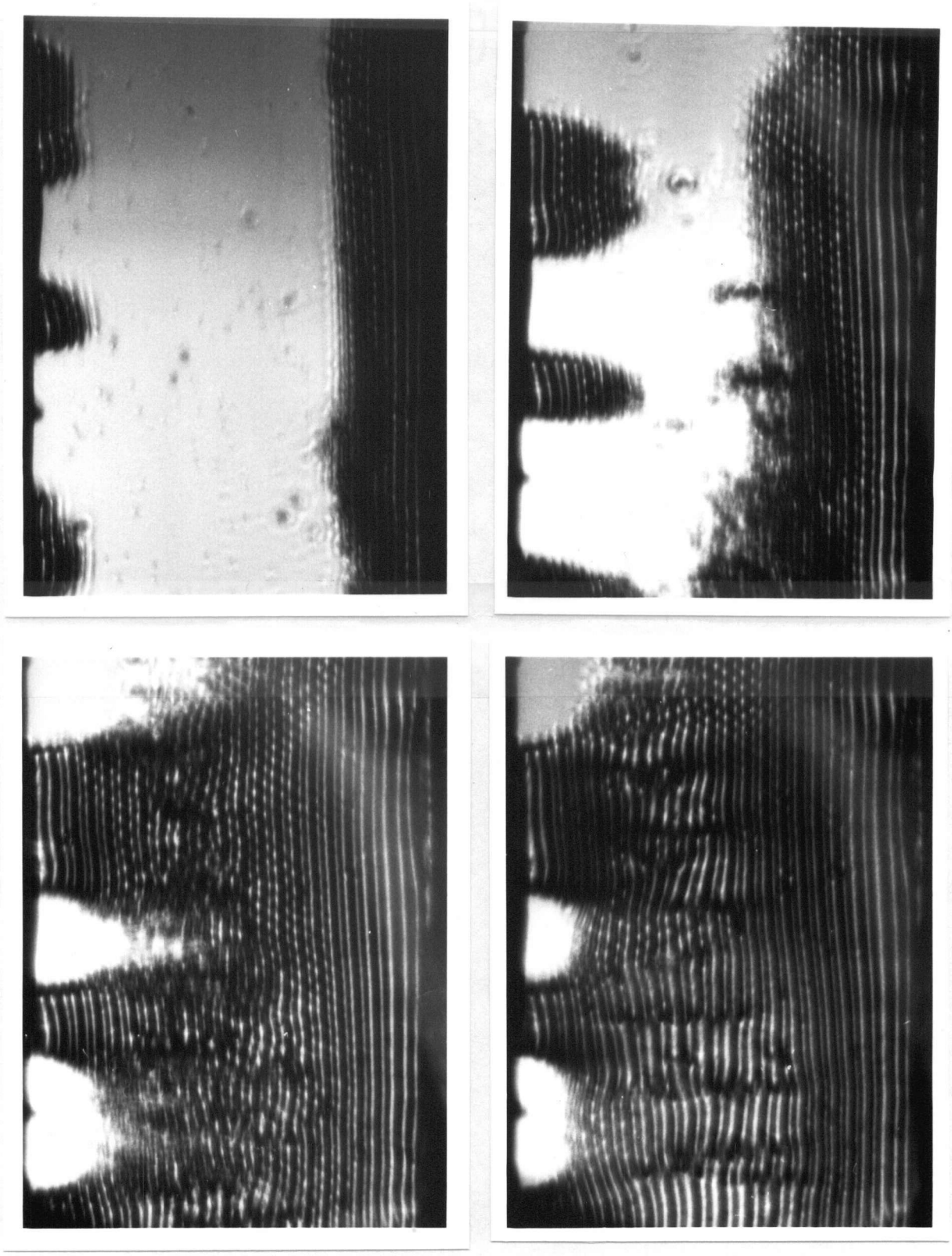

Fig. 24. Photographs of modulated phase.

sample appears to have a more grainy appearance. The grain size grows as the voltage is increased and the dotted pattern seen in the photos of Fig. 24 develops. The stripes grow out of the dotted pattern, basically parallel to the electrodes and perpendicular to the magnetic field; the wavevector of the stripes is along $\hat{x}$. The contrast in the image is best if a single analyzer is used after the cell with its direction of polarization parallel to $\hat{x}$. The transition can be monitored quantitatively by measuring the capacitance, the first visible distortions are accompanied by increases in the capacitance. At higher voltages, the stripes disappear by annealing together, sometimes leaving disclination lines which are slow to disappear. The chronology and geometry of the stripe growth is very reproducible for increasing voltage; the pattern always forms from the same area with similar defects. When the voltage is decreased, the pattern can be quite different; the stripes are not very uniform and they tend to lie along $\hat{x}$, i.e. with a wavevector along $\hat{y}$. This is consistent with the observation that the transition is first order and that the same voltage will be associated with a different θ_m.

When the modulations were first observed, some effort was put into ascertaining whether or not the effect was electrohydrodynamic in nature. The optical properties of Williams domains, the most common electrohydrodynamic modulation, are similar to the domains observed here in that the best contrast is observed when a single analyzer is oriented with its direction of polarization perpendicular to the axis of the domains, and the domains are not visible when this analyzer is oriented parallel to the domains. The most compelling evidence that the domains observed at the electric field induced bend transition are not associated with flow lies in the comparison of the frequency dependence of the two effects. The measurements were generally done with an ac voltage of 1-2 kHz where as Williams domains are typically studied at 50-200 Hz. Figure 25 shows the frequency dependence of the threshold voltage for a cell of width 5.3 mm in the presence of a 0.33 T stabilizing magnetic field. The electrohydrodynamic effects due to both carrier injection and the formation of space charges with

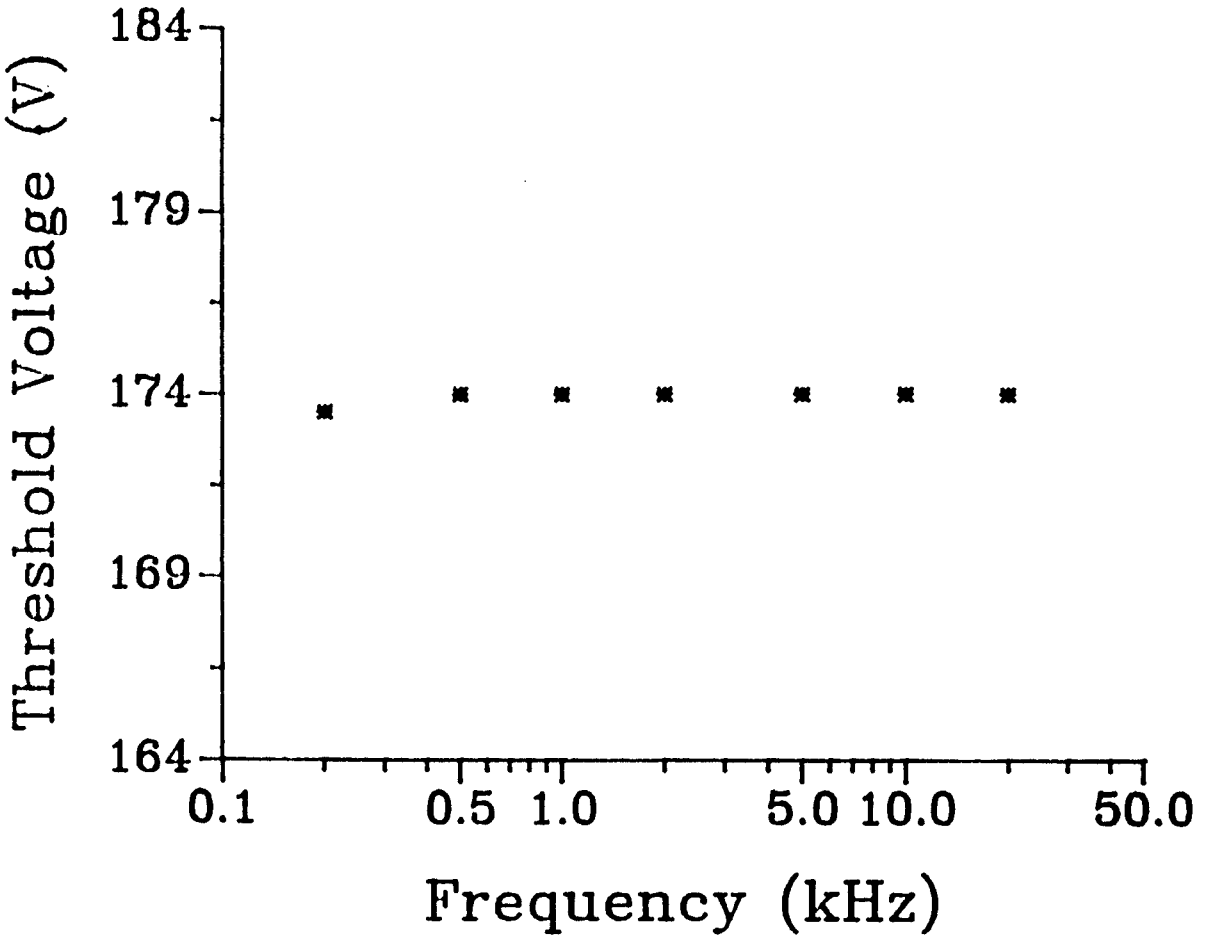

Fig. 25. Frequency dependence of threshold voltage for electric field induced bend Freedericksz transition.

accompanying ion flow are highly frequency dependent, this dependence is absent here where the threshold voltage appears to be essentially constant in frequency over three orders of magnitude. To check the frequency dependence of the threshold for Williams domains, a 40 μm planar cell with homogenous alignment was filled with MBBA, a liquid crystal with negative dielectric anisotropy and positive conductivity anisotropy. Figure 26 shows the frequency dependence of the threshold voltage for Williams domains in this cell, in striking contrast with the results for the stripes observed in conjuction with the electric field induced bend transition. As well, it was obvious that the modulated phase observed here was not a transient effect with associated backflow, as the stripes persist in a stable configuration at constant voltage and magnetic field over a time period of days. Under microscopic observation, the flow of particles can be detected in a Williams domain cell. Unfortunately, such observation was not possible in this geometry.

It is interesting to note that even though the threshold voltage is essentially constant, the nature of the deformation seems to vary somewhat with frequency. At 200 Hz, the stripes start in the center of the 5.3 mm cell, while for higher frequencies the tendency is for the stripes to start along the walls. At lower frequencies of 200 and 500 Hz, the beaded phase is not noticeable, at 1 and 2 kHz, the beads precede the vertical stripes while at higher frequencies, the beads persist longer and the sample has a tendency for horizontal stripes.

The wavelengths of the modulations were measured from the film with the aid of a microscope with a micrometer driven x-y translation stage. The wavelength increases slightly as the voltage is increased but the magnitude of the applied magnetic field has the most noticeable effect. Figure 27 shows the dependence of the inverse wavelength on the magnitude of the magnetic field for two cells of different width. The linear relationship between the inverse wavelength and the applied field is in agreement with the wavelength dependence of the modulated deformations discussed in the last section.

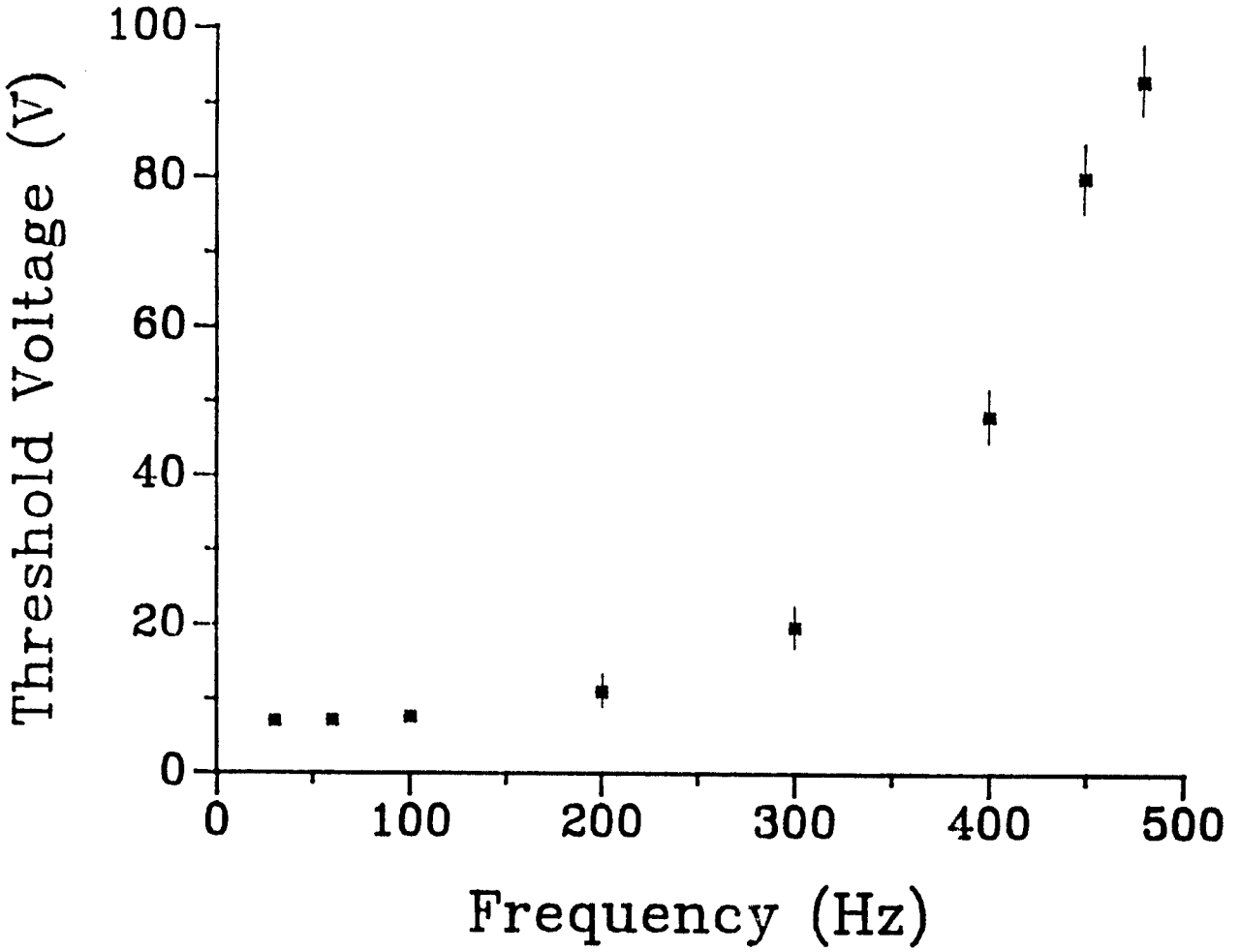

Fig. 26. Frequency dependence of threshold voltage for Williams domains.

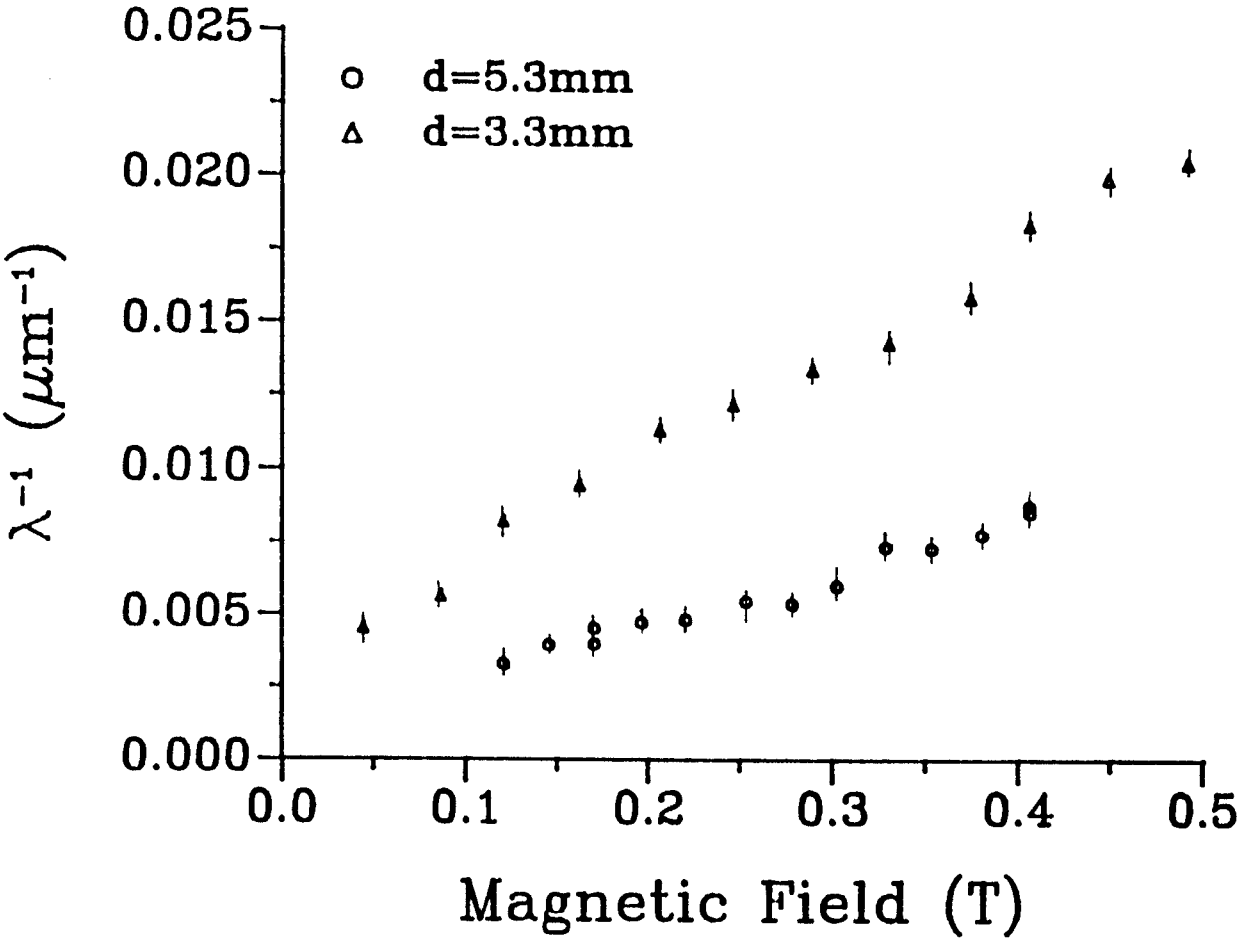

Fig. 27. Effect of magnetic field on inverse wavelength λ^{-1} for two cells of different width d.

The periodic modulated deformation observed here is significantly different from other modulated phases. It is a static, equilibrium deformation in the same class as the stable modulated phases observed by Lonberg and Meyer [1985] and Cladis and Torza [1975]. In contrast to these two stable phases, however, the modulated phase observed during the electric field induced bend transition is characterized by the director staying in the plane of the initial orientation and the fields. The conditions necessary for the existence of this phase are discussed in the next section.

5.3: Theory

Complete theoretical treatment of these stable periodic structures involves solving the Euler-Lagrange equations, a set of coupled nonlinear equations, for the deformation which minimizes the Frank free energy. As it turns out, this is not a very tractable approach, and so a variety of simplifications have been made in attempting to obtain solutions corresponding to the stable modulated phases outlined above. The periodic distortion associated with splay avoidance is the easiest to solve as the transition to the modulated phase precedes the transition to the uniform phase. As the transition is second order, the distortion amplitude should be small close to the transition making it possible to linearize the equations and solve for the corresponding deformation [Lonberg and Meyer, 1985]. On the other hand, the periodic phase associated with the bend Freedericksz transition with diverging bend elastic constant takes place at a field slightly higher than that at which the transition to a uniform distorted phase occurs. The second transition occurs when the uniform phase becomes unstable to the formation of a periodic phase. Solving this problem involves testing the local stability of the uniform distorted phase to a periodic modulation using an experimentally motivated form of the distortion [Allender and Hornreich, 1987]. Recent computational results minimizing the free energy for a finite dimensional director field also offer solutions to these problems [Cohen et al., 1986; Cohen, 1988].

The experimental studies made on the stable periodic structure observed as part of this work on the electric field induced bend transition suggest that this Freedericksz transition is directly to a modulated phase. However, as the transition is first order, the assumption that the distortion is small at threshold is not valid. As a first attempt at the theoretical solution to this problem, it can be shown that a modulated distortion can give a lower free energy than a uniform distortion [Allender et al., 1989]. These calculations are outlined below. Future work will include optimizing the form of the distortion to give the lowest free energy.

First it is worth discussing what may be learned from a theoretical treatment of the periodic distortion. Summarizing the experimental observations:

- the stripes are observed in the electric field induced bend transition, but not in the electric field induced twist transition,
- they develop as the sample is reorienting and disappear at higher voltages and
- the wavelength of the distortion decreases with increasing magnetic field.

It is interesting to note the correlation between the existence of the modulated phase and nonzero values of the $\hat{z}$ component of the electric field in the sample, E_z, given by

$$E_z = -\frac{u\, n_x n_z\, E_x}{1 - u\, n_x^2} \qquad [5.1]$$

where

$$\hat{n} = (\sin\theta, 0, \cos\theta). \qquad [5.2]$$

Below the transition, $n_x = 0$ and there is no modulation. Above the transition, n_x is close to unity and $n_z = 0$. The modulated phase exists in the transition region where E_z is nonzero.

In analyzing this distortion, the director is assumed to be in the $\hat{z}$-$\hat{x}$ plane, defined by the boundary conditions and the applied fields. The director lies at an angle θ with respect to the $\hat{z}$ axis. In previous calculations, the angle θ was assumed to depend only on z. Now, however, the angle θ is allowed to depend on x as well as z, i.e. $\theta = \theta(x,z)$. The free energy due to elastic deformation and field effects (in units of $K_3\left[\frac{\pi}{d}\right]^2$) now takes the form

$$\mathbb{F} = \frac{1}{2}\int d^3r\left\{(K+\kappa\sin^2\theta)\theta_x^{\,2} + \kappa\sin 2\theta\, \theta_x\theta_z + (1-\kappa\sin^2\theta)\theta_z^{\,2} - \frac{e}{1-u\sin^2\theta} + h\cos^2\theta\right\} \qquad [5.3]$$

where $\theta_x = \frac{\partial\theta}{\partial x}$ etc. and the coordinates are expressed in units of $\frac{\pi}{l}$. Here we define $K = \frac{K_1}{K_3}$, $\kappa = 1 - K$, and recall that $e = \frac{\epsilon_o\epsilon_\perp V^2}{K_3}\left[\frac{l}{\pi d}\right]^2$ and $h = \frac{\Delta\chi B^2}{\mu_o K_3}\left[\frac{l}{\pi}\right]^2$.

$\theta(x,z)$ can be written as the sum of the solution of the unmodulated phase θ_o and a modulation term θ_1

$$\theta(x,z) = \theta_o(z) + \theta_1(x,z). \qquad [5.4]$$

For simplicity, we approximate θ_o by $\theta_o(z) = \theta_m \sin(z)$ as before and use a trial function for θ_1 of the form

$$\theta_1 = \delta\theta \left[\cos(z)\cos(qx) + r\sin(2z)\sin(qx)\right]. \qquad [5.5]$$

The amplitude $\delta\theta$ is assumed to be small and r and q are variational parameters. The free energy is expanded in $\delta\theta$ to order $(\delta\theta)^2$ and then in θ_m to order ${\theta_m}^6$. The resulting expression for the free energy is

$$F = F(\theta_o) + \frac{\pi(\delta\theta)^2}{4}\left[-\alpha - 4\beta r^2 + \frac{1}{2}(1+4r^2) - \kappa(\gamma+4\delta r^2) - \kappa\frac{rq}{2}\eta + \frac{\kappa q^2}{8}(\mu+4r^2\nu) + \frac{Kq^2}{2}(1+r^2)\right]$$

where

$$c_o = eu - h \qquad [5.6]$$

$$c_1 = 3eu^2 - c_o$$

$$c_2 = 15eu^3 - 10eu^2 + \frac{2}{3}c_o$$

$$c_3 = 7eu^4 - 7eu^3 + \frac{7}{5}eu^2 - \frac{1}{45}c_o$$

$$\alpha = \frac{1}{2}c_o + \frac{3}{4}c_1{\theta_m}^2 + \frac{5}{16}c_2{\theta_m}^4 + \frac{35}{32}c_3{\theta_m}^6$$

$$\beta = \frac{1}{8}c_o + \frac{1}{8}c_1{\theta_m}^2 + \frac{5}{128}c_2{\theta_m}^4 + \frac{7}{64}c_3{\theta_m}^6$$

$$\gamma = \frac{3}{4}{\theta_m}^2 - \frac{5}{16}{\theta_m}^4 + \frac{7}{144}{\theta_m}^6$$

$$\delta = \frac{5}{16}{\theta_m}^2 - \frac{5}{64}{\theta_m}^4 + \frac{49}{(144)(40)}{\theta_m}^6$$

$$\eta = 3\theta_m - \frac{5}{3}{\theta_m}^3 + \frac{7}{24}{\theta_m}^5$$

$$\mu = 3{\theta_m}^2 - \frac{5}{6}{\theta_m}^4 + \frac{7}{72}{\theta_m}^6$$

$$\nu = \frac{1}{2}{\theta_m}^2 - \frac{5}{48}{\theta_m}^4 + \frac{7}{720}{\theta_m}^6$$

If the coefficient of the $(\delta\theta)^2$ term is negative, the periodic solution is more stable than the uniform solution.

Minimizing the free energy with respect to q and r to optimize these parameters yields a quadratic equation for r^2 in terms of the above parameters, and an equation for q in terms of r:

$$16\,(1 - 2(\beta-\delta\kappa))\,(\kappa\nu+K)^2\,r^4 + 8\,(1 - 2(\beta+\delta\kappa))\,(\kappa\mu+4K)\,(\kappa\nu+K)\,r^2 + (1 - 2(\beta+\delta\kappa))\,(\kappa\mu+4\kappa)^2 - \frac{\kappa^2\eta^2}{4}\,(\kappa\mu+4K) = 0 \qquad [5.7]$$

and $$q = \frac{2\kappa r\eta}{\kappa(\mu+4r^2\nu)+4K(1+r^2)} \qquad [5.8]$$

The range of e for which metastable unmodulated solutions of the Landau free energy exist was examined for solutions to Eqn. [5.7] and Eqn. [5.8]. The modulation makes a negative contribution to the free energy for a range of u values, when .15<K<.8 and h = 0.0 for a range of e around the value of e at the first order transition. For example, for K=.5, the contribution to the free energy is negative for .682<u<.688. Figure 28 shows the dependence of θ_m, the free energy and the wavelength of the deformation on the parameter e.

The theory described above shows that a periodic distortion of the form assumed can minimize the free energy for certain values of the parameters. The form of the distortion assumed may not be appropriate when considering the effect of the magnetic field as including a magnetic field term decreases the range for which a periodic solution exists. Future work will attempt to examine a broader class of functions in order to better describe the deformation.

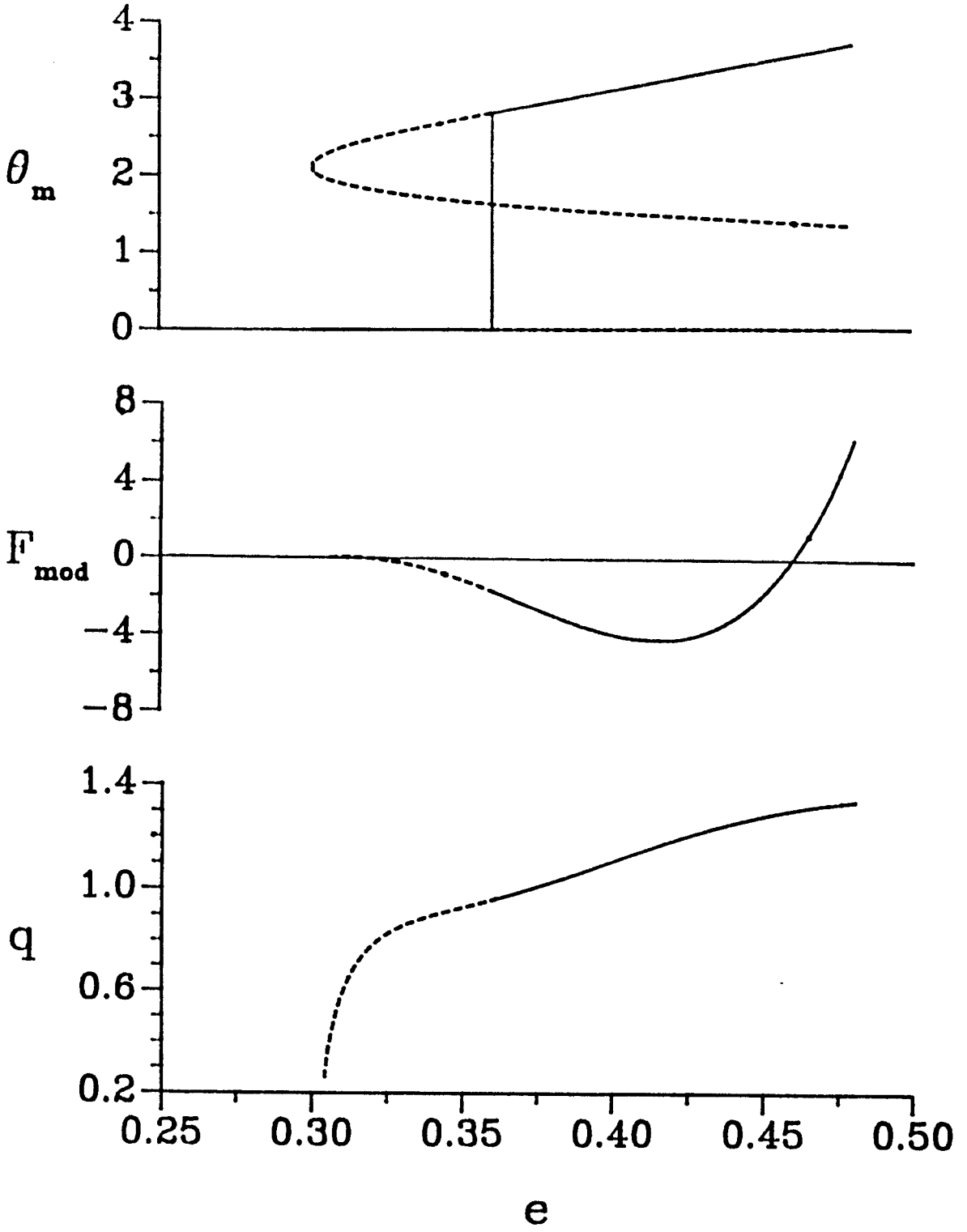

Fig. 28. Dependence of θ_m, the free energy due to the deformation F_{mod} and the wavenumber q of the deformation on the voltage parameter e. $e = \frac{\epsilon_o \epsilon_\perp V^2}{K_3} \left[\frac{l}{\pi d}\right]^2$.

Chapter 6: Conclusions

Several aspects of the interaction of electric and magnetic fields with nematic liquid crystals have been studied.

For the first time, a SQUID magnetometer has been used to study the order parameter of a nematic liquid crystal by measuring the diamagnetic susceptibility. The results are consistent with those of other authors, both in absolute and relative accuracy. Proposed modifications to the experimental apparatus could significantly improve the sensitivity of the magnetometer. Further work could usefully involve the study of the effect of the magnitude of the aligning field on the order parameter.

Mean field theory has been used to study the phase behavior of nematics in the presence of arbitrarily oriented electric and magnetic fields. Calculations of the field dependence of the order parameters and the transition temperatures have been carried out. The results have been used to estimate how the molecular ordering induced by a transverse electric field in a sample of nematic 5CB in the presence of a stabilizing magnetic field would affect the optical properties of the sample.

The effect of a transverse electric field on the director fluctuations in a homeotropically aligned sample of nematic 5CB in the presence of a stabilizing magnetic field has been studied. The first observation of field induced biaxiality in a nematic with positive susceptibility anisotropies due to the differential enhancement of director fluctuations has been made. The measured effects of the induced biaxiality are in good agreement with the predictions of continuum theory.

Freedericksz transitions have been studied in geometries involving two fields, where one is applied along the direction of initial alignment to stabilize the alignment and the other is applied perpendicular to this direction to induce the transition. Landau expansions and calculations of deformations which minimize the free energy exactly

both predict that some of these transitions will be first order. Dielectric measurements have been carried out which show clear evidence of hysteresis in the case of the electric field induced bend transition. Results for the electric field induced twist transition show a small hysteresis. Furthermore, the threshold voltages both in the absence and in the presence of a competing magnetic field are in good agreement with theory. The width of the transitions in the presence of a competing magnetic field is significantly less than predicted by theory. This discrepancy is not wholly understood at this time. The discovery of a first order Freedericksz transition suggests the possibility of optical bistability in these systems; exploring this effect with a view toward device applications is an objective for future work.

A new, static modulated phase associated with the electric field induced bend Freedericksz transition has been observed. This phase is different from static modulated phases previously reported in that the nematic director appears to remain in the plane defined by the initial alignment and the distorting field. Theoretical studies demonstrate that for a film in the bend geometry with an electric field in the film plane, the non-periodic Freedericksz state is unstable against the formation of a periodic state having a wave vector parallel to the field for certain values of the physical parameters. Future work will attempt to achieve quantitative agreement with experiment.

Bibliography

1. D.W. Allender and R.M. Hornreich, Phys. Rev. Lett. 59, 2654 (1987).

2. D.W. Allender, B.J. Frisken and P. Palffy-Muhoray, Liq. Cryst., in press (1989).

3. S.M. Arakelyan, A.S. Karayan, and Yu.S. Chilingaryan, Sov. Phys. Dokl. 29(3), 202 (1984).

4. G. Barbero, E. Miraldi, C. Oldano and P. Valabrega, Z. Naturforsch. A. 43, 547 (1988).

5. B. Bergersen, P. Palffy-Muhoray and D.A. Dunmur, Liquid Crystals 3, 347 (1988).

6. A.L. Berman, E. Gelerinter and A. de Vries, Mol. Cryst. Liq. Cryst. 33, 55 (1976).

7. L.M. Blinov, Electro-optical and magneto-optical properties of liquid crystals, John Wiley and Sons Ltd., Chichester, 1983.

8. A. Buka and W.H. de Jeu, J. Physique 43, 361 (1982).

9. A. Buka and L. Bata, Mol. Cryst. Liq. Cryst. 135, 49 (1986).

10. J.D. Bunning, T.E. Faber and P.L. Sherrel, J. Physique 42, 1175 (1981)

11. E.F. Carr, Mol. Cryst. Liq. Cryst. 34, 159 (1977).

12. S.H. Chen and J.J. Wu, Appl. Phys. Lett. 52, 1998 (1988).

13. K.C. Chu and W. L. McMillan, Phys. Rev. A 15, 337 (1977).

14. P.E. Cladis and S. Torza, J. Appl. Phys. 46, 584 (1975).

15. R.A. Cohen, R. Hardt, D. Kinderlehrer, S.Y. Lin and M. Luskin, Minimum energy configurations for liquid crystals: computational results, Theory and applications of liquid crystals, IMA Volumes in math. and appl. 5 (J.L. Ericksen and D. Kinderlehrer, eds), Springer-Verlag, 1987.

16. R.A. Cohen, Ph.D. Thesis, University of Minnesota, 1988.

17. E.P. Day, Ph.D. Thesis, Stanford, 1972.

18. P.G. de Gennes, C.R. Acad. Sci. Ser. B 266, 15 (1968).

19. P.G. de Gennes,The Physics of Liquid Crystals, Oxford University Press, Oxford, 1974.

20. W.H. de Jeu, C.J. Gerritsma and Th.W. Lathouwers, Chem. Phys. Lett. 14, 503 (1972).

21. W.H. de Jeu and W.A.P. Claassen, J. Chem. Phys. 68, 102 (1978).

22. H.J. Deuling, Mol. Cryst. Liq. Cryst. 19, 123 (1972).

23. H.J. Deuling and W. Helfrich, Appl. Phys. Lett 25, 129 (1974).

24. D.A. Dunmur, M.R. Manterfield, W.H. Miller and J.K. Dunleavy, Mol. Cryst. Liq. Cryst. 45, 127 (1978).

25. D.A. Dunmur and A.E. Tomes, Mol. Cryst. Liq. Cryst. 97, 241 (1983).

26. D.A. Dunmur, T.F. Waterworth and P. Palffy-Muhoray, Mol. Cryst. Liq. Cryst. 124, 73 (1985).

27. D.A. Dunmur, K. Szumilin and T.F. Waterworth, Mol. Cryst. Liq. Cryst. 149, 385 (1987).

28. S. D. Durbin, S. M. Arakelian and Y.R. Shen, Phys. Rev. Lett. 47, 1411 (1981).

29. C.P. Fan and M.P. Stephen, Phys. Rev. Lett. 25, 500 (1970).

30. L.G. Fel and G.E. Lasene, Sov. Phys. Crystallogr. 31(4), 428 (1986).

31. N.J. Felici, Rev. Gen. Electr. 78, 717 (1969).

32. F.C. Frank, Discuss. Faraday Soc. 25, 19 (1958).

33. V. Freedericksz and V. Zolina, Trans. Faraday Soc. 29, 919 (1933).

34. B.J. Frisken, J.F. Carolan, P. Palffy-Muhoray, J.A.A.J. Perenboom and G.S. Bates, Mol. Cryst. Liq. Cryst. Lett. 3(3-4), 57 (1986).

35. B.J. Frisken, B. Bergersen and P. Palffy-Muhoray, Mol. Cryst. Liq. Cryst. 148, 45 (1987).

36. B.J. Frisken and P. Palffy-Muhoray, Phys. Rev. A 39, 1513 (1989).

37. B.J. Frisken and P. Palffy-Muhoray, Liq. Cryst., in press (1989).

38. W.M. Gelbart, J. Phys. Chem. 86, 4298 (1982).

39. J.T. Gleeson, M.Sc. Thesis, University of British Columbia, 1988.

40. J.T. Gleeson and P. Palffy-Muhoray, Liq. Cryst., in press, (1989).

41. C. Gooden, R. Mahmood, D. Brisbin, A. Baldwin and D.L. Johnson, Phys. Rev. Lett. 54, 1035 (1985).

42. E.F. Gramsbergen, L. Longa and W. H. de Jeu, Physics Reports 135, 195 (1986) and references therin.

43. H. Gruler, T.J. Scheffer and G. Meier, Z. Naturforsch. 27a, 966 (1972).

44. E. Guyon, R. Meyer and J. Salan, Mol. Cryst. Liq. Cryst. 54, 261 (1979).

45. Handbook of Chemistry and Physics, Chemical Rubber Co., Cleveland OH, 1970.

46. F. Hessel and H. Finkelmann, Polymer Bulletin 15, 349 (1986).

47. A.J. Hurd, S. Fraden, F. Lonberg and R.B. Meyer, J. Phys. 46, 905 (1985).

48. A. Joets and R. Ribotta, J. Phys. 47, 595 (1986).

49. A.J. Karn, S.M. Arakelian and Y.R. Shen, Phys. Rev. Lett. 57, 448 (1986).

50. P.H. Keyes, Phys. Lett. 67A, 132 (1978).

51. H. Kneppe, V. Reiffenrath and F. Schneider, Chem. Phy. Lett. 87, 59 (1982).

52. G.F. Kventsel and T.J. Sluckin, Phys. Rev. A 36, 4486 (1987).

53. L.D. Landau and E.M. Lifshitz, Statistical Physics, 3rd. Edition, (Pergamon Press), Chapter XII.

54. F. Lonberg and R.B. Meyer, Phys. Rev. Lett. 55, 718 (1985).

55. W. Maier and A. Saupe, Z. Naturforsch. 13a, 564 (1958).

56. W. Maier and A. Saupe, Z. Naturforsch. 14a, 882 (1959).

57. W. Maier and A. Saupe, Z. Naturforsch. 15a, 287 (1960).

58. B. Malraison, Y. Poggi and E. Guyon, Phys. Rev. A 21, 1012 (1980).

59. J. Malthete, L. Liebert, A.M. Levelut and Y. Galerne, C.R. Acad. Sc. Paris 303 II, 1073 (1986).

60. J.L. Martinand and G. Durand, Sol. St. Comm. 10, 815 (1972).

61. E. Miraldi, C. Oldano and A. Strigazzi, Phys. Rev. A 34, 4348 (1986).

62. S.W. Morris, P. Palffy-Muhoray and D.A. Balzarini, Mol. Cryst. Liq. Cryst. 139, 263 (1986).

63. T. Motooka and A. Fukuhara, J. Appl. Phys. 50, 3322 (1979).

64. M. Nakagawa and T. Akahane, J. Phys. Soc. J. 52, 3773 (1983a).

65. M. Nakagawa and T. Akahane, J. Phys. Soc. J. 52, 3782 (1983b).

66. S.R. Nersisyan and N.V. Tabiryan, Mol. Cryst. Liq. Cryst. 116, 111 (1984).

67. H.L. Ong, Phys. Rev. A 28, 2393 (1983).

68. H.L. Ong, Phys. Rev. A 31, 3450 (1985).

69. H. Onnagawa and K. Miyashita, Japan. J. Appl. Phys. 13, 1741 (1974).

70. Orsay Liquid Crystal Group, Phys. Rev. A 25, 1642 (1970).

71. P. Palffy-Muhoray and D.A. Dunmur, Mol. Cryst. Liq. Cryst. 97, 337 (1983).

72. P. Palffy-Muhoray, J. de Bruyn and D.A. Dunmur, Mol. Cryst. Liq. Cryst. 127, 301 (1985).

73. J. Philo and W.M. Fairbank, Rev. Sci. Instr. 48, 1529 (1977).

74. J. Philo, Ph.D. Thesis, Stanford. 1977.

75. Y. Poggi and J.C. Filippini, Phys. Rev. Lett. 39, 150 (1977).

76. W.H. Press, B.P. Flannery, S.A. Teukolsky and W.T. Vetterling, Numerical Recipes: The Art of Scientific Computing, Cambridge University Press, Cambridge, 1986.

77. R.G. Priest, Phys. Lett. 47A, 474 (1975).

78. B.R. Ratna and R. Shashidhar, Mol. Cryst. Liq. Cryst. 42, 113 (1977).

79. C. Rosenblatt, Phys. Rev. A 24, 2236 (1981).

80. A. Seppen, G. Maret, A.G.M. Jansen, P. Wyder, J.J.M. Janssen and W.H. de Jeu, Springer Proc. Phys. 11, 18 (1986).

81. P.L. Sherell and D.A. Crellin, J. Physique, 40, C3-211 (1979).

82. J.P. Straley, Phys. Rev. A 10, 1881 (1974).

83. M.F. Vuks, Opt. and Spect. 20, 361 (1966).

84. Peng-ye Wang, Hong-jun Zhang and Jian-hua Dai, Opt. Lett. 12, 654 (1987).

85. R. Williams, J. Chem. Phys. 39, 384 (1963).

86. P.J. Wojtowicz and P. Sheng, Phys. Lett. 48A, 235 (1974).

87. L.J. Yu and A. Saupe, Phys. Rev. Lett. 45, 1000 (1980).

88. B. Ya. Zel'dovich, N.V. Tabiryan and Yu. S. Chilingaryan, Sov. Phys JETP 54, 32 (1981).

89. H.M. Zenginoglou, J. Phys. 48, 1599 (1987).

Appendix A:

```
      program nmx
c
c     this program calculates values for the order parameter and
c     temperature of a rod like nematic in crossed fields
c     using the maier saupe model and integrating with the
c     calling function dquank. choose the field strengths
c     and iterate delta to find the order parameters
c
c     output to 7
c
      implicit real*8(a-h,o-z)
      implicit integer*4(i-n)
      real*8 lwbnd,upbnd
      integer b1,b2,b3,c1,c2,c3
      common /ab/ alpha,delta,pi,sqrtpi
      external fz,fq,fp
c
c     data
c
      ndelta=1000
      pi=2.d0*darcos(0.d0)
      lwbnd=0.d0
      upbnd=2.d0*pi
      sqrtpi=dsqrt(pi)
      deps=1.d-5
      write(7,10)
10    format(1x,'alpha',8x,'q',12x,'p',12x,'t',12x,'f')
c
c     choose field strengths
c
      a=4.541458d0
      write(5,*) 'Enter magnetic field strength, b'
      read(5,*) b
      write(5,*) 'Enter direction of b, eg.  1  0  0 '
      read(5,*) b1,b2,b3
      write(5,50) b,b1,b2,b3
      ba=-0.5d0*b1*b-0.5d0*b2*b+b3*b
      bd=0.5d0*b1*b-0.5d0*b2*b
      write(5,*) 'Enter electric field strength, c'
      read(5,*) c
      write(5,*) 'Enter direction of c, eg.  0  1  0 '
      read(5,*) c1,c2,c3
      write(5,60) c,c1,c2,c3
      ca=-0.5d0*c1*c-0.5d0*c2*c+c3*c
      cd=0.5d0*c1*c-0.5d0*c2*c
      write(5,*) ba,bd
      write(5,*) ca,cd
      write(7,50) b,b1,b2,b3
      write(7,60) c,c1,c2,c3
50    format(1x,'b=',g12.5,'*(',i1,',',i1,',',i1,')')
60    format(1x,'c=',g12.5,'*(',i1,',',i1,',',i1,')')
c
c     choose alpha, delta
c
```

```
70      format(1x,'nalpha=',i2,1x,'stepsize=',g15.7)
        delta=0.d0
        do 500 ialpha=1,100
          write(5,*) 'Enter the minimum value of alpha required'
          read(5,*) alpmin
          if (alpmin.eq.0.d0) go to 600
          write(5,*) 'Enter the maximum value of alpha required'
          read(5,*) alpmax
          write(5,*) 'Enter the number of alpha values required'
          read(5,*) nalpha
          stepsz=(alpmax-alpmin)/(nalpha-1)
          write(5,70) nalpha,stepsz
          do 100 j=1,nalpha
            alpha=alpmin+stepsz*(j-1)
            if (alpha.eq.0.d0) go to 100
c
c     calculate order parameters using dquank
c
            do 200 i=1,ndelta
              zz=dquank(fz,lwbnd,upbnd,deps,tolz,fifthz)
              q=dquank(fq,lwbnd,upbnd,deps,tolq,fifthq)
              qq=1.5d0*q/zz-0.5d0
              p=dquank(fp,lwbnd,upbnd,deps,tolp,fifthp)
              pp=1.5d0*p/zz
c
c     calculate t and new delta and check criterion
c
              t=(qq+ba+ca)*a/alpha
              delta1=(pp/3.d0+bd+cd)*a/t
              diff=dabs(delta1-delta)
              delta=delta1
              if (delta1.ge.1.d-4) go to 250
              if (diff.ge.1.d-7) go to 200
              go to 260
250           reldif=dabs(diff/delta1)
              if (reldif.ge.1.d-4) go to 200
260           f=(qq*qq+pp*pp/3.d0)/2.d0-t*(-1.d0*dlog(4.d0*pi)-alpha/2.d0
     #          +dlog(zz))/a
              if (b3.ne.1) then
                if (b1.eq.1) then
                  qq=-0.5*(qq+pp)
                  pp=-0.5*(-3.*qq+pp)
                else if (b2.eq.1) then
                  qq=-0.5*(qq-pp)
                  pp=-0.5*(3.*qq+pp)
                endif
              endif
              write (6,210) alpha,qq,pp,t,f
              write (7,210) alpha,qq,pp,t,f
              go to 100
200         continue
100       continue
210       format (1x,5(d12.5,1x))
220       format (14x,2(d12.5,1x))
500     continue
600     stop
```

```
      end
c
c
c
c
c     this is the integrand for calculating z
c
      double precision function fz(x)
      implicit real*8(a-h,o-z)
      common /ab/ alpha, delta, pi,sqrtpi
      complex*16 arg,y
      aa=delta*dcos(2.d0*x)
      gmmasq=1.5d0*(aa-alpha)
      if (gmmasq.eq.0.d0) go to 11
      kb=0
      if (gmmasq.gt.0.d0) kb=1
      gmmsq=dabs(gmmasq)
      gmma=dsqrt(gmmsq)
      gmmar=kb*gmma
      gmmai=(1-kb)*gmma
      arg=dcmplx(gmmar,gmmai)
      call cerf(arg,y)
      r=((1-kb)*dimag(y)+kb*dreal(y))*sqrtpi/gmma
      go to 10
11    r=2.d0
10    fz=dexp(1.5d0*aa)*r
      return
      end
c
c
c
c
c     this is the integrand for q
c
      double precision function fq(x)
      implicit real*8(a-h,o-z)
      common /ab/ alpha, delta, pi,sqrtpi
      complex*16 arg,y
      aa=delta*dcos(2.d0*x)
      gmmasq=1.5d0*(aa-alpha)
      if (gmmasq.eq.0.d0) go to 11
      kb=0
      if (gmmasq.gt.0.d0) kb=1
      gmmsq=dabs(gmmasq)
      gmma=dsqrt(gmmsq)
      gmmar=kb*gmma
      gmmai=(1-kb)*gmma
      arg=dcmplx(gmmar,gmmai)
      call cerf(arg,y)
      r=((1-kb)*dimag(y)+kb*dreal(y))
      ff=(r*sqrtpi/2.d0-gmma*dexp(-1.d0*gmmasq))/(gmma**3)*(2*kb-1)
      go to 10
11    ff=2.d0/3.d0
10    fq=dexp(1.5d0*aa)*ff
      return
      end
```

```
c
c
c
c
c     this is the integrand for p
c
      double precision function fp(x)
      implicit real*8(a-h,o-z)
      common /ab/ alpha, delta, pi, sqrtpi
      complex*16 arg,y
      aa=delta*dcos(2.d0*x)
      gmmasq=1.5d0*(aa-alpha)
      if (gmmasq.eq.0.d0) go to 11
      kb=0
      if (gmmasq.gt.0.d0) kb=1
      gmmsq=dabs(gmmasq)
      gmma=dsqrt(gmmsq)
      gmmar=kb*gmma
      gmmai=(1-kb)*gmma
      arg=dcmplx(gmmar,gmmai)
      call cerf(arg,y)
      r=((1-kb)*dimag(y)+kb*dreal(y))
      part1=r*sqrtpi/gmma
      part2=(r*sqrtpi/2.d0-gmma*dexp(-1.d0*gmmasq))/(gmma**3)*(2*kb-1)
      go to 10
11    part1=2.d0
      part2=2.d0/3.d0
10    fp=dcos(2.d0*x)*dexp(1.5d0*aa)*(part1-part2)
      return
      end
c
c
c
c
c     this program looks for crossings in the free energy
c
      program cross
      implicit real*8(a-h,o-z)
      implicit integer*4(i-n)
      dimension q(1000), p(1000), t(1000), f(1000), slope(1000)
      dimension alp(1000)
c
c     input data
c
      read(4,30) kkk
      read(4,35)b
      read(4,35)c
30    format(a2)
35    format(3x,g12.5)
      npts=0
      do 40 ip=1,1000
        read(4,*,end=45) alp(ip),q(ip),p(ip),t(ip),f(ip)
        npts=npts+1
40    continue
45    do 100 i=1,npts
        deltat=t(i+1)-t(i)
```

```
          if (deltat.eq.0.d0) go to 490
          slope(i)=(f(i+1)-f(i))/(t(i+1)-t(i))
100     continue
        do 200 i=1,npts
          nb=i
          ii=i+2
          do 300 j=ii,npts
            if (t(j).gt.t(i+1)) go to 300
            if (t(j+1).lt.t(i)) go to 300
            if (f(j).gt.f(i+1)) go to 300
            if (f(j+1).lt.f(i)) go to 300
            deltas=slope(j)-slope(i)
            if (deltas.eq.0.d0) go to 300
            deltat=t(j)-t(i)
            tt=(slope(j)*t(j)-slope(i)*t(i)+f(i)-f(j))/deltas
            ff=(slope(i)*slope(j)*deltat+slope(j)*f(i)-slope(i)*f(j))/deltas
            na=j
            write(6,565)tt,ff
            if (tt.ge.t(j)) go to 330
            go to 300
330         if (tt.le.t(j+1)) go to 340
            go to 300
340         if (tt.ge.t(i)) go to 350
            go to 300
350         if (tt.le.t(i+1)) go to 500
300       continue
200     continue
        write(6,540)
        go to 570
490     write(6,530)
        go to 570
500     tni=tt
        q1=(q(nb+1)-q(nb))/(t(nb+1)-t(nb))*(tt-t(nb))+q(nb)
        q2=(q(na+1)-q(na))/(t(na+1)-t(na))*(tt-t(na))+q(na)
        write(6,550) tni
        write(6,555) q1,q2
        write(7,520)
        write(7,560) b,c,ff,tni,q1,q2
        if (i.ne.npts) go to 200
520     format(1x,'b',12x,'c',12x,'f',12x,'tni',10x,'q1',11x,'q2')
530     format(1x,'there are two identical adjacent temperatures')
540     format(1x,'no crossing was found')
550     format(1x,'the crossing of f occurs at t=',g15.8)
555     format(1x,'above the transition, q=',g12.5,'  below, q=',g12.5)
560     format(1x,6(g12.5,1x))
565     format(1x,2(g15.8,1x))
570     stop
        end
```

Appendix B:

```
      program frng
c
c     Calculates maximum deformation angle, free energy and capacitance
c     for bend freedericksz transion in two fields
c     Input thm, h, calculate e and free energy
c     Output to unit 7
c
      implicit real*8(a-h,o-z)
      implicit integer*4(i-n)
      character*64 filename
c
c     e=reduced voltage parameter
c     h=reduced magnetic field paramenter
c     F=free energy
c     THM=maximum deformation angle
c
      common /a/ ineg
      common /d/ u,ek,h,pi
      common /ee/ etasq
      common /f/ f1n0,f1d0,f10
      external fcne,fcnf,fcnc
c
c     material parameters and other data
c     u=(epspar-epsperp)/epspar, this changes sign
c     when e < 0.d0
c     ek=(k3-k1)/k3
c     d=3.3mm, width of cell in x direction
c     cl=.5mm, length of the cell in the z direction
c     ch=2.54cm, height of the cell (y)
c
      pi=2.d0*dacos(0.d0)
      e0=8.85d-12
      eperp=8.5d0
      write(*,*) 'Input elastic parameter ek'
      read(*,*) ek
      write(*,*) 'Input dielectric parameter u'
      read(*,*) u
      d=3.3d-3
      ch=2.54d-2
      cl=5.d-4
      epse=1.d-5
c
c     set up input/output files
c
      write(*,*) 'Data to device:filename'
      read(*,1) filename
1     format(a)
      open(7,file=filename,status='new')
c
c      input magnetic field
c
2     write(*,*) 'Input magnetic field parameter: '
      read(*,*) h
      write(*,3) h
```

```
      write(7,3) h
3     format(1x,'Magnetic field parameter is',e10.5)
      write(7,*)
      write(7,5)
5     format(1x,2x,'theta max',2x,3x,'e parameter',3x,1x,'free energy',1x,
     * 1x,'capacitance')
c
c   now we want to vary thm, iterate to find
c   e and then calculate f for
c   each value of the voltage and find where f=f0
c
      write(*,*) 'Lower bound on thm?'
      read(*,*) thmin
      write(*,*) 'Upper bound on thm?'
      read(*,*) thmax
      write(*,*) 'Number of steps?'
      read(*,*) nthm
      iflag=0
      ineg=0
      do 25 i=1,nthm
20      if (ineg.eq.1) then
          u=-1.d0*u
          iflag=1
          ineg=0
        end if
      thm=float(i-1)/float(nthm-1)*(thmax-thmin)+thmin
c
c   can now calculate numerator and denomenator without e for
c   f1 for phi=pi/2
c
      etasq=dsin(thm)**2
      f1n0=(1.-ek*etasq)*(1.-u*etasq)*(1.-u*etasq)
      f1d0=-h*(1.d0-u*etasq)*(1.d0-u*etasq)
c
c   set limits for e
c
      if (h.lt.0.d0.and.iflag.eq.0) then
        elow=0.0
        ehigh=1.d5
      else if (h.lt.0.d0.and.iflag.eq.1) then
        elow=h*(1.d0-u*etasq)**2+1.d-6
        ehigh=0.d0
      else if (h.ge.0.d0.and.iflag.eq.0) then
        elow=h*(1.d0-u*etasq)+1.d-6
        ehigh=1.d6
      end if
c
c   iterate to find e, criterion epse
c
      e=rtbis(fcne,elow,ehigh,epse)
c
c   calculate free energy and capacitance
c
      call frngcap(thm,e,f,c)
      c=2.d0*e0*eperp*ch*cl/d*c
      write(*,30) thm,e,f,c
```

```
      write(7,30) thm,e,f,c
c
c     new theta max
c
25    continue
30    format(1x,4(d13.6,1x))
      write(*,*) 'Continue (y or n)?'
      read(*,1) check
      if (check.eq.'n') then
        go to 100
      else
        go to 2
      end if
100   stop
      end
c
c
c
c
c     function to find e by bisection method, criterion epse
c     further documentation in Press et al. [1986]
c
      function rtbis(func,x1,x2,xacc)
      implicit real*8(a-h,o-z)
      implicit integer*4(i-n)
      parameter (jmax=40)
      fmid=func(x2)
      f=func(x1)
      if (f*fmid.ge.0.) pause 'Root must be bracketed for bisection.'
      if(f.lt.0.)then
        rtbis=x1
        dx=x2-x1
      else
        rtbis=x2
        dx=x1-x2
      endif
      do 11 j=1,jmax
        dx=dx*.5
        xmid=rtbis+dx
        fmid=func(xmid)
        if(fmid.lt.0.)rtbis=xmid
        if(abs(dx).lt.xacc .or. fmid.eq.0.) return
11    continue
      pause 'too many bisections'
      end
c
c
c
c
c     function to be zeroed
c
      function fcne(e)
      implicit real*8(a-h,o-z)
      implicit integer*4(i-n)
      common /d/ u,ek,h,pi
      common /ee/ etasq
```

```
      common /f/ f1n0,f1d0,f10
      external fcn1
c
c   integrating to precision epsint
c
      ck=dsqrt(1.d0-etasq)
      cappa=cel(ck.1.d0,1.d0,1.d0)
      epsint=1.d-5
      f10=dsqrt(f1n0/(e+f1d0))
      g1=simp(e,0.d0,pi/2.d0,epsint,n,fcn1)
      fcne=g1+f10*cappa-5.d-1
      return
      end
c
c
c
c
c   function to calculate integrand for fcne
c
      function fcn1(e,phi)
      implicit real*8(a-h,o-z)
      implicit integer*4(i-n)
      common /d/ u,ek,h,pi
      common /ee/ etasq
      common /f/ f1n0,f1d0,f10
      ysq=dsin(phi)**2
      fn=(1.d0-ek*etasq*ysq)*(1.d0-u*etasq*ysq)*(1.d0-u*etasq)
      fd=e-h*(1.d0-u*etasq*ysq)*(1.d0-u*etasq)
      fcn1=(dsqrt(fn/fd)-f10)/dsqrt(1.-etasq*ysq)
      return
      end
c
c
c
c
c   function to perform integration via adaptive simpson's rule
c
      function simp(e,a,b,error,n,ffn)
      implicit real*8(a-h,o-z)
      implicit integer*4(i-n)
      dimension as(1000),bs(1000)
      if(a.eq.b) then
        simp = 0.d0
        return
      endif
      do 3 i=1,1000
      as(i) = 0.d0
      bs(i) = 0.d0
3     continue
      i = 0
      s = 0.
      imax=0
      eps = error
c
c   calculate error criterion
c
```

```
      err=dabs(eps/(b-a))
c
c     initialise stacks
c
      i=i+1
      as(i)=b
      bs(i)=ffn(e,b)
      i=i+1
      c=(a+b)/2.
      as(i)=c
      bs(i)=ffn(e,c)
      i=i+1
      as(i)=a
      bs(i)=ffn(e,a)
c
c     update stacks
c
1     ta1=as(i)
      tb1=bs(i)
      i=i-1
      ta2=as(i)
      tb2=bs(i)
      c=(as(i-1)+ta2)/2.
      as(i)=c
      bs(i)=ffn(e,c)
      i=i+1
      as(i)=ta2
      bs(i)=tb2
      i=i+1
      c=(ta2+ta1)/2.
      as(i)=c
      bs(i)=ffn(e,c)
      i=i+1
      as(i)=ta1
      bs(i)=tb1
c
c     evaluate error
c
      if(i.ge.imax) imax=i
      xi1=bs(i)+4*bs(i-2)+bs(i-4)
      xi2=bs(i)+4*bs(i-1)+bs(i-2)
      xi3=bs(i-2)+4*bs(i-3)+bs(i-4)
      diff=xi1-0.5*(xi2+xi3)
      if(dabs(diff).le.err)then
        s=s+xi1*(as(i-4)-as(i))/6.
        i=i-4
        if(i.le.1)then
          simp = s
          go to 2
        endif
      endif
      go to 1
2     continue
      n=(imax-5)/2+1
      return
      end
```

```
c
c
c
c
c     subroutine to calculate free energy and capacitance
c     once thm, e are known
c
      subroutine frngcap(th,eknown,fr,cap)
      implicit real*8(a-h,o-z)
      implicit integer*4(i-n)
      common /d/ u,ek,h,pi
      common /ee/ etasq
      common /g/ f20,f30
      external fcn2,fcn3
c
c     calculate free energy for thm=0
c
      f0=(-eknown/u-h)/2.d0
c
c     calculate integrands for phi=pi/2
c
      fn0=(eknown-h*(1.d0-u*etasq)*(1.d0-u*etasq))
      fd0=(1.d0-ek*etasq)*(1.d0-u*etasq)*(1.d0-u*etasq)
      gth0=dsqrt(fn0/fd0)
      a0=0.d0
      b0=(eknown/u+h*(1.d0-u*etasq)*(1.d0-etasq))/(1.d0-u*etasq)
      f20=a0*gth0-b0/gth0
      f30=1./(1.-u*etasq)/gth0
c
c     complete equation for free energy
c
      ck=dsqrt(1.d0-etasq)
      cappa=cel(ck,1.d0,1.d0,1.d0)
      epsint=1.d-5
      g2=simp(eknown,0.d0,pi/2.d0,epsint,n,fcn2)
      epsint=1.d-5
      g3=simp(eknown,0.d0,pi/2.d0,epsint,n,fcn3)
      fr=g2+f20*cappa-f0
      cap=g3+f30*cappa
      return
      end
c
c
c
c
c     function to calculate integrand for free energy
c
      function fcn2(e,phi)
      implicit real*8(a-h,o-z)
      implicit integer*4(i-n)
      common /d/ u,ek,h,pi
      common /ee/ etasq
      common /g/ f20,f30
      ysq=dsin(phi)**2
      fn=(e-h*(1.d0-u*etasq)*(1.d0-u*etasq*ysq))
      fd=(1.d0-ek*etasq*ysq)*(1.d0-u*etasq*ysq)*(1.d0-u*etasq)
```

```
      gth=dsqrt(fn/fd)
      alpha=(1.d0-ek*etasq*ysq)*etasq*(1.d0-ysq)
      beta=(e/u+h*(1.d0-u*etasq*ysq)*(1.d0-etasq*ysq))
     *            /(1.d0-u*etasq*ysq)
      fcn2=(alpha*gth-beta/gth-f20)/dsqrt(1.d0-etasq*ysq)
      return
      end
c
c
c
c
c     function to calculate capacitance
c
      function fcn3(e,phi)
      implicit real*8(a-h,o-z)
      implicit integer*4(i-n)
      common /d/ u,ek,h,pi
      common /ee/ etasq
      common /g/ f20,f30
      ysq=dsin(phi)**2
      fn=(e-h*(1.d0-u*etasq)*(1.d0-u*etasq*ysq))
      fd=(1.d0-ek*etasq*ysq)*(1.d0-u*etasq*ysq)*(1.d0-u*etasq)
      gth=dsqrt(fn/fd)
      fcn3=(1./(1.-u*etasq*ysq)/gth - f30)/dsqrt(1.-etasq*ysq)
      return
      end
c
c
c
c
c     function to evaluate elliptic integral
c     qqc is 1-k*k
c     for integral of the first kind, pp=aa=bb=1
c     further documentation in Press et al. [1986]
c
      function cel(qqc,pp,aa,bb)
      implicit real*8(a-h,o-z)
      implicit integer*4(i-n)
      parameter (ca=.0003, pio2=1.5707963268)
      if(qqc.eq.0.)pause 'Failure in CEL'
      qc=abs(qqc)
      a=aa
      b=bb
      p=pp
      e=qc
      em=1.
      if(p.gt.0.)then
        p=sqrt(p)
        b=b/p
      else
        f=qc*qc
        q=1.-f
        g=1.-p
        f=f-p
        q=q*(b-a*p)
        p=sqrt(f/g)
```

```
      a=(a-b)/g
      b=-q/(g*g*p)+a*p
    endif
1   f=a
    a=a+b/p
    g=e/p
    b=b+f*g
    b=b+b
    p=g+p
    g=em
    em=qc+em
    if(abs(g-qc).gt.g*ca)then
      qc=sqrt(e)
      qc=qc+qc
      e=qc*em
      go to 1
    endif
    cel=pio2*(b+a*em)/(em*(em+p))
    return
    end
```

PUBLICATIONS:

B.J. Frisken and P. Palffy-Muhoray, 'Effects of a Transverse Electric Field in Nematics: Induced Biaxiality and the Freedericksz Transition', to be published in Liquid Crystals.

D.W. Allender, B.J. Frisken and P.Palffy-Muhoray, 'Theory of an Electric Field Induced Periodic Phase in a Nematic Film', to be published in Liquid Crystals.

B.J. Frisken and P. Palffy-Muhoray, 'Electric Field Induced Twist and Bend Freedericksz Transitions in Nematic Liquid Crystals', Phys. Rev. A 39, 1513 (1989).

B.J. Frisken, B. Bergersen and P. Palffy-Muhoray, 'Phase Behaviour of Nematics in the Presence of Electric and Magnetic Fields', Mol.Cryst.Liq.Cryst 148, 45 (1987).

B.J. Frisken, J.F. Carolan, P. Palffy-Muhoray, J.A.A.J. Perenboom and G.S. Bates, 'SQUID Susceptibility Measurements on 5CB', Mol.Cryst.Liq.Cryst.Letters 3, 57 (1986).

B. Frisken, F. Guillon, J.P. Harrison and J.H. Page, 'Low Frequency Phonons in Sintered Copper', J. Phys. Colloq. 42, C6, 858-60 (1981).